Geotechnical Characterization and Slope Stability Assessment along selected section of Tercha-Chida Road, Southern Ethiopia

Emebet Ejgu Werku

A Thesis Submitted to the Department of Applied Geology,

School of Applied Natural Science

Presented in Partial Fulfillment of the Requirement for the Degree of Master's in Engineering Geology

Office of Graduate Studies

Adama Science and Technology University

June 2022

Adama, Ethiopia

Geotechnical Characterization and Slope Stability Assessment along selected section of Tercha-Chida Road, Southern Ethiopia

Emebet Ejgu Werku

Advisor

Endalu Tadele (Ph.D.)

Co-Advisor

Tola Garo (MSc)

A Thesis Submitted to the Department of Applied Geology

School of Applied Natural Science

Presented in Partial Fulfillment of the Requirement for the Degree of Master's in Engineering Geology

Office of Graduate Studies

Adama Science and Technology University

June 2022

Adama, Ethiopia

Declaration

I hereby declare that this Master Thesis entitled is "**Geotechnical Characterization and Slope Stability Assessment along the selected section of Tercha-Chida Road, Southern, Ethiopia"** my original work. That is, it has not been submitted for the award of any academic degree, diploma, or certificate in any other university. All sources of materials that are used for this thesis have been duly acknowledged through citation

________________________	________________________	________________
Name of the Student	Signature	Date

Recommendation

We, the advisors of this thesis, hereby certify that we have read the revised version of the thesis entitled "**Geotechnical Characterization and Slope Stability Assessment along the selected section of Tercha-Chida Road, Southern, Ethiopia**" was prepared under our guidance by **Emebet Ejgu** and submitted in partial fulfillment of the requirements for the degree of Masters of Science in **Engineering Geology**. Therefore, we recommend the submission of a revised version of the thesis to the department following the applicable procedures.

______________________	______________________	______________________
Major Advisor	Signature	Date
______________________	______________________	______________________
Co-advisor	Signature	Date

Approval Page

We, the advisors of the thesis entitled "**Geotechnical Characterization and Slope Stability Assessment along selected sections of Tercha-Chida Road, Southern, Ethiopia**" and developed by Emebet Ejgu, hereby certify that the recommendation and suggestions made by the board of examiners are appropriately incorporated into the final version of the thesis.

Major Advisor	Signature	Date
Co-Advisor	Signature	Date

We, the undersigned, members of the Board of Examiners of the thesis by **Emebet Ejgu** have read and evaluated the thesis entitled "**Geotechnical Characterization and Slope Stability Assessment along selected sections of Tercha-Chida Road, Southern, Ethiopia**" and examined the candidate during the open defense. This is, therefore, to certify that the thesis is accepted for partial fulfillment of the requirement of the degree of Master of Science in **Engineering geology**.

Chairperson	Signature	Date
Internal Examiner	Signature	Date
External Examiner	Signature	Date

Final approval and acceptance of the thesis is contingent upon the submission of its final copy to the Office of Postgraduate Studies (OPGS) through the Department Graduate Council (DGC) and School Graduate Committee (SGC).

Department Head	Signature	Date
School Dean	Signature	Date
Office of Postgraduate Studies, Dean	Signature	Date

ACKNOWLEDGEMENT

This work would not have been possible without the financial support and laboratory facilities of Adama Science and Technology University. I would like to express my special gratitude to my advisor Dr. Endalu Tadele as well as to my co-advisor Mr. Tola Garo who made this work possible. Their guidance and advice helped me through all stages of writing this thesis. Detailed subsurface data, geophysical and borehole data were collected from ECDSWC and I want to thank the ECDSWC for providing the data and their support. I am grateful to the staff in the civil and geotechnical engineering department of Addis Ababa Science and Technology University, who permitted me to use the necessary tools in the lab. Last but not least I would like to thank my friend and families for helping me through this project.

Table of Contents

LIST OF TABLES

List of Figures and Illustrations

List of Acronyms and Abbreviations

ASTU…..…… Adama Science and Technology University

AASHTO…. America Association of State Highway and Transportation Officials

ASTM……. American Society for Testing and Materials

ECDSWC…… Ethiopia Construction Design and Supervision Works Corporation

FEM……..…. Finite Element Method

FOS………...Factor of Safety

GIS……..…. Geographic Information System

LEM……..…Limit Equilibrium method

SNNP……...South Nation, Nationality and Peoples 'Region

SRF……… Strength Reduction Factor

UCS………Unconfined Compressive Strength

USCS………Unified Soil Classification System

VES……..…Vertical Electrical Sounding

ABSTRACT

Slope stability assessment is essential for the safety and sustainable development of mining, civil, and environmental engineering projects worldwide. It is also important for the long-term survivability of existing and excavated slopes. Geotechnical characterization and Slope stability analysis has been carried out to evaluate the potential for failure of the cut slope. The study area was along a road section between Tercha in the Dawro zone and Chida in Konta woreda. The main objective of the study is a geotechnical characterization of soil and rock mass along the selected road sections, assessing the potential failure by determining the factor of safety of the critical slope sections and proposing the remedial measure. Along the road sections of Tercha in the Dawro zone and Chida in Konta, eight sections have been selected. Out of that six of them are rock slopes and the other two slopes are soil slope. On the rock slope, detailed joint mapping was carried out and the result of the discontinuity survey indicates that the dominant joint orientation is sub-horizontal to vertical. The subsurface conditions of the critical slope section were studied through six boreholes and seismic refraction data obtained from ECDSWC; accordingly, the selected slope sections were classified into three geological formations namely; (1) top soils (a pyroclastic deposit with 10m thickness (2) weathered and fractured rock (20m thickness) and (3) bed rock. The disturbed and remolded sample was obtained from 2 pit excavations. The clayey gravel soil is brown with a specific gravity of 2.68, Natural water content of 3.6%, Plastic limit of 31.93, and a liquid limit value of 51.983. the optimum moisture content, which was 22.1%, and maximum dry density with the value of 1.58g/cm3. the direct shear test result shows the cohesion and friction angle 12.2 and 30.5° values respectively. Similarly, all rock units observed in the critical slope sections including Tuff, Ignimbrite, Rhyolite, Basalt, and unwelded tuffs are identified and their respective point load strength, dry and saturated density and slake durability were determined. The critical slope section analysis was carried out using limit equilibrium, finite element, and kinematic analysis methods. Two structurally controlled rock slope failures have been identified and each has a planar and a toppling failure. The effect of saturation, material properties and loading conditions significantly affect the stability of the slope. Benching and Constructing pressure Berms at the toe and the replacement of slipped material with free-draining material is important to increase the stability of the slopes.

Key words: Geotechnical characterization, Slope stability, Factor of safety, SRF, Limit equilibrium method, Finite element method, Benching and Berms.

CHAPTER ONE

INTRODUCTION

1.1 Background of the Study

Slope stability assessment is essential for the safety and sustainable development of mining, civil, and environmental engineering projects worldwide. It is also important for the long-term survivability of existing and excavated slopes. Slope stability analysis is vital to preventing slope failures in a variety of engineering applications including landfill design, roads, dams, and embankments, to name a few. Proper analysis anticipates both natural and manmade slopes and failure of foundations and retaining walls. (Moudabel, 2013). The main interest of slope stability analysis is typically to determine a factor of safety value (FS) against slope failure. A lot of researches have been performed in the last the past few decades but slope stability analysis still remains a challenge in geotechnical engineering

Slope stability analysis is the investigation of potential failure mechanisms and the sensitivity to various triggering mechanisms. Slope stability analysis involves the design of optimal slope concerning safety, reliability and, economics and, the design of possible remedial measures. The geometry of the slope, incorporated materials, soil, environmental conditions and geological forces (seismic and groundwater) are only a few of the factors to consider in determining slope stability.

Slope stability analysis determines stability based on a "factor of safety." The factor of safety is a ratio of material shear strength properties to applied shear stress. It can also be thought of as a ratio of the maximum load a slope can sustain to the actual load that is applied. There are many different ways to conduct slope stability analysis, and each of them have their benefits and limitations. According to Azeze (2020), Slope stability analysis can be perform using limit equilibrium and finite element numerical methods. The limit equilibrium method is one of the oldest and the best well-known numerical methods that has been used routinely in geotechnical engineering work because of its simplistic and accurate results (Carol Matthews and Zeena Farook, 2014) However, it cannot help to determine the response of the ground under stress. For this purpose, the finite element method is preferable. Furthermore, the limit equilibrium method is better when the analysis does not expect material response under stress whereas the finite element method is appropriate when the analysis considers mechanical responses of the materials (Carol Matthews and Zeena Farook, 2014).

In Ethiopia, slope failures are mostly concentrated in the north, south, and western part of the Ethiopia plateau, and rift margins. Moreover, according to (Woldearegay, 2013) these slope failures mostly occur in broad regions that possess characteristics of soil and rock materials, geologic structures, and, topographic settings mainly in terms of deep-seated rotational slumps.

The selected site is located between Tercha and Chida cities in the South of Ethiopia, which is found 530km away from Addis Ababa city. A landslide has been countered around the study area early on 28 May 2019 in the Gamo Zone of the Southern Nations, Nationalities, and Peoples' Region (SNNPR), and this hazard has killed at least 10 people due to a landslide triggered by heavy rainfall. This study will enable the designers, administration, and planners to make a judgment on the safety of local people, and damage to road infrastructures in the study area due to slope instability.

The main objective of this study is to determine the factor of safety to identify critical slope sections and to design the remedial measures. To improve the accuracy of a slope stability analysis different physio- mechanical properties of the material are determined by laboratory tests and fieldwork. Limit equilibrium, finite element methods and borehole and geophysical data are used to determine the stability of the slope in the study area.

1.2 Description of the Study

1.2.1 Location and Accessibility

The study area for research work is located between Tercha and Chida towns in the Dawro zone of South Nation, Nationality, and, People's region, Southern Ethiopia as shown in Figure 1.1. It is bounded by geographic coordinates of 36˚20'0'' to 37˚10'0'' Easting and 6˚30'0'' to 7˚30'0'' Northing.

This area can be accessible via 545 km long Addis Ababa-Butajira-SodoBele-Tercha-Chida route or through 450 km Addis Ababa-Welkite-Jimma-Chida-Tercha route. Sodo-Chida is a gravel road that is under construction to be upgraded to an asphalt road.

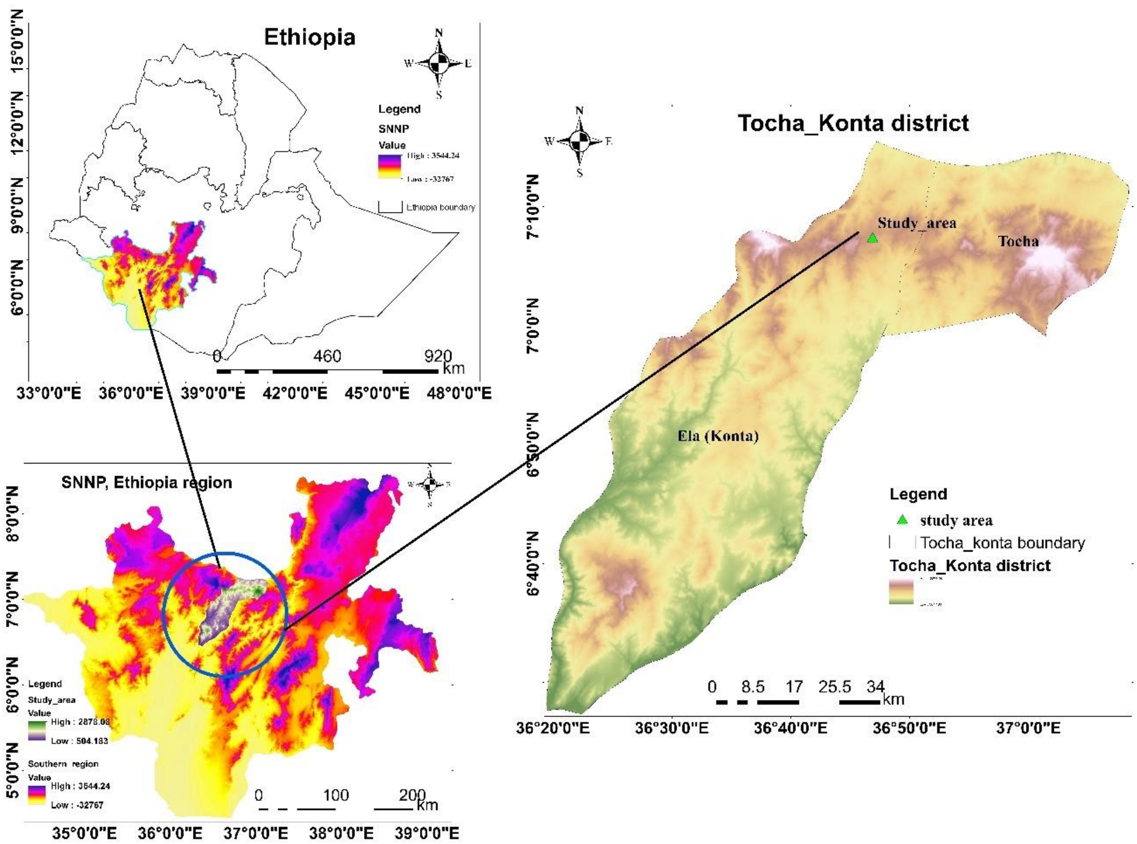

Figure 1.1 Location map of a study area

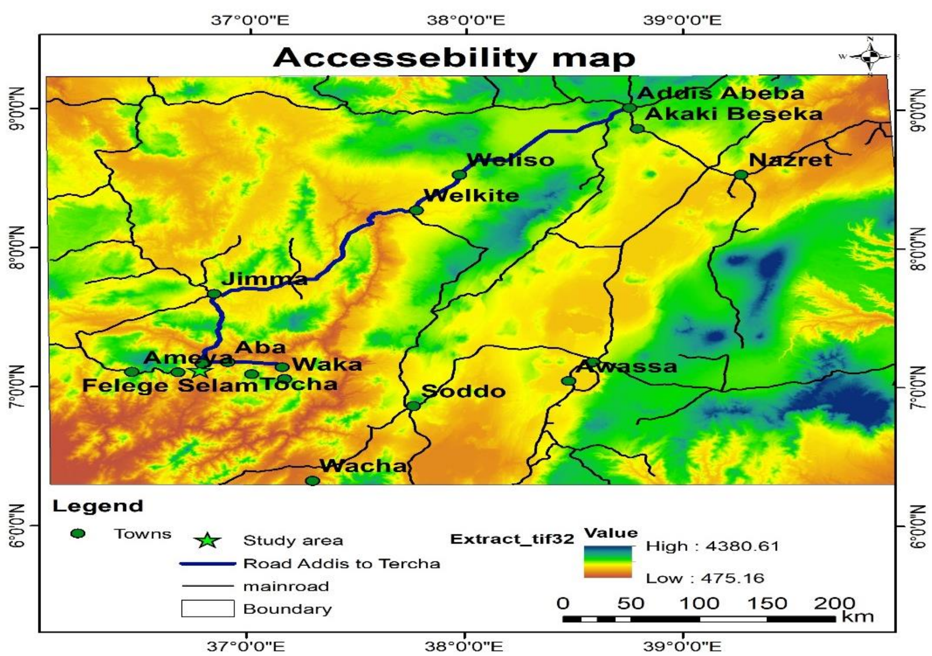

Figure 1.2 Accessibility map of the study area

1.2.2 Physiography and Climate

The area comprises different topographic terrains that vary from rugged and hilly terrains to planar surfaces ranging from below 1000 meters above sea level in the eastern part to 2400 meters above sea level in the western part. Morphological depressions are related to a series of EW and NS trending fault systems (Wube, 2003).

The southwestern Ethiopia physiography subdivision consists of the highlands of Wellega, Illuababor, Jimma, Kaffa, Gamo, and Gofa. This region is separated from the adjacent highlands by the Abay and Omo River valleys. It extends from the Abay gorge in the north to the Kenya border and Chew Bahir in the south. It accounts for 22.7% of the area of the region. The region is the second-largest in the Western highlands. About 70% of its area lies within 1,000-2,000 meters altitude. The southwestern plateau is the wettest in Ethiopia. It is drained by Dabus, Deddessa (tributaries of Abay), Baro, Akobo and the Ghibe/Omo rivers. With a height of 4,200 meters above sea level, Guge Mountain is the highest peak in this physiographic subdivision.

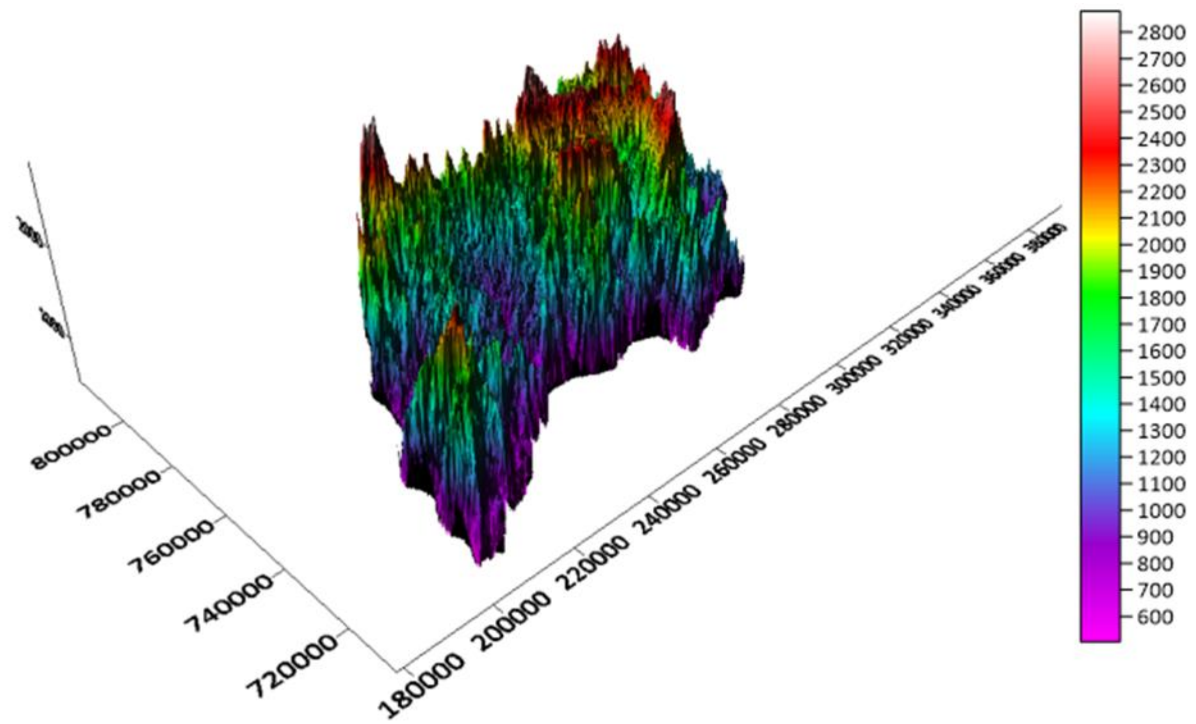

Figure 1.3 Physiography of the study area

According to the data taken from 2010 and 2021, (NASA, 2022) the southwestern Ethiopia has a maximum and minimum annual rainfall of 9.89mm/day and 1.23mm/day respectively.

The main rainy season extends from June to October (kiremt) and a short rainy season (belg) occurs between March and May. The mean annual temperature ranges from 20.8˚c to 23.2˚c. the highest temperature is recorded in February. The area is generally characterized by warm and humid subtropical climatic conditions with pronounced temperature variations depending on the elevation differences (warm in the Valleys and mild on higher elevations).

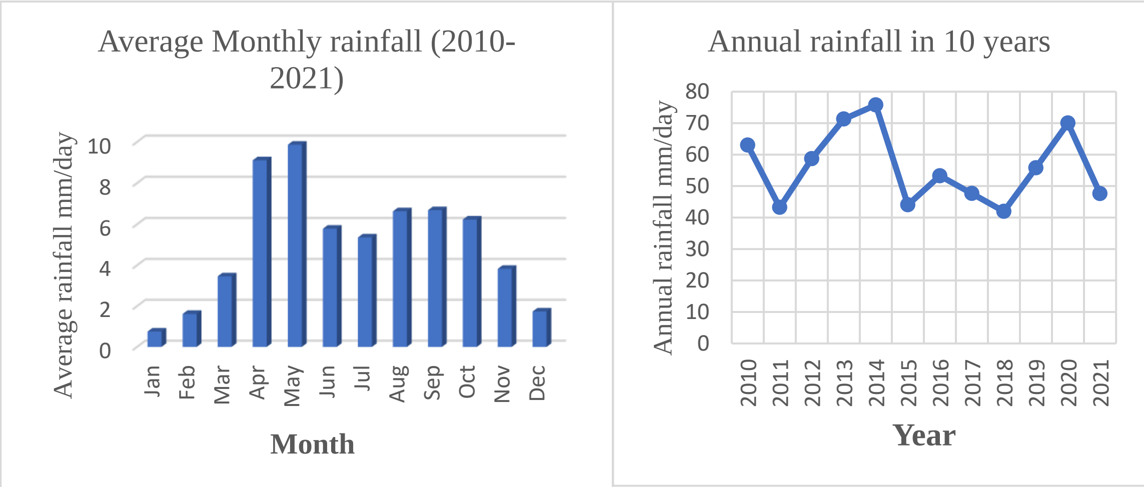

Figure1. 4 Average annual and monthly rainfall of 11 years (2010-2021)

1.2.3 Vegetation

Vegetation of the area also consists of sparse bushy types mainly acacia and is densely covered by grass. Remnants of tropical rain forests are confined along with stream courses as well. The vegetation includes woody forest along the valley and some mountain ranges. Different dense, tall and broad-leaved, evergreen trees characterize Jima, Kaficho and Konta regions.

1.2.4 Seismicity of the Study Area

Seismic hazard in South Ethiopia (6,0°- 8,5°N, 37,5°- 39,5°) is conditioned by the rift character of the region. From a global point of view, seismicity is related with rifts (both oceanic and continental) which represents about 6% of the seismic energy release. Continental rifts are characterized by a special type of seismicity, including seismic swarms and volcanic earthquakes (Valenta, 2021).

The earthquakes have been observed around the study area with a magnitude of (7). Depending on the Ethiopia building code standards zoning (EBCS-8), the site falls at zone 2 with a ground acceleration of 0.05. This showed that the study area is seismically active area.

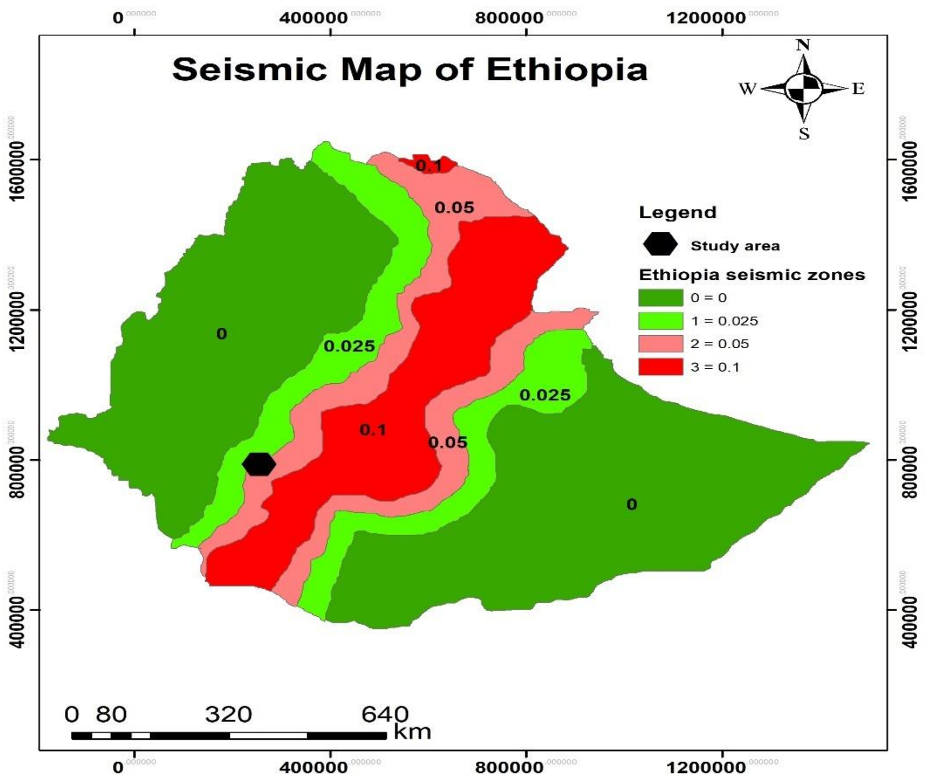

Figure 1.5 seismic map of the study area (Dulbal, 2020)

1.3 Statement of the Problem

The Slope stability is the resistance of an inclined surface to failure by sliding or collapsing. The failure of a slope may lead to loss of life and property. It is, therefore, essential to check the stability of the proposed area. To assess a safe design of a man-made or natural slope, we need to analyze its stability. Southwestern Ethiopia passes through an extremely rugged terrain characterized by steep hill slopes and deep valleys. The study is for road construction, assessing the slope of the road is important before any damage occurred. The one condition for slope instability to occur is a decrease in shear strength which can be occur due to moisture content also weathering. The study area is covered by highly weathered and loose material and the slope of this formation will have low shear strength, so it cannot resist any external and internal forces as it fails easily. The ground acceleration of the study area is 0.05, which shows that the study area is closed to the or near to seismically active area.

1.4 OBJECTIVES

1.4.1 General objective

The main objective of this study is to carry out the slope stability analysis around Tercha-Chida Road, Dawro Zone, Southern Ethiopia.

1.4.2 Specific Objective

1. To assess and determine geological and geotechnical properties of soils and rocks
2. To determine the factor of safety and identify potential failure surface
3. To propose remedial measures for the identified problems.

1.5 Significance of the Study

The finding of this study will be used as input data for the design of countermeasures against slope instability problems along roads in the study area. This will enable the designers, administration, and planners to make a decision on the safety of local people, and reduce the damage to road infrastructures in the study area due to slope instability. Moreover, the findings of this study will be also used as a reference for other roads that are intended to be constructed in similar or related topographic and geological set up.

1.6 Limitation of the Study

The scope of the study was to determine the factor of safety of the non- structurally controlled and structurally controlled slope failures present in the study area. For non-structurally controlled slope a numerical method like; Limit equilibrium and finite element method were used. For structurally controlled slope faces, the kinematic analysis was used. A geotechnical test has been implemented for identification and classification of geologic materials. This study is limited to the use of empirical methods due lack of data rock discontinuity data.

CHAPTER TWO

LITERATURE REVIEW

2.1 INTRODUCTION

Slope instability is one of the foremost imperative and sensitive issues in civil engineering, particularly in huge project ventures such as dams, highways, and, tunnels, (Pourhosravani, 2011). The stability of natural and man-made slopes such as roads and railway embankments, road cuts, etc. are causing a genuine issue for geotechnical engineers. These vulnerable slopes are making the problem worst and hence, it should be analyzed and designed very carefully.

According to Sazzad, (2017), Slope stability analysis is one of the foremost imperative intrigues in the geotechnical engineering. In construction areas, the slope may fail due to overwhelming precipitation, increment in groundwater table and change in stress condition. So also, natural slopes that have been steady for numerous a long time may abruptly come up short due to alterations in topography, external forces, loss of shear strength, and, weathering (Abramson, 2002). In this manner, it may be a common challenge for both analysts and experts to analyze the stability of a slope and assess the certainty of a factor of safety.

Gentle slopes are usually stable. As the slope's inclination angle increases, the risk of failure increases accordingly. This can be attributed to the instability of the soil mass when the geometry results in the soil strength being unable to provide adequate support and its natural tendency to achieve stability and equilibrium. Failures in slopes usually occur in the form of soil movement, where the unstable mass topples or slides downwards or sideways to achieve stability (Yang., 2021).

2.2 Factors Affecting Slope Stability

It is important to understand the causes of instability in slopes for purposes of designing and constructing new slopes and repairing failed slopes. For stability of a slope, the shear strength of the soil must be greater than the shear stress for equilibrium. The instability condition can be reached through two mechanisms (Duncan, 2005).

• A decrease in the shear strength: The loss of the shear strength may occur due to an increase in moisture content, pore water pressure, shock or cyclic loads, weathering, etc.

• An increase in the shear stress: The stresses may increase due to the weight of water causing saturation of soils, surcharge loads, seepage pressure, etc.

Understanding whether there is loading or unloading is the first step in approaching a slope stability problem. Embankment and reclamation operations where the slope is raised from an existing grade and load is added to the soil. These are common sources of loading issues. When the earth is dug from an existing ground, the load on the soil is reduced, causing unloading problems, Nelson (2013), mentioned the factor affecting slope instability by classifying the factors into five components.

2.2.1 Gravity

Gravity is the primary force that causes a mass to move. Gravity is a force that operates on everything on the earth's surface. By drawing everything in the direction of the earth's center. The force of gravity acts downward on a flat surface. The substance will not move under the force of gravity as long as it remains on a flat surface (Nelson, 2013).

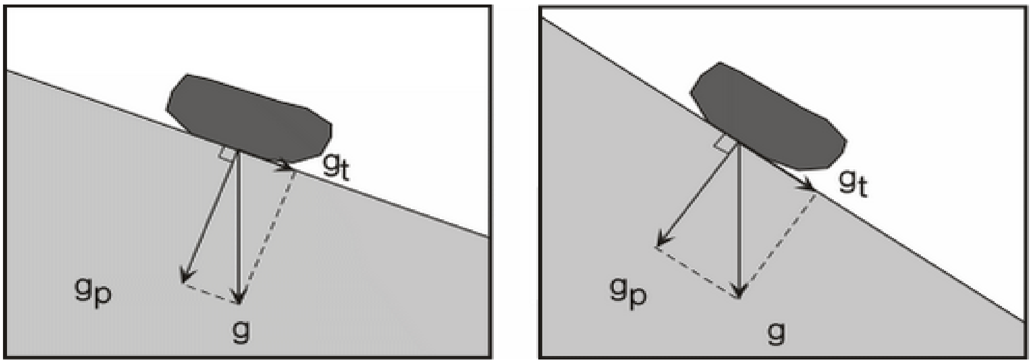

Figure 2. 1 Force of gravity acting on the slope (Nelson, 2013)

Slightly steeper slope angles, which increase shear stress, and anything that reduces shear strength, such as lowering particle cohesiveness or frictional resistance, promote down-slope movement. The safety factor, FS, is the ratio of shear strength to shear stress that is frequently used.

$$Fs = \text{Shear Strength/Shear Stress}$$

The force holding the material on the slopes which could include friction and cohesive forces that hold the rock or soil together, is referred to as shear strength. Slope failure is likely if the safety factor falls below 1.0. Gravity would tend to flatten out slopes if it was not for the cohesion and friction forces of rocks and soils. However, the stability conditions may change due to temporary adjustments of equilibrium or because of external perturbations. In this case, a landslide may be triggered Gholipoor (2015).

2.2.2 Role of Water

Although water is not always directly involved as the transporting medium in mass movement processes, it does play an important role (Nelson, 2013).

Water becomes important for several reasons

1. The addition of water from rainfall or snowmelt adds weight to the slope.
2. Water can change the angle of repose (the slope angle which is the stable angle for the slope).

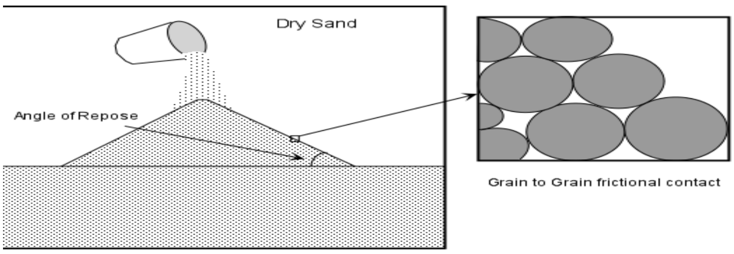

Figure 2.2 The effect of water on the angle of response (Nelson, 2013)

3. Water can be adsorbed or absorbed by minerals in the soil. Adsorption, causes the electronically polar water molecule to attach itself to the surface of the minerals. If adsorption occurs then the surface frictional contact between mineral grains could be lost resulting in a loss of cohesion, thus reducing the strength of the soil.
4. Water can dissolve the mineral cement that holds grains together.
5. Liquefaction -, liquefaction occurs when loose sediment becomes oversaturated with water and individual grains lose grain to grain contact with one another as the water gets between them.
6. Groundwater exists nearly everywhere beneath the surface of the earth. It is water that fills the pore spaces between grains in rock or soil or fills fractures in the rock. The water table tends to rise during wet seasons when more water infiltrates into the system and falls during dry seasons when less water infiltrates.
7. Fluid pressure is another feature of water that influences slope stability. The grains of soil and rock can rearrange themselves to form a more compact structure as they are buried deeper in the earth but pore water is restricted to occupy the same space. This can raise the fluid pressure to the point where the water can support the weight of the rock pile above it.

When this happens, friction decreases and the shear strength of the material holding it on the slope decreases resulting in slope failure.

2.2.3 Troublesome Earth Materials

- ✓ Expansive and Hydro compacting Soils - These are soils that contain a high proportion of a type of clay mineral called smectites or montmorillonites. Such clay minerals expand when they become wet as water enters the crystal structure and increases the volume of the mineral.
- ✓ Sensitive Soils - In some soils, the clay minerals are arranged randomly, with much pore space between the individual grains. Often the grains are held in this position by salts (such as gypsum, calcite, or halite) precipitated in the pore space that "glue" the particles together. Compaction of the soil or shaking of the soil can thus cause a rapid change in the structure of the material.
- ✓ Some clays, called thixotropic clays (which the apparent viscosity is temporarily reduced by previous deformation), when left undisturbed can strengthen, but when disturbed they lose their shear strength. Thus, small earthquakes or vibrations caused by humans or the wind can suddenly cause a loss of strength in such materials.

According to Gholipoor (2015), a recent volcaniclastic material may become very unstable and collapse into debris flows and lahars following intense precipitation. In contrast, hard and compact rock like intact gneiss is normally very stable.

2.2.4 Weak Materials and Structures

- ➢ Bedding Planes - These are planar layers of rocks upon which original deposition occurred. Since they are planar and since they may have a dip down-slope, they can form surfaces upon which sliding occurs, particularly if water can enter along the bedding plane to reduce cohesion.
- ➢ Weak Layers - Some rocks are stronger than others. In particular, clay minerals generally tend to have a low shear strength. If a weak rock or soil occurs between stronger rocks or soils, the weak layer will be the most likely place for failure to occur.

2.2.5 Triggering Factors

A mass movement event can occur any time a slope becomes unstable. Sometimes, as in the case of creep or solifluction, the slope is unstable all the time and the process are continuous.

- Shocks – an unexpected shock, such as an earthquake, can cause a slope to become unstable. Minor shocks, like huge trucks crashing down the road, trees falling in the wind, or human-caused explosions, can also cause mass movement.
- Slope Modification – changing the slope angle, whether by people or natural forces, can result in the slope no longer being at the angle of repose the slope can then be restored to its resting angle by mass movement events.
- Undercutting – a slope can be undercut by streams eroding their banks or by surf activity along the shore, rendering it unstable.
- Changes in Hydrologic Characteristics – heavy rains can saturate regolith, reducing grain to grain contact and lowering the angle of repose, resulting in a mass movement event. Heavy rain can also soak rock, making it heavier. Changes in the groundwater system can cause fluid pressure in rock to rise or fail, as well as mass movement events.
- Volcanic Eruptions – explosions and earthquakes are caused by volcanic eruptions. They can also cause snow to melt or crater lakes to empty, releasing significant amounts of water that can mix with regolith and generate debris flows, mudflows, and landslides by reducing grain to grain contact.
- Changes in Slope Strength – anything that changes the slope intensity abruptly or gradually can operate as a triggering mechanism.

2.3 Slope Failure Mechanism

In geotechnical terms, an earth or soil slope is a surface of soil mass that is inclined. Slopes can be natural or manmade. It is important to monitor earth slopes such as their balance, shear strength and, ability to withstand movement and to ensure that slope failure does not occur. There are mainly four types of failures which are described as follows, (Stead, 2015).

1. **Plane failure**

A planar failure of rock slope occurs when a mass of rock in a slope slide down along a relatively planar failure surface. The failure surface is usually structural discontinuities such as bedding planes, faults, joints or the interface between bedrock and an overlying layer of weathered rock. The favorable conditions for plane failure are as follows:

- The dip direction of the planar discontinuity must be within (±20˚) of the dip direction of the slope face.

- The dip of the planar discontinuity must be less than the dip of the slope face.
- The dip of the planar discontinuity must be greater than the angle of friction on the surface.

2. Wedge failure

Wedge failure can occur in a rock mass with two or more sets of discontinuities whose lines of intersection are approximately perpendicular to the strike of the slope and dip towards the plane of the slope.

- The trend of the line of intersection must approximate the dip direction of the slope face.
- The plunge of the line of intersection must be less than the dip of the slope face. The line of intersection under this condition should daylight on the slope.
- The plunge of the line of intersection must be greater than the angle of friction of the surface.

3. Toppling failure

Toppling failure occurs when columns of rock, formed by steeply dipping discontinuities in the rock rotate about an essentially fixed point at or near the base of the slope followed by slippage between the layers. Jointed rock mass closely spaced and steeply dipping discontinuity sets dip away from the slope surface are necessary prerequisites for toppling failure.

4. Rotational failure

The failure surface in a section of rotating slips can be a circular arc or non-circular curve. Circular slips are generally associated with homogeneous soil conditions, whereas non-circular slips are associated with non-homogeneous conditions. When the shape of the failure surface is altered by the presence of a neighboring stratum of significantly differing strength, translation and compound slides occur. Translational slips are most common where the next stratum is at a shallow depth below the surface and the neighboring stratum is planar and generally parallel to the slope. When the next stratum is at a larger depth, compound slips occur, with the failure surface comprising curved and planar parts. A rotating slide is the movement of material along a curved surface.

2.4 Shear Strength Failure Criteria of Rock

2.4.1 Mohr-Coulomb Strength Criteria

The Mohr-Coulomb criterion assumes that the maximum shear stress controls failure and this failure due to shear stress is dependent on the normal stress. This can be shown by graphing Mohr's circle in terms of maximum and minimum main stresses for states at failure. The best straight line that touches these Mohr's circles is the Mohr-Coulomb failure line. As a result, the Mohr-Coulomb criterion is expressed as, (Coulomb, 1972):

$$\tau = C + \sigma tan\emptyset \tag{2.1}$$

where τ is the shear stress, σ is the normal stress (negative in compression), c is the cohesion of the material and ϕ is the material angle of friction.

Effective stress controls the shear strength of soils, independent of whether the failure occurs under drained or undrained conditions. The Mohr-Coulomb strength envelope depicts the connection between shear strength and effective stress.

2.4.2 Hoek Brown Strength Criteria

Because representative specimens are too large for laboratory testing, estimating the mechanical behavior of closely jointed rock masses is one of the fundamental challenges in rock mechanics.

For design purposes, practitioners are frequently asked to anticipate the strength of large-scale rock masses. Fortunately, Hoek and Brown (1980) established an empirical failure criterion for intact and jointed rock masses based on the curve fitting of triaxial test data. The criterion is based on the Geological Strength Index classification system (GSI). One of the few non-linear criteria widely accepted and used by engineers to evaluate the strength of a rock mass is the Hoek–Brown criterion. (Li, 2008) Details of the implementation of the Hoek–Brown criterion into the numerical analysis formulations can be found in Merifield (2006). In this study, the latest version of Hoek–Brown failure criterion [(Hoek E C.-T. C., 2002) is employed.

$$\sigma_1' = \sigma_3' + \sigma_{ci}(m_b \frac{\sigma_3'}{\sigma_{ci}} + s)^a \tag{2.2}$$

where $\sigma 1'$ and $\sigma 3'$ are the maximum and minimum effective principal stresses at failure, mb is the value of the Hoek-Brown constant for the rock mass, s and a are constants which depend upon the rock mass characteristics, and σci is the uniaxial compressive strength of the intact rock pieces.

Where:

$$mb = mi \exp(\frac{GSI-100}{28-14D}) \quad (2.3)$$

$$S = \exp(\frac{GSI-100}{9-3D}) \quad (2.4)$$

$$\alpha = \frac{1}{2} + \frac{1}{6} \left(e^{\frac{-GSI}{15}} - e^{\frac{-20}{3}}\right) \quad (2.5)$$

The GSI was introduced because Bieniawski's rock mass rating (RMR) system (Bieniawski,1989) and the Q-system (Barton, 2002) were deemed to be unsuitable for poor rock masses. The GSI ranges from about 10, for extremely poor rock masses, to 100 for intact rock. The parameter D is a factor that depends on the degree of disturbance.

The uniaxial compressive strength is obtained by setting σ_3=0,

$$\sigma_c = \sigma_{ci} S^{\alpha} \quad (6)$$

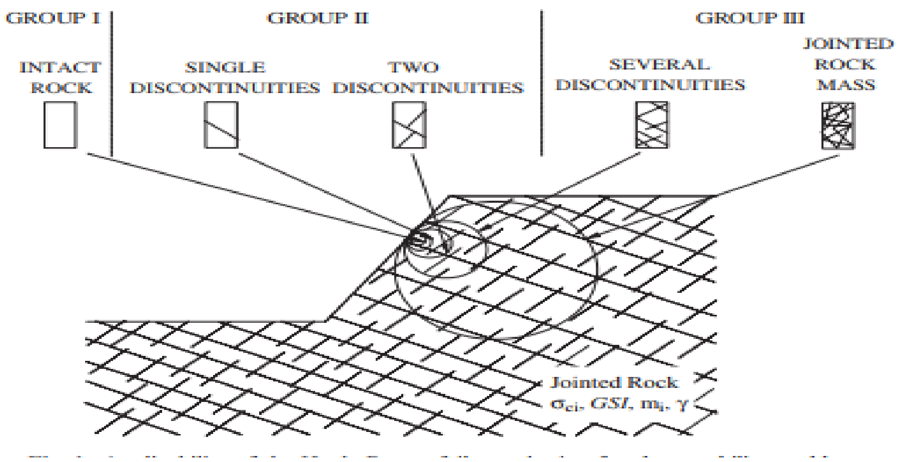

Figure 2.3 Applicability of the Hoek–Brown failure criterion for slope stability problems (Li, 2008).

2.5 Stability Analysis Method

Engineers can use a variety of analytical techniques to determine if a particular natural or constructed slope is stable. The 'limit equilibrium approach,' in which a single value of factor of safety is derived to estimate the stability of a slope, is the classic method for slope stability analysis. Following that, some academics created finite element methods as a useful tool for studying slope stability issues (Kaur, 2016).

2.5.1 Limit Equilibrium Method

For slope stability analysis, limit equilibrium approaches have been utilized for decades, and several methodologies have been developed. The size of the factor of safety is determined using limit equilibrium analysis in design. When a slope fails, however, the factor of safety is one, and the analysis can be used to estimate the average shearing resistance along the failure surface or a portion of the failure surface if the shearing resistance is assumed to be known along with the rest of the failure surface (Sangrey, 1978).

The most frequent way is based on limit equilibrium, in which it is considered that the soil is at the point of failure. In this method, the theory of elasticity or plasticity is also being progressively applied. The analysis of the limit equilibrium is statically uncertain. Because the stress-strain connection over the assumed surface is unknown, the system must be statically determined to be studied using the equation of equilibrium (Digvijay and Salunkhe, 2017).

2.5.1.1 Analytical Methods of Limit Equilibrium

2.5.1.1.1 Method of Slices

The most widely used limit equilibrium technique is using method of slices. The soil bulk is split into vertical slices in this method. There are several variations of the approach in use. Because of differing assumptions and inter-slice boundary constraints, these variations can produce different results (factor of safety).

A. Swedish slip circle method

The frictional angle of soil or rock is assumed to be zero in the Swedish slip circle approach. The frictional angle is assumed to be zero as a result of this assumption. As a result, the effective stress term is zero. As a result, shear strength is equal to the soil's cohesiveness parameter. This method examines stress and strength characteristics utilizing circular geometry and statics, assuming a circular failure interface. The moment produced by a slope's internal driving forces is compared to the moment produced by forces that resist slope failure. The slope is deemed to be stable if the resisting forces are larger than the driving forces. In saturated clays, undrained studies yielded a value of 0. Here, a circular surface is acceptable for somewhat thick zones of weaker materials, (Digvijay and Salunkhe, 2017).

B. Ordinary method of slices

Fellenius discovered the ordinary method of slices in 1927. The sliding mass above the failure surface is separated into multiple slices using the slices method, also known as the Fellenius method. The forces operating on each slice are calculated using the slices' mechanical (force and moment) equilibrium. There is only one equation for the moment of equilibrium in the total mass in this manner of a slice. Nonhomogeneous slopes and c –soils are good candidates for a circular surface. It's useful for doing calculations by hand. Effective stress analyses with large pore pressures, it is inaccurate.

C. Modified Bishop's method of analysis

This method differs slightly from the traditional method of slicing. The interslice shear force is zero because the normal contact forces between neighboring slices are considered to be collinear. It has been demonstrated that the procedure produces a factor of safety values that are within a few percent of the "right" values. This method achieves vertical force equilibrium for each slice as well as overall moment equilibrium around the trial surface's center. All failure surfaces must be circular for the bishop approach to be correctly applied.

D. Spencer's method

Spencer (1967) based his analysis on Fellenius's (1927) and Bishop's (1927) slices approach in 1955. Spencer's approach is reasonably accurate for slope stability analysis with general, arbitrarily formed failure surfaces. The sliding mass's moment and force equilibrium are both satisfied by this procedure. However, to acquire an accurate value of a factor of safety that satisfies the entire equilibrium, numerous iterations are required. It can be used on almost any slope. For computing the factor of safety, this is the simplest full equilibrium approach.

2.5.2 Finite Element Method

The contact between the bedrock and the debris overburden experiences the greatest shear strain toward the slope toe, according to the FEM stability study. This could be the zone with the least resistance, allowing the sliding surface to develop. To avoid the early formation of a sliding surface, excavation at the slope toe should be restricted. The results of the LEMs were compared to those of the finite-element model-based technique (FEM). According to previous studies, the FEM produces a lower global safety factor (FS) than the LEM and better assesses the slopes' stability condition (Pradhan, 2020) and (Bushira, 2018).

These methods have several advantages including the ability to model slopes with a high level of realism (complex geometry, loading sequences, presence of reinforcement material, water action, and laws for complex soil behavior) and the ability to better visualize the deformations of soils in place. Due to the higher number of variables available to the engineer, it is vital to interpret the analysis output.

2.5.2.1 The Shear Strength Reduction (SSR) Technique

The shear Strength Reduction method is a new technique in the finite element method to obtain the factor of safety of earth slopes. The finite element method was first applied to geotechnical engineering in 1966 (Rocscience, 2004). In the mid-1970s, slope stability analysis started by appearing in the literature. According to the SSR method, soil shear strength is reduced to bring a slope to the verge of failure (Duncan, 2005)). In the finite element method, such a state is detected by the inability to reach equilibrium. In the SSR technique, it is assumed that the slope materials have elastic-plastic behavior. The material strength is reduced until failure occurs.

In this technique, the Mohr-Coulomb material shear strength is reduced by a factor F, which is also called the "factor of safety". The definition is expressed as:

$$\tau = \frac{C}{F} + \frac{\sigma n tan\varphi}{F} \quad (2.6)$$

For Mohr-Coulomb materials, the steps for systematically searching for the critical factor of safety value, F, which brings a previously stable slope to the verge of failure, are given below (Rocscience, 2004):

Step 1: Develop an FE model of a slope, using the deformation and strength properties established for the slope materials. Compute and record the maximum total deformation in the slope by using the finite element method.

Step 2: Increase the value of F and calculate factored Mohr-Coulomb material parameters as described above. Enter the new strength properties into the slope model and re-compute deformation. Record the maximum total deformation.

Step 3: Repeat step 2, using systematic increments of F, until the FE model does not converge to a solution. In other words, continue to reduce material strength until the slope fails. The critical F value beyond which failure occurs will be the slope factor of safety, based on the finite element method.

For an initially unstable slope, the factor of safety values in steps 2 and 3 must be reduced until the finite element model converges to a solution (Rocscience, 2004).

2.5.3 Slope Classification System

Classification systems are empirical relations that relate rock mass properties either directly or via a rating system to an engineering application, e.g., slope, tunnel, (Hack, 2016).

2.5.3.1 Rock Mass Rating (RMR) (Bieniawski)

One of the oldest but still used systems is RMR (Bieniawski, 1989). Developed in South Africa for underground mining but currently widely used in civil engineering as well excavation and support are determined by the RMR value and result in five different support classes. Adjustment factors and refinements are possible. Based on a combination of five parameters Each parameter is expressed by a point rating.

Table 2.1 Rock mass parameters and range of values, (De Mulder et. al, 2012)

Parameter	**Range of values**				
Intact material strength UCS (MPa)	>250	100-250	50-100	25-50	5-25 1-5 <1
Rating:	15	12	7	4	2 1 0
Drill core quality-RQD (%)	90-100	75-90	50-75	25-50	<25
Rating:	20	17	13	8	3
Discontinuity spacing (cm)	>200	60-200	20-60	6-20	<6
Rating:	20	15	10	8	5
Condition of discontinuities	Very rough surface Not continuous No separation Unweather wall rock	slightly rough surface separation <1mm slightly weathered walls	slightly rough surface separation <1mm highly weathered walls	Slickensides surface or gouge <5mm thick, or separation 1-5mm continuous	Soft gouge >5mm thick or separation>5mm continuous
Rating:	30	25	20	10	0
Ground water – Inflow per 10m tunnel length (L/min)	None	<10	10-25	25-125	>125
Ground water – Ratio of joint water pressure over major principal stress	0	<0.1	0.1-0.2	0.2-0.5	>0.5
Ground water – General observation	Completely dry	Damp	Wet	Dripping	Flowing
Ground water – Rating:	15	10	7	4	0

The addition of the points results in the RMR rating, *RMR = (IRS + RQD + spacing + condition + groundwater)+ reduction factor*(*s*) *reduction factors for orientation, excavation damage, etc.)*

Table 2.2 Rock mass classes with rock mass rating, (De Mulder et. al, 2012).

	Rock mass classes				
RMR rating	100-81	80-61	60-41	40-21	<20
Class number	I	II	III	IV	V
Description	Very good rock	Good rock	Fair rock	Poor rock	Very poor rock
Average stands up time	20 years for 15m span	1 year for 10m span	1 week for 5m span	10 hours for 2-5m span	30 minutes for 1m span
Rock mass cohesion (KPa)	>400	300-400	200-300	100-200	<100
Rock mass angle of internal friction (degrees)	>45	35-45	25-35	15-25	<15

This method is simple but developed for tunneling in a high surrounding stress environment. Cohesion is generally considered too high for a low-stress environment (i.e., not suitable on slopes).

2.5.4 Kinematic Analysis

Kinematics is also called as ‘geometry of the motion’. It is the branch of classical mechanics that evaluates the motion of the point/ object/ body irrespective of its cause of motion (Shi, 1989). It is a purely geometric evaluation of slopes that determines the angular relationships among slope face and discontinuities in the rock mass. It identifies the potential for different modes of structurally controlled failures due to unfavorably oriented discontinuities. It is widely conducted on Schmid- type stereonet. It does not consider external forces such as water pressure or reinforcement which can have a significant effect on stability (Wyllie, 2004).

Only qualitative assessment of various structurally controlled failures like planar, toppling, and wedge mode can be made by this method. The angle of internal friction plotted as friction cone on stereonet, the orientation of pertaining discontinuities and slopes represented by great circles or as their poles are some keys and essential inputs for the kinematic evaluation of slopes. According to Rocscience, the Friction cone defines the limits of frictional stability on a stereonet while considering dip vectors. The angular relationship between structural discontinuities in rocks and the gradient along with the aspect of topography defines the probability for different modes of failure (Shi, 1989; Hoek, 1981; Wyllie, 2004).

Planar:

If the strike of discontinuity is nearly parallel (±20º) the trend of slope and dip of

discontinuity is gentler than that of the slope, then planar failure is likely to occur.
Toppling:

If the strike of discontinuity is nearly parallel (±20º) to the trend of the slope but discontinuity is dipping steeply in opposite to that of slope direction, it will give rise to a toppling failure mode.

Wedge:

Wedge failure is likely to occur when two discontinuities individually do not form any failure but they intersect in such a way that the line formed by their intersection daylight into a slope face i.e., the amount of plunge is smaller than the angle of slope provided the plunge of the the intersection should also exceed the friction angle. However, Goodman (1989) suggested that parallelism in direction may vary from ±20º to ±30º. The exact angle is not fixed, the vulnerability is most at zero degrees and decreases gradually as it approaches a higher degree

Circular failure

Under these conditions, one or more of the discontinuities normally define the slide surface. However, in the case of a closely fractured or highly weathered rock, a well-defined structural pattern no longer exists, and the slide surface is free to find the line of the least resistance through the slope. Observations of slope failures in these materials suggest that this sliding surface generally takes the form of a circle. The conditions under which circular failure will occur arise when the individual particles in a soil or rock mass are very small compared with the size of the slope. Hence, broken rock in a fill will tend to behave as a 'soil' and fail in a circular mode when the slope dimensions are substantially greater than the dimensions of the rock fragments. Similarly, soil consisting of sand, silt and smaller particle sizes will exhibit circular slide surfaces, even on slopes only a few meters in height. Highly altered and weathered rocks, as well as rock with closely spaced, randomly oriented discontinuities such as some rapidly cooled basalts, will also tend to fail in this manner. It is appropriate to design slopes in these materials on the assumption that a circular failure process will develop, (Goodman, 1989).

2.5.5 Factor of Safety

The factor of safety is that factor by which the shear strength parameters may be reduced to bring the slope into a state of limiting equilibrium along a given slip surface. According to this definition, the factor of safety relates to the strength parameters and not to the strength itself, which in the case of an effective stress analysis depends on the effective normal stress as well. Moreover, this definition implies that the factor of safety is uniform along the entire slip surface (Sangrey, 1978).

The factor of safety is commonly thought as the ratio of the maximum load or stress that a soil can sustain to the actual load or stress that is applied. The factor of safety (FOS), concerning strength, may be expressed as follows, (Guide, 2002):

$$F = \frac{\tau_{ff}}{\tau} \tag{2.7}$$

where τff is the maximum shear stress that the soil can sustain at the value of normal stress of σn, τ is the actual shear stress applied to the soil.

$$\tau = \frac{C}{F} + \frac{\sigma n tan\varphi}{F} \tag{2.8}$$

Two other factors of safety that are occasionally used are the factor of safety with cohesion, Fc, and the factor of safety with friction, Fφ. The factor of safety with cohesion may be defined as the ratio between the actual cohesion and the cohesion required for stability when the frictional component of strength is fully mobilized.

The most widely used definition of the factor of safety for a slope is the ratio of shear strength of the soil to shear stress required for equilibrium. Shear strength is often the largest uncertainty in slope stability analyses. A value of F=1.0 indicates that a slope is on the boundary between stability and instability. If all the factors are computed precisely, even a value of 1.01 would be acceptable. However, the computed values of FOS are not precise, due to the uncertainty of variables. Therefore, the factor of safety should be larger to be on the safe side (Duncan, 2005).

2.6 Other Related Research

1. Matthews and Farook (2014): published “Slope stability analysis using limits equilibrium or the finite element method”. They concluded that as computers and their application evolve in geotechnical analysis; it seems that we should be looking to more advanced ways to analyze slope stability. This study has shown that there are significant opportunities in using the more comprehensive finite element analysis. However, the traditional Limit Equilibrium method remains able to produce accurate and reliable results. Both have their advantages and disadvantages with the choice of

which method to use depending on some of the considerations described below, the method the user selects should be based on the complexity of the problem to be modeled.

2. Khaled Farah et.al, (2015) published “A Study of Probabilistic FEMs for a Slope Reliability Analysis Using the Stress Fields”. In this paper, they concluded the perturbation method and the spectral stochastic finite element method (SSFEM) using random field theory were presented. These methods are applied to analyze the stability of a homogeneous slope assuming an elastic soil behavior. To overcome the absence of the analytical solution of the mean and standard deviation of the factor of safety, the Monte Carlo simulation combined with the deterministic finite element code is applied. The perturbation method provides satisfactory results and it is easy to apply even with high random field expansion order.
3. Bacicn (2014) deals about “Slope stability analysis” in that paper they conclude a methodology of slope stability analysis and provide an insight into the basics of landslides and their general terms. The natural process of constant affected by the change in the relationship between shearing stress and resistance.
4. Burman (2015) deals about "A comparison of the classic limit equilibrium method versus the finite element method for slope stability analysis". They conclude that in the current study, limit equilibrium techniques (ordinary slice method, Bishop's method, Spencer's method, Morgenstern-Price method) and finite element methods were utilized to investigate various slope stability problems. Among all the limit equilibrium techniques studied in this study, the ordinary slice method provides the most conservative estimation of a factor of safety value. As a result, any slope design done with a traditional slice method is likely to be on the safe side at all times. Other limit equilibrium approaches, such as Ordinary Bishop's Method, Spencer's Method, and Morgenstern and Price's Method, aim to arrive at a more accurate estimate of interstice forces.
5. Reginald Hammah et.al, (1999): studied "A comparison of finite element slope stability analysis and traditional limit equilibrium analysis". Opinions that the FE SSR is difficult, as indicated by Griffiths and Lane, miss the fact that 'slip circle' analysis might generate deceptive results. As a result, we recommend geotechnical engineers use the SSR as another reliable and strong tool for slope design and analysis. It can assist in the detection of critical activity that might otherwise go missed.

CHAPTER THREE

MATERIALS AND METHODS

3.1 METHODS

3.1.1 General

Slope stability analysis involves a proper site investigation and determining the characteristics of geologic material. The critical surface is a surface that is prone to slide problems. The surface is selected based on the site that has a weak (loose) material and structure, slope, and the existence of water around the site. To accurately document and report soil and rock conditions, borehole data is collected to understand the subsurface condition of the study area, the geophysical data is collected. These data are collected from ECDSWC which have been done and done before the fieldwork.

3.1.2 Field surveying and sampling

In the field, 8 critical slope sections were selected for slope stability analysis. From the critical surface, 6 of them were rock slopes among which 2 rock slopes are structurally controlled slope failures but the rest of them are non-structurally controlled slopes failures. The other critical surfaces are soil slope which is residual soil. Different structures were also observed, these are minor faults, fractures, angular unconformity, and exfoliation. The fresh samples of rock have been taken for a detailed laboratory test that shows the critical condition and are labeled and disturbed soil samples of 25kg are taken from two pits and each pit that has a depth of 1-4m. The samples are used to determine the geotechnical properties most importantly the strength parameters and the unit weight of the materials. For structurally controlled slopes dip and strike of joints were measured and, in the field, able to observe the critical benching system and measured the bench width and the height of the slope. Benching system help to stabilize the road and the land sliding. Coordinates were taken for each lithology using GPS and a geologic structure’s dip and strike were also measured and observed using Bruno compass to prepare the geological map.

Figure 3.1 Sample collection A) soil sample collection from test pit-1, B) soil sample collection from test pit-2, c) rock sample

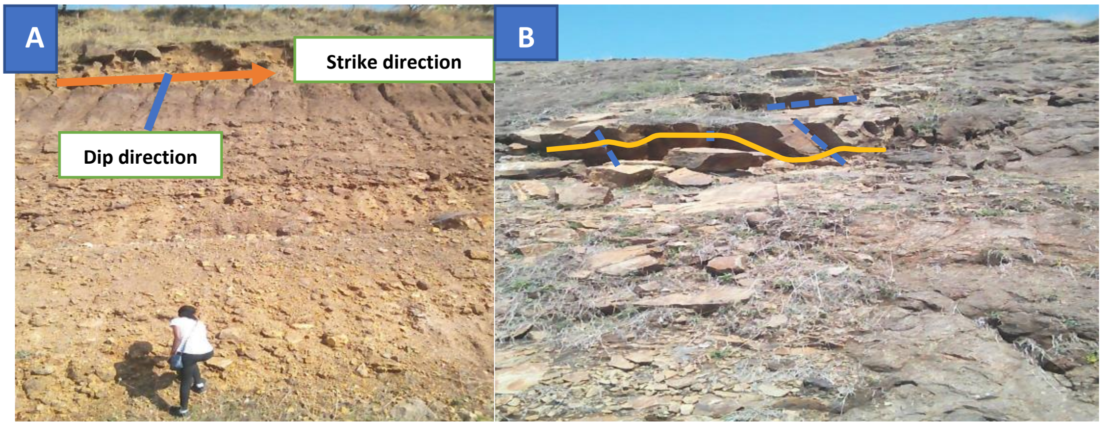

Figure 3.2 Joint orientation measurement A) strike and dip data collection B) joint sets of rhyolite slope

3.1.2.1 Visual estimation of the slope instability

The slope surface around the road section is mainly characterized by unwelded pyroclastic deposits, unconsolidated sediments, and weathered rocks. Most of the road sections have a benching system, some of these slopes show critical condition. A colluvial soil around the study area is more prone to sliding as compared to other sections. The slope does not have a high height, to create catastrophic problems on the road, but it can cause damage to the drainage system by filling it with the soil or other materials and to the road infrastructure. In some sections actually, the system has been covered by the soil due to sliding triggered by erosion. Most of the rock slopes face the road section, and around 8 critical sections have been selected for this research. Figure 3.7 shows a critical sections of soil slope and rock slope.

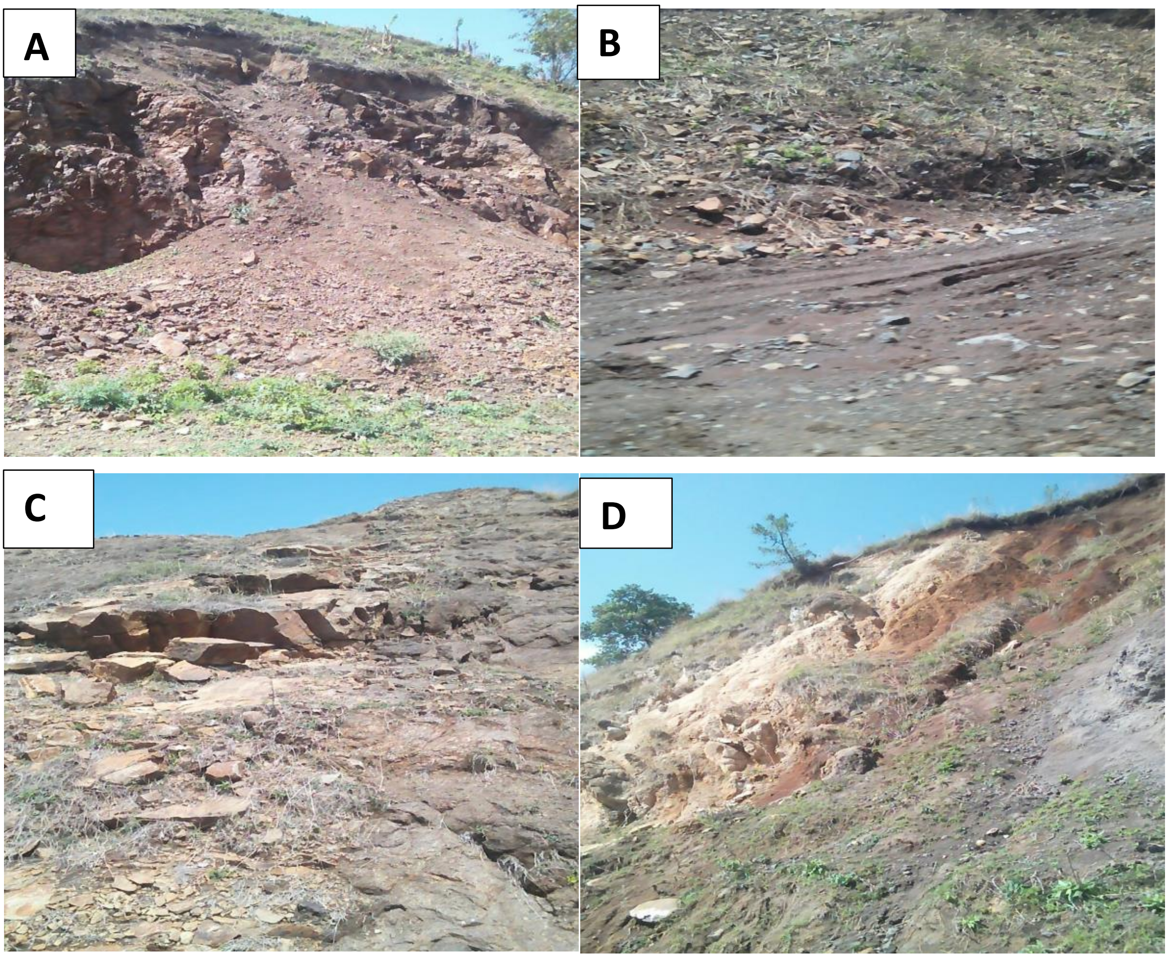

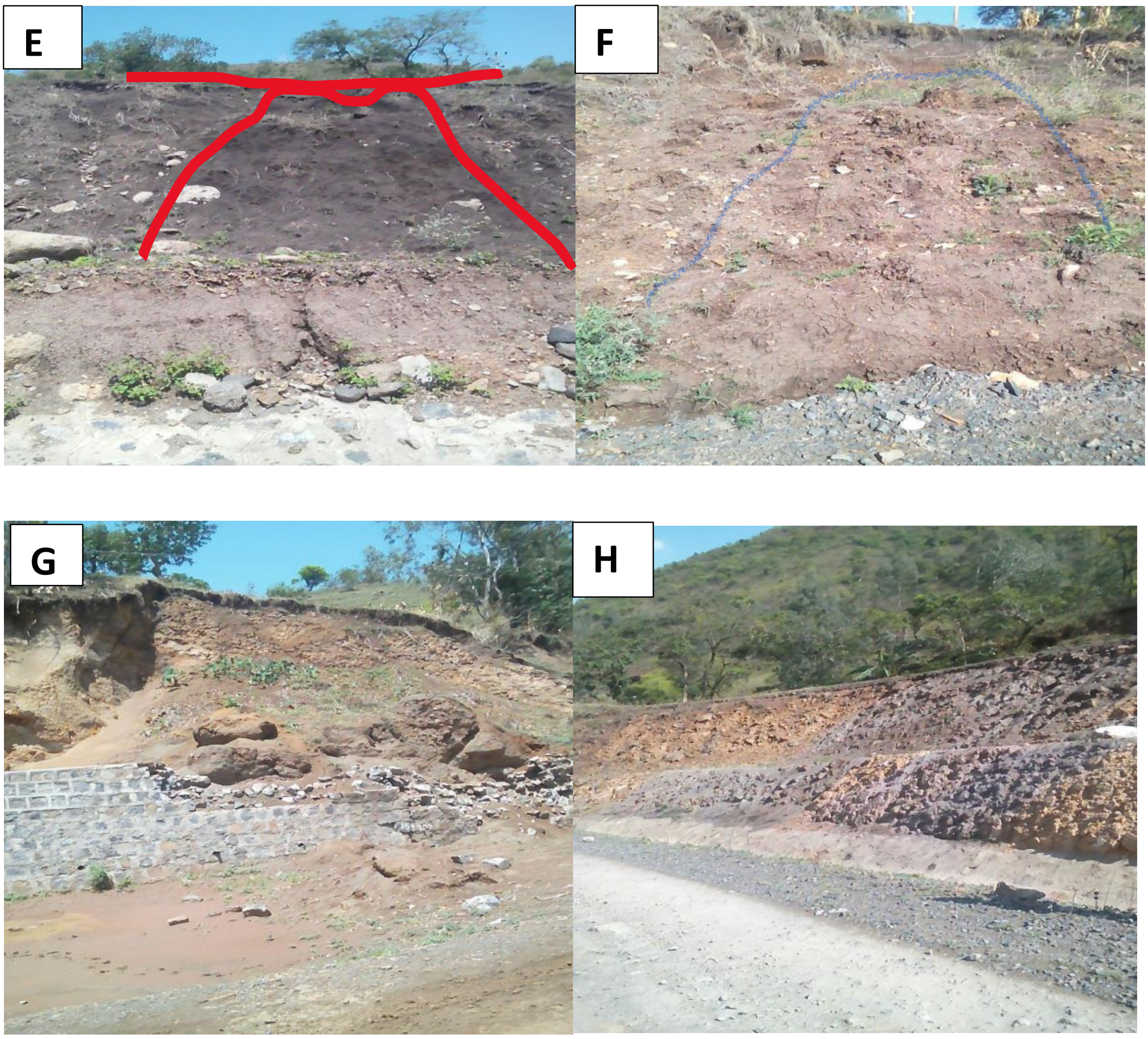

Figure 3.3 Critical sections of soil and rock slopes, A) a homogeneous basaltic slope, B) a basalt slope with a soil base, C) structurally controlled rhyolite slope, D) non-homogeneous rhyolite, soil, and pyroclastic deposit tilted parallel to each other, E) soil-2 slope F) soil-1 slope G) highly weathered basalt rock, H) angular unconformity between tuff and ignimbrite

3.1.3 Laboratory analysis

Slope stability analysis involves determining the strength parameters of materials which is done in the laboratory. For soils and rocks, different laboratory tests have been taken. Soil laboratory test involves particle size distribution, hydrometer, water content determination, and specific gravity, these tests were conducted for test pit - 1, and the rest tests that are done for both soils were compaction and direct shear test. The tests that were performed for rock are point load, dry and saturated density, intact Schmidt hammer, and slake durability test.

Table 3.1 Analytical method adopted for soil

Parameters	Method	Standard
Index property	Sieve analysis	ASTM D422
	Atterberg limit	ASTM4318
	Hydrometer	ASTM D 7928H
Unit weight	Compaction	AASHTO T-99
Strength parameters (cohesion, friction angle	Direct shear method	ASTM D 3080
Specific gravity	Specific gravity test	ASTMD8541919
Moisture content	Natural Water content determination	ASTMD2216

3.2 Physical property determination

This method is used to identify and classify soils and rocks based on their engineering properties. For index property determination a sieve and a hydrometer analysis have been conducted.

3.2.1 Index property determination

- ✓ **Sieve analysis**

This method is conducted for soil samples that have a particle size greater than 0.075mm. The method is done by shaking the soil sample that is in the sieve that has a different opening that decreases from top to bottom. In this analysis around a 3kg, soil sample was air-dried due to the moistness behavior of the soil. Air-dried sample was taken to the sample and the sieve method was conducted using the ASTM D 422 standard. Before and after shaking, all samples that are on each sieve were measured and recorded.

- ✓ **Hydrometer**

This test is conducted for soil samples that have a particle size less than 0.075mm. This test is used to determine the percent silt size and clay size fraction of soil. For this test, a 50g soil sample that pass a 0.075mm sieve was taken. A chemical that was used to disperse a soil was sodium hexa meta phosphate with 5g weight. This test is conducted by the ASTM D 7928 standard.

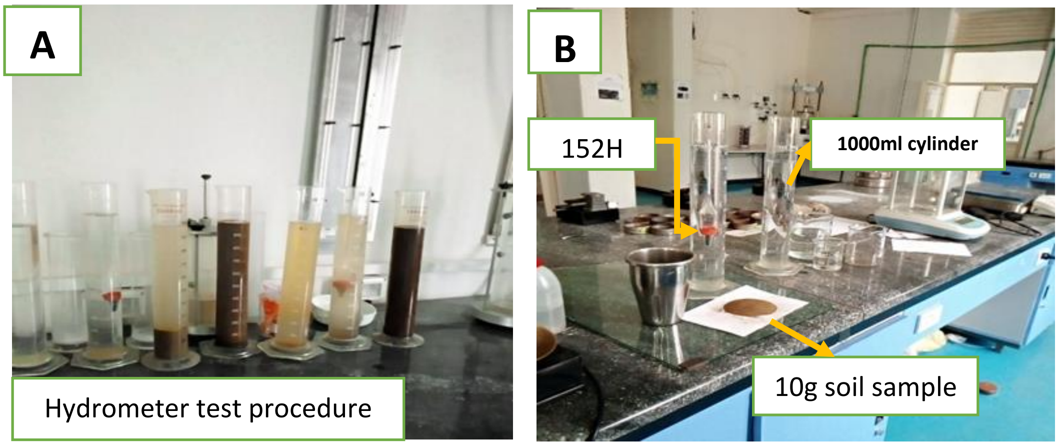

Figure 3.4 Hydrometer analysis, A) dispersed soil in 1000ml cylinder, B) materials used for the hydrometer analysis of a soil sample, 1000ml cylinder, and hydrometer 152H

- ✓ **Atterberg limit**
  - ➢ **Liquid limit**

The test is done to determine the liquid limit of soil as per ASTM 4318 standard by passing a 0.425mm sieve sample. The soil was mixed with water to evaporate dish. The wet soil was placed on a liquid limit device (Casagrande), and the grooving tool cut through the sample along the symmetrical axis of the top. The 13mm sample that is closed to the grove was collected after the number of blows. The collected samples were placed in the can and put into the oven for moisture content determination.

- ➢ **Plastic limit**

The test is used to determine the plastic limit of a soil sample. The test involves using a sample passing a 0.425mm sieve as per ASTM 4318 standard. The soil is mixed with water on a glass plate and rolled until it reaches 3mm thread with hand’s palm. The thread soil was placed in the can and put in the oven for 24 hours for water content determination.

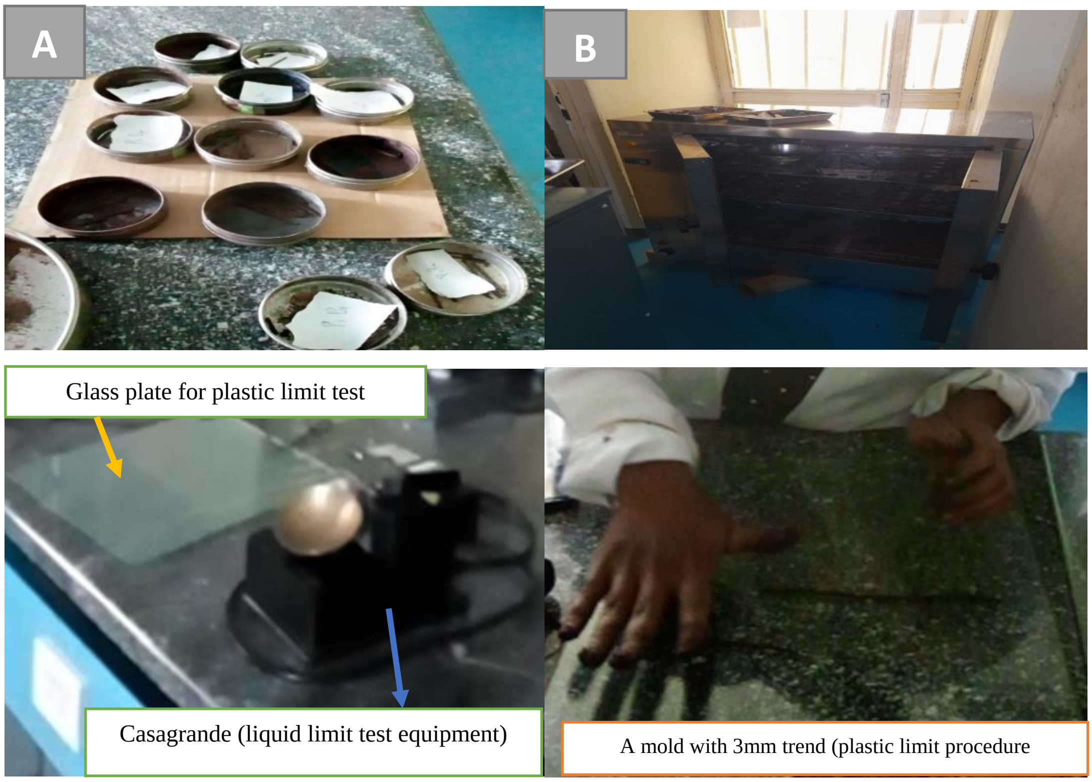

Figure 3.5 Methodology for Atterberg test, A) samples for LL and PL test, B) oven for water content determination

3.2.2 Density bottle method (Specific gravity)

The test is aimed to determine the specific gravity of soil. For the test, the empty density bottle is weighted and 10gm of oven-dried soil is added to it. The water is added to the soil on the density bottle and stirred and weighted. The clean water in the density bottle was weighed after the stirred sample is removed. The standard used for this test was ASTM D 8541919.

3.2.3 Natural moisture content determination

The test is performed to determine the moisture content of the soil. The standard reference that was used for this study was ASTM D 2216. The moist soil is weighed and placed in the weighted empty moisture can. The sample in the moisture can is left in the oven. This test is essential for determining soil properties.

3.2.4 Slake durability test

The aim of the slake durability test is to provide an index that is related to the resistance of rock against degradation when subject to two standard cycles of wetting and drying. For this test 10 rock fragments, each fragment weighing 40 – 60g with a total mass between 450-

550g were taken. This process has been repeated for the second cycle. The test was based on ASTM D 4644-87 standard procedure.

Figure 3.6 slake durability test, A) slake durability apparatus B) 10 rock samples for the slake durability test

3.3 Mechanical Properties determination

3.3.1 Compaction test

This laboratory test is performed to determine the relationship between the moisture content and the dry density of soil. A 2.5kg soil that passed 4.75mm was used depending on the standard proctor test procedure. The sample was mixed with 50ml water, put in the mold with 3 equal layers that are subjected to 25 drops of a hammer and weighted. The standard reference that was used for this study was AASHTO T-99.

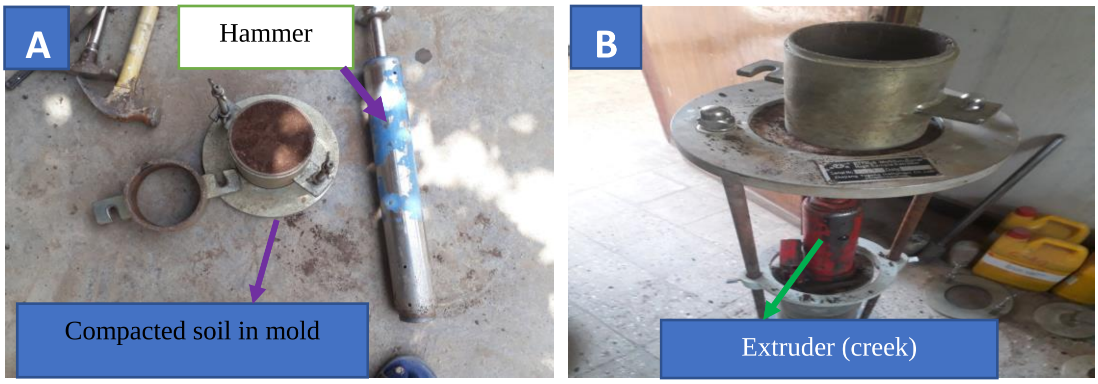

Figure 3.7 Compaction test equipment A) hammer, mold and soil sample, B) extruder to extrude the sample from the mold

3.3.2 Direct shear test

The compacted soil was placed on the shear box and weighted. The box was placed on the direct shear device. The gauges, the horizontal displacement gauge, and the shear load gauge were adjusted to zero, then the motor is started. The horizontal displacement and the shear load reading were taken until the shear load reaches the peaks and falls. The test used the standard reference of ASTM D 3080 and conducted for 3 different shear loads, these are 100kpa, 200kpa, and 300kpa.

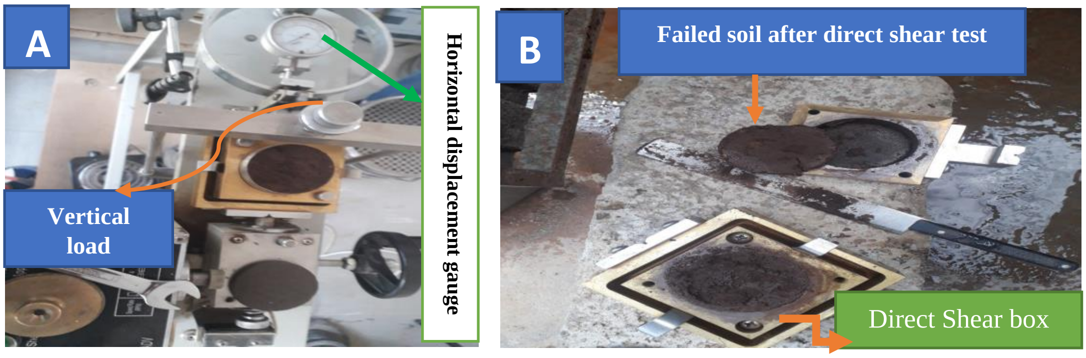

Figure 3.8 Direct shear test, A) Top view of direct shear device, B) shear box, and failed soil sample

Table 3.2 Analytical method adopted for rock sample

Parameter	Methods	Standard
Strength	Point load test	ASTM D 2938
Density	Dry density determination	ISRM 1978
	Saturated density test	ISRM 1978
Durability	Slake durability test	ASTM D 4644

3.3.3 Strength test

3.4.3.1 Point load test

Point Load (PL) is a test that aims at characterizing rock materials in terms of strength. The rock sample with the ratio of its diameter to average width is greater than 0.3mm and half of the diameter is less than the length of the rock sample is placed in the point load tester model PIL-7. The steady load was added until failure occur and recorded the pressure. The standard reference used for this study was ASTM D 2938.

Figure 3.9 Point load test PIL7 apparatus and samples after failure

3.3.4 Dry density determination

This test is used to determine the dry density of the rock. The samples were weighed and placed in the oven for 24hours, then the dry sample was weighted and put in the measuring cylinder with water, the volume of water has been recorded before the sample is in it. The volume of water was recorded after the sample was put. The ratio between the mass of the dried rock sample and the volume change will give us the dry density of the rock sample.

3.3.5 Saturated density determination

The sample was placed for 1 day in the water. The wet sample was weighted and put in the cylinder. The volume difference after the sample was put in the cylinder was taken. The test also helps indirectly to find the saturated weight of the rock sample by multiplying the saturated density by gravity.

3.4 Data processing and analysis

The information that was collected during the site investigation and from the laboratory forms the basis for the slope stability analysis. This analysis allows the relative stability of a slope to be expressed numerically in terms of a factor of safety.

3.4.1 Shear strength parameters

The shear strength parameters of soil were determined from a laboratory direct shear test. The recorded horizontal displacement, the area of the shear box, the shear load, and the shear stress were the input parameters for the determination of cohesion and friction angle of soil in excel.

3.4.2 Rock mass property

Roc data software was used to determine the rock mass properties of a material that are going to be used as input parameters for the analysis and these are cohesion, friction angle and young’s modulus. It is used to understand rock and soil material properties by analyzing their strength characteristics and constitutive behavior to determine strength envelopes and other material parameters. It used an input of geological strength index and unified compression strength data.

Table 3.3 Input data for rock mass property determination in Rocdata software

Rock id	Rock type	UCS (Mpa)	GSI	Mi (for intact rock)
RS-1	Tuff	61.105	35±5	14.2
RS-2	Ignimbrite	90.36	55±5	15.46
RS-3	Pumice with Ash	21.975		22.7
RS-4	Rhyolite	83.482	40±5	26.07
RS-5	Basalt	140.985	25±5	35.24

3.5 Slope stability analysis

3.5.1 Limit equilibrium method

Limit Equilibrium (LE) methods use the Mohr-Coulomb failure criterion to determine the shear strength along the slip surface. Slide 6.009 was used for evaluating the safety factor or probability of failure, of circular or failure surfaces in soil and rock slopes. For the present study, four different approaches to the limit equilibrium method were used, these are Bishop, Janbu simplified, Spencer, and Morgesten for better results and to compare the factor of safety. The method needs cohesion, friction angle, unit weight of the rock or the soil and the slope geometry as an input parameter to compute the factor safety. The result is determined for each dry, wet condition and static and dynamic condition to identify the effect of this parameter on the slope section. Homogenous slopes and heterogenous slopes were the cases that were analyzed.

3.5.2 Finite element method

The safety factor was determined using the $\emptyset/c$ reduction approach where the strength parameters ($\tan\emptyset$) and (c) of the soil are successively reduced until failure of the structure occurs. Phase 2 was used to determine the safety factor of a simple homogeneous slope and non-homogeneous slope using the shear strength reduction (SSR) method. The method determined the factor of safety by clearly identifying cohesion, friction angle, unit weight, young's modulus, and the slope geometry of material as input data. Designing the slope geometry was the important task that was done before the input data after the strength reduction method was selected. The input parameters are added in the material property option. The input data were computed after the geometry was created and the computed data gives the strength reduction factor.

3.5.3 Kinematic analysis

Kinematic analysis is a method of determining the probable modes of failure and failure zones for unfavorable jointed rock slopes. The Burno compass was used to measure the dip and dip direction of the rock discontinuity orientation. From field visual estimation 2 slope sections show structurally controlled failure mode. This slope was in the western part of the study area and the slope is characterized as basalt rock and it shows a planar failure type. The other failure was found in the middle of the road section around Aba town which is covered by slightly weathered rhyolite showing a toppling failure. The structural orientation for each failure was collected joint dip and dip direction that were used as input data for dip software to determine the failure type and the critical section. For this analysis dip 6.008 was used. After the determination of the failure type and critical surface by the dip software the factor of safety was calculated using rocplane and swedge software for the planar and wedge failure respectively depending on the failure that gives a higher failure percentage.

Dips

DIPS is a program designed for the interactive analysis of orientation-based geological data. The software is a kinematic analysis software that is used to determine the failure type and critical surfaces. Dip 6.008 used the dip and dip direction of a joint. It is used to perform the kinematic analysis of rock slopes and used to be capable of analyzing the potential for the various structurally controlled modes of rock slope failures (plane, wedge and toppling).

3.6 Slope model

3.6.1 Slope geometry

For the present study, 8 different critical slope sections were selected each having different slope geometry and property. Four different slope gradients of 1.1H:1V, 1.5H:1V, 1.54H:1V and 2H:1V were modeled with a soil base.

Table 3.4 Indicative maximum cut slope angles (H: V) for rock slopes (without discontinuity control), *(authority, 2013)*

Type of material	Cut slope heights			Remark
	<10m	10-15m	15-20m	
Fractured and slightly to moderately weathered basalt	0.25:1	0.75:1	1.00:1	Remove hanging blocks before cutting, this minimizes the formation of overhanging
Fractured and weathered basalt in blocks, cobbles and gravels of all sizes in a matrix of silt or clay	1.00:1	1.25:1	1.50:1	
Weathered tuff, volcanic breccias or agglomerate	1.00-1	1.25:1	1.50:1	
Fractured, slightly weathered, thickly bedded limestone with intercalation	0.25:1	0.50:1	1.00:1	Apply controlled excavation: benches and drainage are needed at different heights
Slightly weathered and fractured mudstone and marl	1.00:1	1.25:1	1.50:1	Remove weathered and unconsolidated portion at low angles, drainage is important to keep the slope dry, reinforcement works and erosion controlling measures may be needed
Slightly weathered, poorly cemented sandstone, with poorly defined stratification	0.25:1	0.50:1	1.00:1	Controlled or trim blasting is recommended so as not to damage the rock behind the cut face
Weathered, highly friable shale and jointed mudstone	1.00:1	1.50:1	2.00:1	Shale has a characteristic of being deformed when wet. Hence, drainage systems are needed to keep the slope dry. Benches may also be required

3.6.2 Material property

The slope of the study area is classified as rock slope and soil slope each having different properties. For the soil slope, 2 slope sections were selected and 6 rock slopes were analyzed for stability analysis. The model was analyzed for homogeneous and heterogeneous materials depending on their presence in the slope section. Unit weight, cohesion and friction angle were the mechanical properties of soils and rock that were used for limit equilibrium analysis and finite element analysis which also used similar property as LEM except young's modulus and Poisson ratio.

3.6.3 Loading and groundwater condition

From the visual estimation in the field the slope did not have an external load. So, the analysis assumes that there is no external load on the slope except a body force. Since the study area was found in seismic zone 2 with a moderate gravitational acceleration coefficient of 0.05, the analysis was done for the dynamic and static conditions. Some of the slopes in the road section are found near a spring or pond but from the secondary borehole data, the groundwater is shown as dry. From the borehole data, the groundwater around Tercha was encountered at a depth of 4.70m. For this study, the wet conditions are analyzed with a water table depth of 4.70m from the surface.

3.7 Methodology flow chart

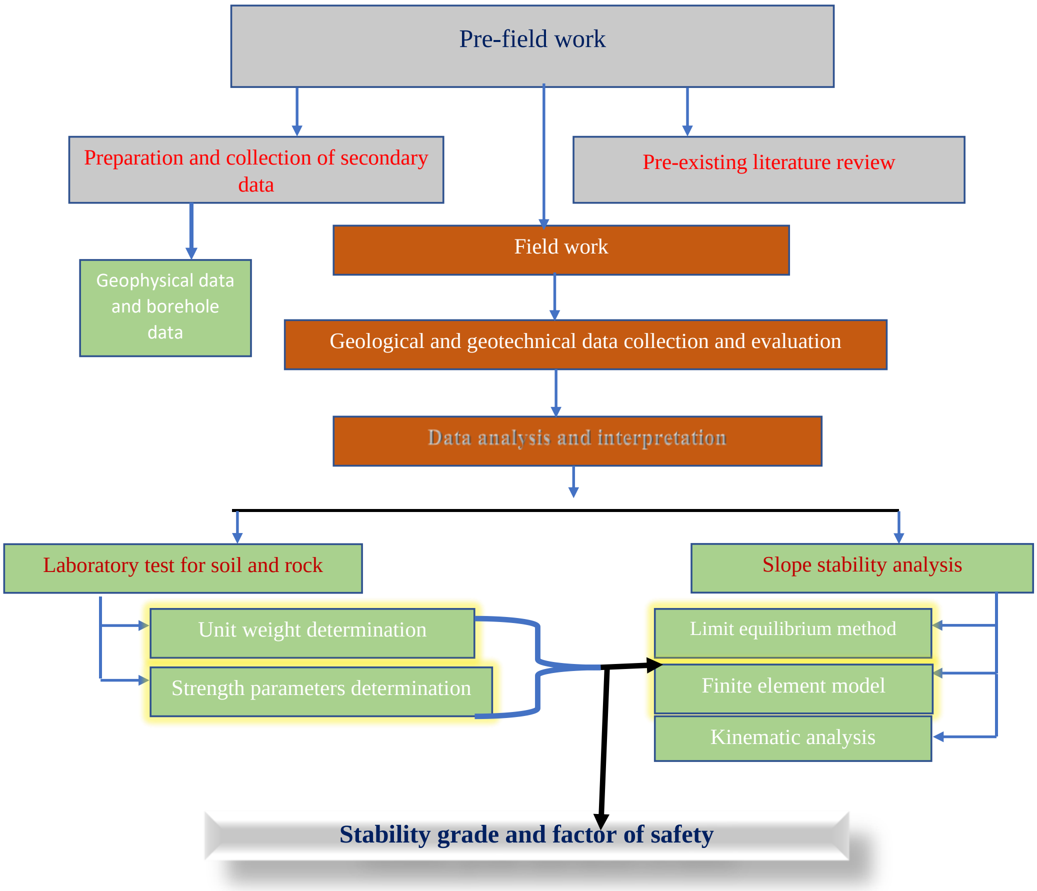

Figure 3.10 Methodology flow chart

CHAPTER FOUR

GEOLOGY

4.1 Regional Geology and Stratigraphy

4.1.1 Regional Geology and Structural Setting

Ethiopia can be divided into four major physiographic regions widely known as the western plateau, southeastern plateau, the Main Ethiopian Rift and Afar Depression. The Ethiopian plateau is underlain at depth by Precambrian rocks of the Afro-Arabian Shield. The Precambrian basement is covered for the most part by glacial and marine sediments of Permian to Paleogene period and Tertiary volcanic rocks with related sediments. The Cenozoic volcanic successions split apart by parts of the Great East African Rift System in Ethiopia (i.e., The Afar Depression, Main Ethiopian Rift and related rifts). The geological units in Ethiopia fall into one of the following three major categories; the Precambrian Basement, Late Paleozoic to Early Tertiary sediments and the Cenozoic volcanic and associated sedimentary rock, Haro et.al (1999).

According to Kazmin et al. (1980), initial sagging of the MER started about 15 Ma and was followed by major episodes of rifting at 10, 5, 4 and 1.8 to 1.6 Ma. Each stage of rifting and downfaulting was accompanied by a bimodal (felsic-mafic) volcanism in the rift and formation of basaltic and trachytic shield volcanoes on the rift shoulder and margins. The general consensus is that downfaulting of the Afar Depression started at a much earlier age and that rifting was accompanied by a voluminous flood basalt volcanicity. Some workers consider initial phases of stretching started as early as in the Early Miocene (Barberi et al., 1975) and the opening of the depression was preceded by alkaline granite intrusions along its margins and was followed by the deposition of detrital sediments shown on the map as the Danakil Group.

Following the initiation of subsidence of the Afar Depression and the MER; subsequent volcanism was restricted at first to the evolving rifts and then to the axial zones which later became a focus of Quaternary and recent volcanic activity. The East African Rift System in Ethiopia comprises the elements of the following major structural and physiographic features of the region.

1. The Gulf of Aden Rift which affects Ethiopia in that faults of this system form the southern boundary of the Afar Depression and determined the trend of regional lineaments such as the Addis Ababa - Ambo - Nekemte lineament on the northwestern plateau.
2. The Red Sea Rift; faulting of which forms the northern Eritrean coast and the Danakil Horst which separates the Red Sea and the Afar Depression and the western escarpment of the Afar Depression with faulting of the same trend extending as far south as the Marda Faults on the southeastern plateau.
3. The Afar Depression where the three important rift systems, i.e., the Main Ethiopian Rift, the Red Sea Rift and the Gulf of Aden Rifts intersect.
4. The Main Ethiopian Rift running NNE from Lake Chamo to about the latitude of Addis Ababa where the rift starts to funnel out into the Afar Depression.
5. The Lake Turkan~, Lake Chew Bahir Rifts and Heireba proto-rifts in southern Ethiopia which are not directly connected but progressively displaced to the east due north.

Regional uplifting around the study area occurred during Oligocene-Miocene that extends from Sidamo through Gamogofa, Keffa to Illubabor (Davidson, 1984). According to Beicip's structural study of southwestern Ethiopia in 1990, this pull-apart basin is bounded by ENE-WSW trending Didessa- Ambo- Addis ababa shear zone to the north and Omo- Amaro shear zone to the south. To the west, it is bounded by a hypothetical boundary that starts from the middle Omo trough NNE-SSW trending and bent northeastward in a WSW-ENE direction through the Gojeb area and to the east, it is bounded by the western border of the main Ethiopian rift.

According to Beicip’s structural study of southern-western Ethiopia in 1990, the NE-SW-trending pull-apart basin is bounded by:

- Two main trans-tensional (strike-slip) faults which are represented by left-lateral shear zones of the ENE-WSW trending Didessa-Ambo-Addis ababa shear zone to the north and Omo-Amaro shear zone to the south.

- Two main low angle detachment faults create major downthrow between the two shear zones: bounded to the west by a hypothetical boundary that starts from the middle Omo trough trending NNE-SSW and bent north-eastward in a WSW-ENE direction through Gojeb area and to the east, by the western border of the main Ethiopian rift.

The NNW-SSE trending faults that created graben and half-graben (Berhe, 1987) which were driven by the advancement of the Ashenghe fracture (Eocene-early Oligocene), are linked to the development of the Delbi-Moye to Gojeb-Chida graben (Berhe, 1987). The commencement of the major Ethiopian rift to the Chew Bahir rift and its continuation into the Gregory rift in Kenya as well as the Omo trough, a northern extension of the Turkana trough, happened during the Neogene (late Oligocene-early Miocene) period (Beicip, 1990)

Merla (1979) gave the trachyte basalt and rhyolites that cover most of southwestern Ethiopia the name Jima volcanic. The Jima volcanic includes a deep succession of basalt and felsic rocks, with basalt dominating the lower half of most sections, and are regarded as analogous that of Davidson (1984) the main series. The Jima volcano has age of 42.7 to 30.5 million years, (Davidson, 1984). There are two units (the lower Jima volcanic consists primarily of basalts while the higher Jima volcanic consists primarily of trachytes, rhyolites, ignimbrites and uncommon tuffs) that demonstrate a conformable relationship. The latter is comparable to Kazmin's Magdela Group (1972). The Precambrian basement is almost usually found beneath the Jima volcano. A remnant sandstone at the base of an unconformity marks it. In some areas, the base flows to form a continuous succession several hundred meters thick. Some silicic rocks are intercalated with flows near the base or form a thick succession just above the basal basalt in some regions.

The Nazareth series rocks are post-rift rocks that are younger. In this area, the Nazareth series forms rift shoulder deposits. The thick succession of welded ignimbrite, minor basalt and rhyolite flows is known as the Nazareth series. According to Tefera (1996) the isolated peaks of basalt represent center basaltic flows. Some basalts have been compared to the Tarmaber basalts which erupted in central Ethiopia. These are pre-rift flows that are younger. Mursi and Bofa basalts are post-rift volcanics that are younger. There are younger quaternary valley deposits (Q). They are interlayered with lacustrine deposits in some areas.

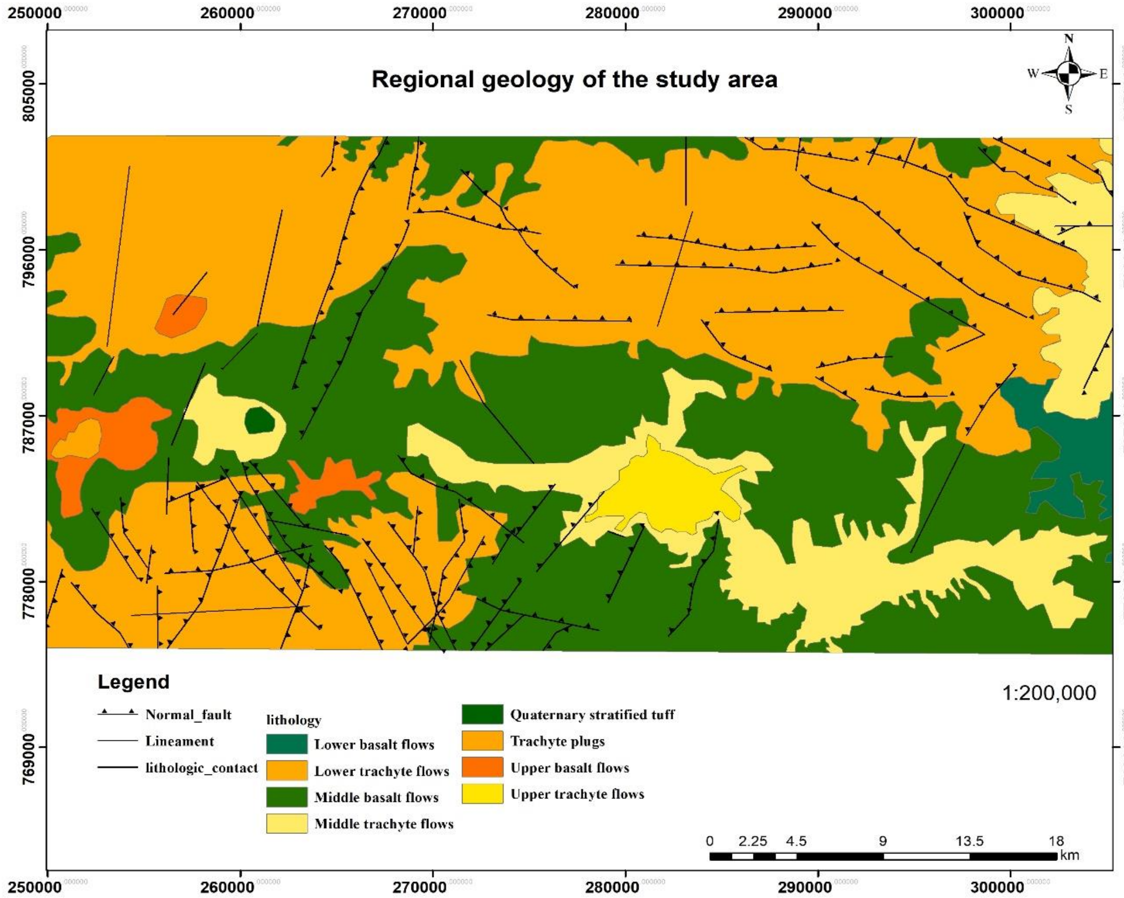

Figure 4.1 Regional geology of study area along Tercha_Chida road, (Haro et al., 2010)

4.1.2 Stratigraphy

According to Haro (2012), the Omo trachyte is the region's oldest rock. This is visible in the Omo valley's lower reaches. The lower lava flows are then overlain by lower trachyte flows. The lower pyroclastic is directly overlain by the basalt in the map. However, the lower trachyte is overlain by lower pyroclastic deposits in the caldera area east of Omo. The intermediate basalt flow follows the lower pyroclastic flows. Middle trachyte flows are overlain by middle volcano flows.

This is on the intermediate trachyte and covers the upper topography. The upper trachyte flows on the top of the upper basalt. Rhyolite flows, which occur east of Nada, come next. The Asendabo graben was filled with down-faulted rhyolite. Then there's the upper pyroclastic which is thought to be younger than the rhyolite in some areas. The Kobech phonolite is the next younger unit. This is also linked to central eruptions of the Sentema type. The trachyte plug is next, which is mostly visible in the map sheet's southcentral region. Sentema basalt is the most recent basalt flow from a central type eruption. After the creation of Asendabo graben to be core eruption effusion. With this eruption, the tertiary period comes to a close, (Haro, 2012).

4.2 Local geology

The study area consists of basalt, pyroclastic deposit, fluvial-lacustrine sediment and felsic volcanic rock that can be categorized into four lithologic units: basalt, sedimentary rocks, felsic rocks and pyroclastic deposits. The study area is outcropped by Oligocene to Miocene volcanic, which is mainly covered by Jima volcanics.

4.2.1 Jima Volcanics

This unit is exposed in the southwestern part of the study area, dominating the lower part of the section. It is composed of rhyolite and basaltic rock the name was adopted from Chernet (1996). The basalt is highly weathered even though some are changed to the soil. The color of the rock is black to brown. The rhyolite rock was observed in some sections, but it was not well exposed in the study area. It was slightly too highly weathered with a color of white to brown.

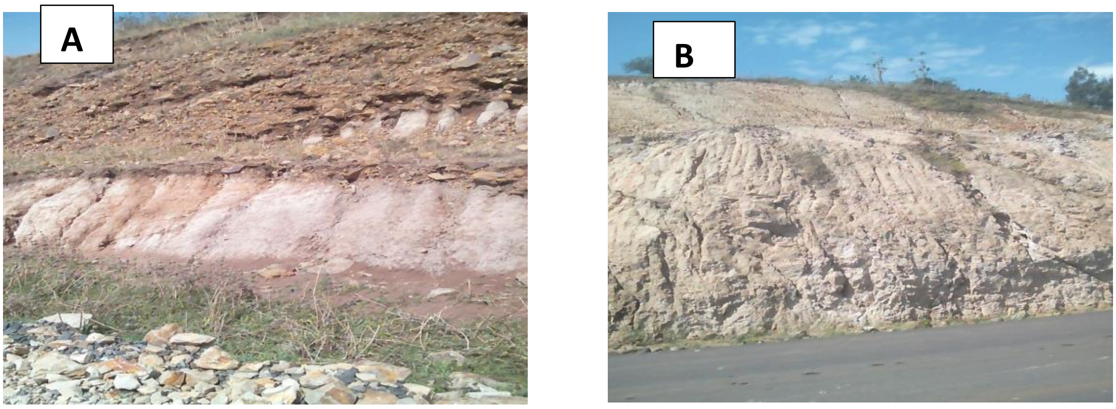

Figure 4.2 Jimma volcanic unit A) rhyolite rock with basalt rock at the top, B) rhyolite slope

4.2.2 Makonnen Basalt

This unit consists of the main basalt with paleosol at the bottom and the name was adopted from Davidson (1984). The Makonnen Basalts are physically separated and are readily distinguishable based on similar basal elevation, columnar form, the thickness of flows and the fact that they have a basal paleosol rather than a residual sandstone. The unit is exposed in the western part of the study area and it is moderately to highly weathered rock characterized by developed joint, fracture, and columnar joint.

Figure 4.3 Mekonnen basalt, a basalt rock with a paleosol at the base

4.2.3 Omo group

This unit consists of tuff, clayey silt and gravel and the name was adopted from Davidson, (1984). The Omo Group sediments (between 3 and 1.3 Ma) include at least 750 meters of brown gray- and buff-colored clays, silt, sand, gravel and tuff.

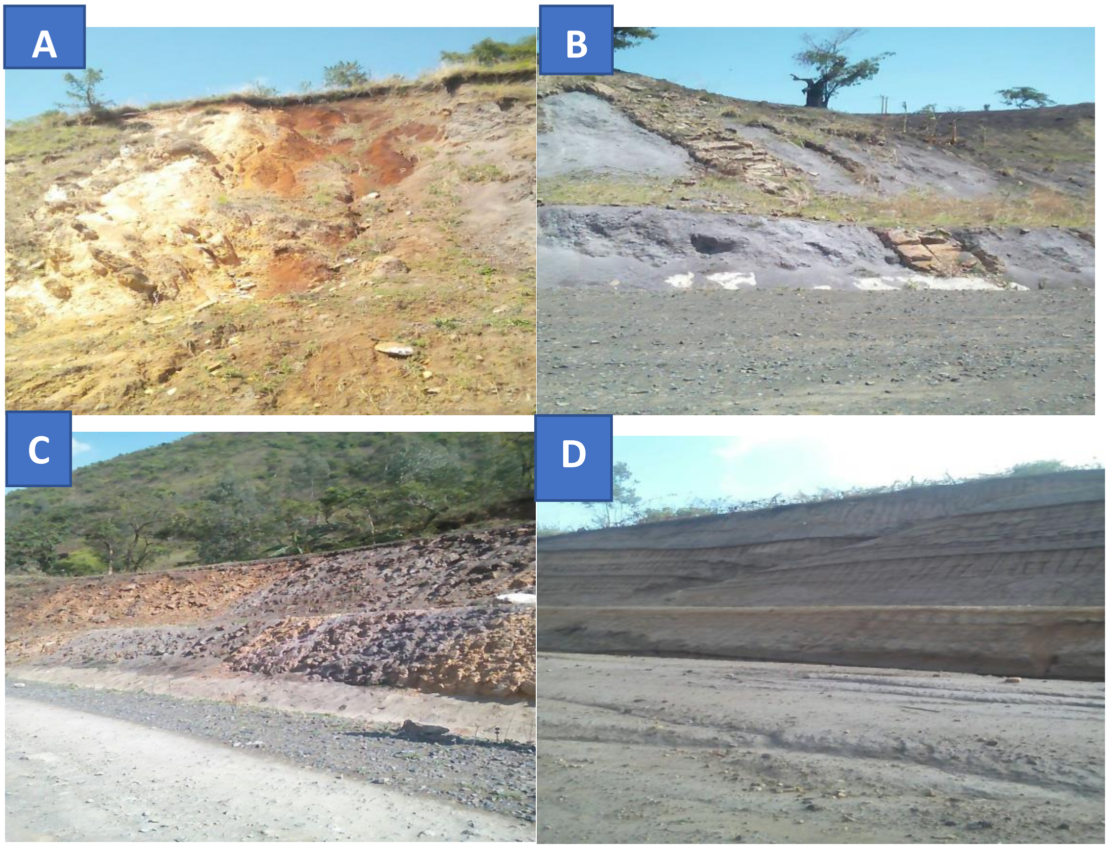

Figure 4.4 Omo unit A) rhyolite with soil and pyroclastic B) rhyolite with pyroclastic deposit C) tuff and ignimbrite deposit D) ash and tuff deposit

4.2.4 Unwelded pyroclastic deposit

The unit comprises unwelded tuff, ash, and pumice, and it covers most of the study area. In most of the sections, the rock in the unit are found intercalated with each other.

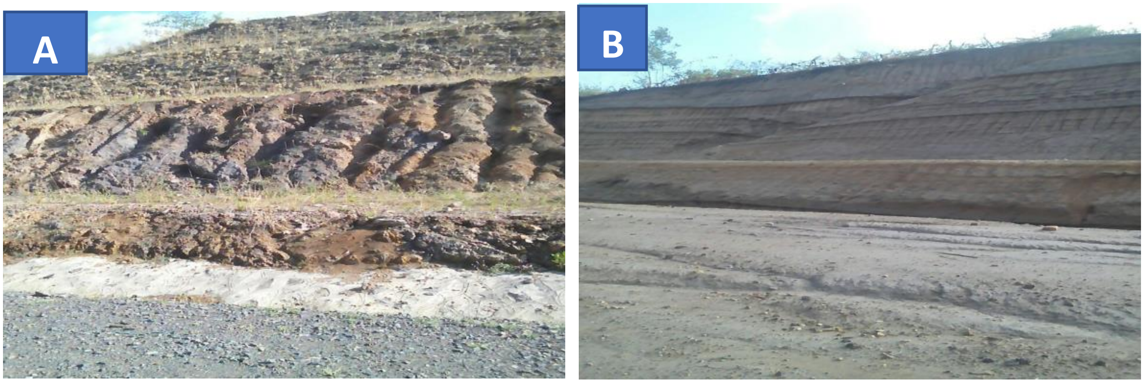

Figure4.5 unwelded tuff, ash and pumice deposit A) unwelded tuff with gravel and boulder deposit B) tuff deposit

4.*2.5* Unconsolidated unit

4.2.5.1 Colluvial soil

Colluvium is a loose deposit of sharp-edged rock debris accumulated through the action of gravity at the base of a cliff or Slope. Colluvium is sediment that has moved downhill to the bottom of the slope without the help of running water in streams. The deposit was found at the bottom of the slope which is composed of fragmented basalt and soil.

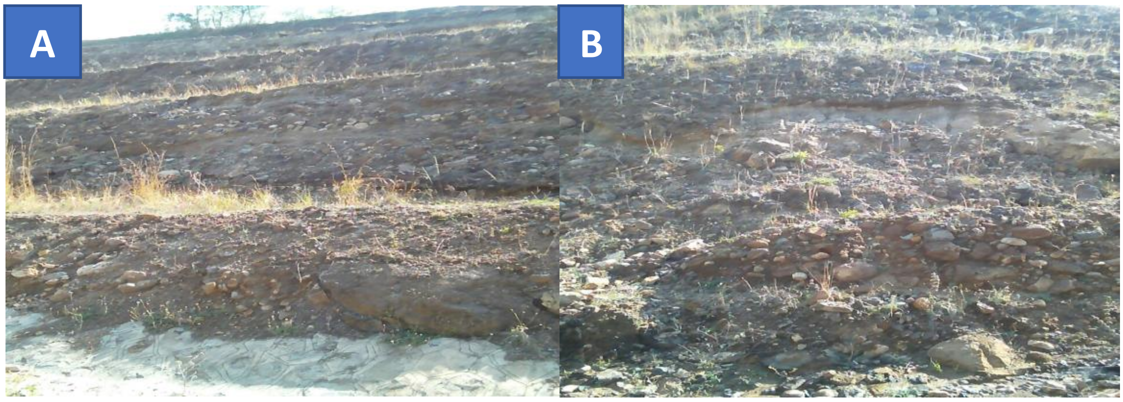

Figure 4.6 A colluvial soil in the study area A) gravel with boulder deposit B) gravel with tuff deposit

4.2.5.2 Residual soil

Residual soil is defined as a soil material that is derived from rock bedding and has not undergone transportation, usually found in tropical climates with relatively high temperatures and rainfall. The soil was found at the top of the soil and was characterized by black and red color, Encyclopedia science (2004).

Figure 4.7 Residual soil in the study area

4.3 Geological structures

The study area is the makeup of different geological structures, like, fractures, joints, and exfoliation. These geological structures are developed in different units with diverse orientations The main structural feature observed in the study area was NW.

4.3.1 Sill

In geology, a sill is a tabular sheet intrusion that has intruded between older layers of sedimentary rock, beds of volcanic lava or tuff, or even along the direction of foliation in metamorphic rock (Holmes, 1978). The term sill is synonymous with concordant intrusive sheet. The sill which was observed in the study area was an intrusion of rhyolite rock in tuff deposit as shown in figure 4.8.

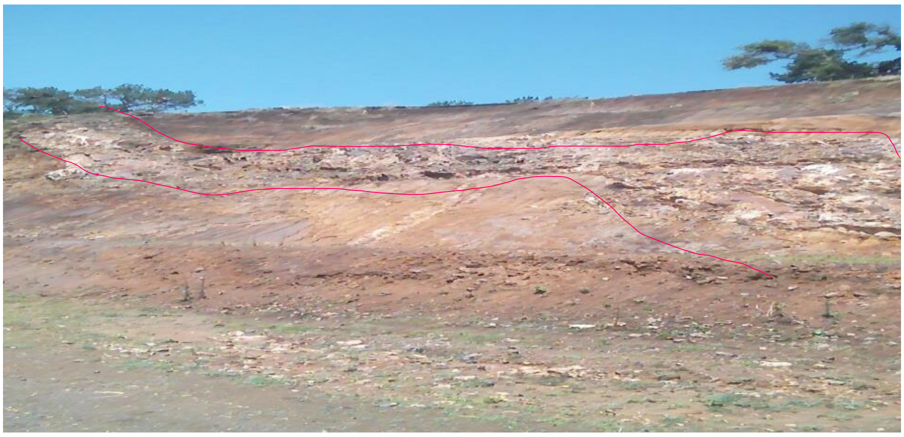

Figure 4.8 Sill, Rhyolite intrusion to pyroclastic deposit

4.3.2 Exfoliation

Exfoliation**,** the separation of successive thin shells, or spalls, from massive rock such as granite or basalt; is common in regions that have moderate rainfall. The thickness of an individual sheet or plate may be from a few millimeters to a few meters. The exfoliation observed in the study area was a basaltic rock, as shown in figure 4.9.

Figure 4.9 Exfoliation of basaltic rock

4.3.3 Joints

A joint is a brittle-fracture surface in rocks along which little or no displacement has occurred. Present in nearly all surface rocks, joints extend in various directions, generally more toward the vertical than to the horizontal. In the study area, the joints were observed in basalt and rhyolite rocks and a columnar joint was observed on a basaltic rock surface. Figure 4.10 A shows a columnar joint of a basaltic rock with 2 joint sets and figure 4.10 B represents a rhyolite rock slope with 3 joint sets. Both joints are characterized as slightly rough surfaces with a joint spacing range of 0.04 to 1m.

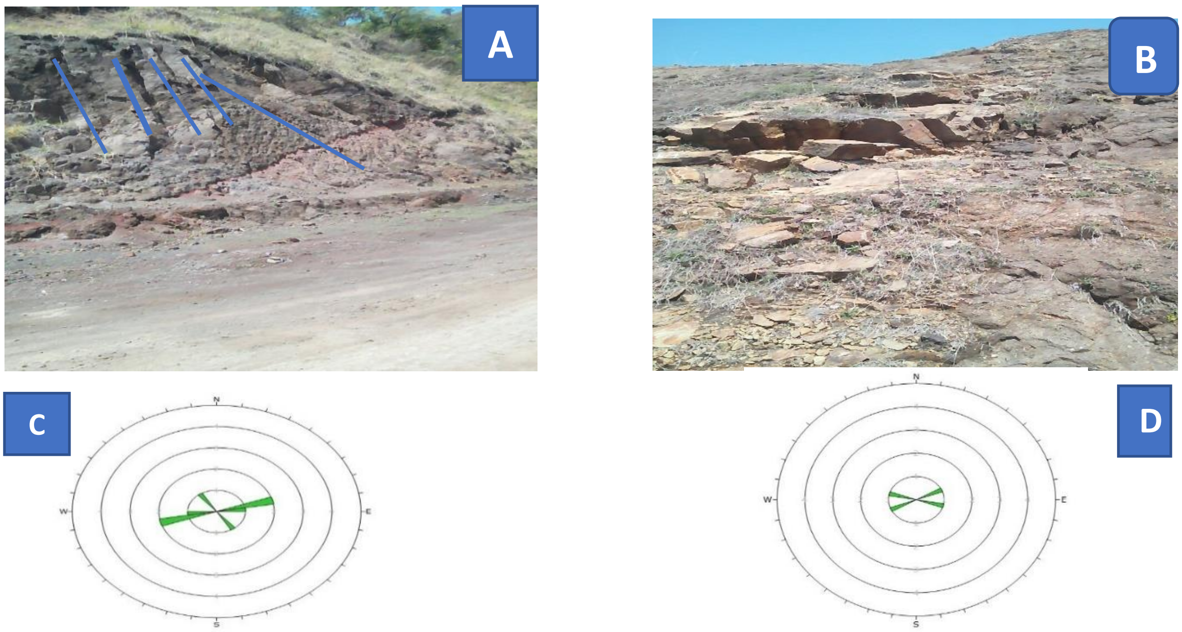

Figure 4.10 joints observed in the study area A) columnar joint in the basaltic rock, B) a rhyolite slope, C) Rosette projection for basalt rock, and D) Rosette projection for rhyolite rock.

4.4 Geological map and cross-section

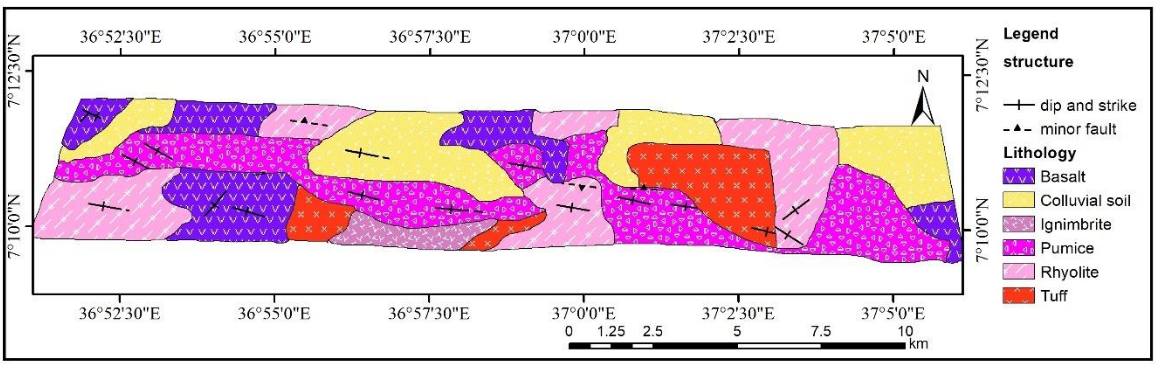

Figure 4.11 Geological map along Tercha-Chida Road

4.5 Subsurface Geology

The subsurface data was collected from ECDSWC and the data includes the borehole data and the geophysical data. Six boreholes were drilled for the maximum depth of 30m. The profile of the borehole shows six lithologic layers. These are gravel with a fine deposit, pyroclastic deposit, basalt, tuff and gravel with sand deposit were found respectively from top to bottom. The groundwater information in the borehole presented as dry or groundwater has not been observed in five of the borehole data but it was observed in borehole six at the depth of 4.7m. Seismic refraction, electrical resistivity imaging, and Vertical Electrical Sounding (VES) are methods used for geophysical investigation.

From Seismic refraction data analysis, subsurface rocks were classified into three geological formations. The upper formation with a velocity of 320- 850 m/s corresponds to the topsoil and highly weathered rocks having less than 10 m thickness. The second stratum with a velocity of 850-2500 m/s signifies weathered and fractured rocks extending to more than 20 m depth. The bottom layer (> 2500 m/s velocity) is detected below 20 m depth.

From Electrical resistivity imaging data analysis, the resistivity of subsurface rocks increase with depth, implying a decrease in weathering and fracturing depth-wise. Generally, the low resistivity upper part is attributed to the topsoil and highly weathered rocks that appear to be about 20 m in most cases.

Vertical Electrical Sounding revealed low resistivity formation extending to more than 25 meter depth which could correspond to highly weathered and fractured rocks, particularly low resistivity features extend deeper in the southern part of the investigation area, showing deep weathering.

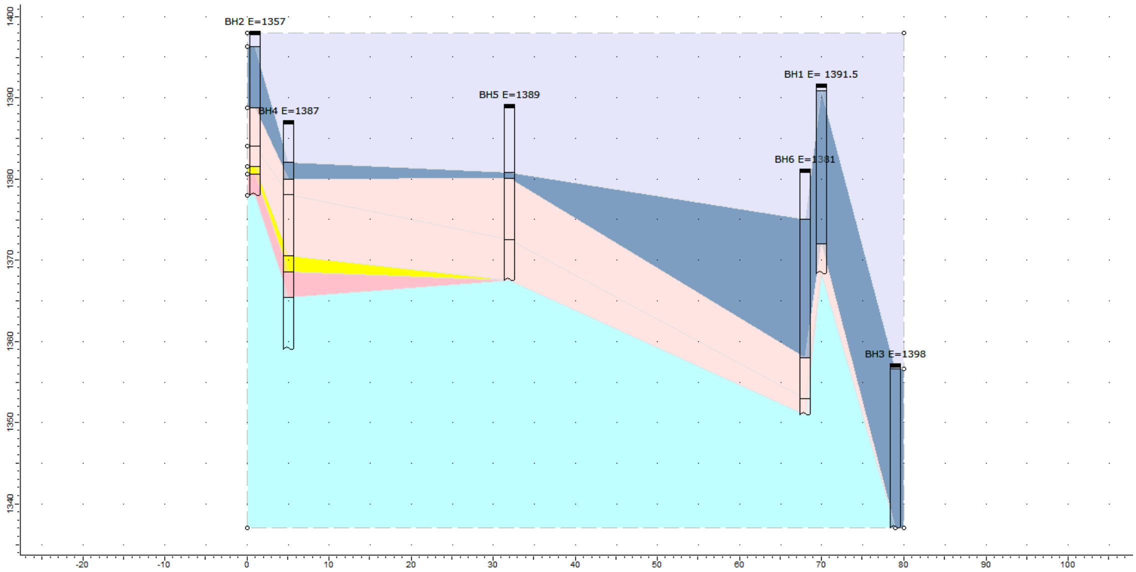

Figure 4.12 Borehole cross-section

CHAPTER FIVE

RESULT and DISCUSSION

5.1 Permeable

In the present study, a finite and a limit equilibrium analysis method were performed to determine the factor of safety of the critical slope section. For the software, laboratory tests for rock and soil were inputted. Soil laboratory tests include sieve, hydrometer, compaction test, direct shear test, Atterberg limit, specific gravity and water content. Dry and saturated density, point load test, Schmidt hammer, and slake durability tests were the tests that were used to determine the rock sample properties. The results from the finite element method were compared with the limit equilibrium method and with swedge and roc plane since there are 2 sites that showed planar and wedge failures.

5.2 Engineering characterization of soils

The test was performed for two test pits to determine the geotechnical property of the soil, where the samples were taken with 4m and 1m for test pit 1 and test pit 2 respectively. The soil sample that was taken from test pit 1 was a brown color with a specific gravity of 2.68. The soil is classified as high plasticity clay soil with a 31.93 plastic limit and 51.983 liquid limit value. From the AASHTO classification the soil was classified as clayey gravel soil which has a water content value of 3.6%. The mechanical parameters were calculated from the direct shear test and these parameters were the cohesion and friction angle, having 12.2KN/m^2 and 30.5° values.

5.2.1 Particle size distribution curve

The results of mechanical analysis (sieve and hydrometer analyses) are generally presented by semi-logarithmic plots known as particle-size distribution curves. This curve is obtained from the percentage finer results of both coarse- and fine-grained portions. The graph shows a soil with all particles of different size which represent a well-graded soil.

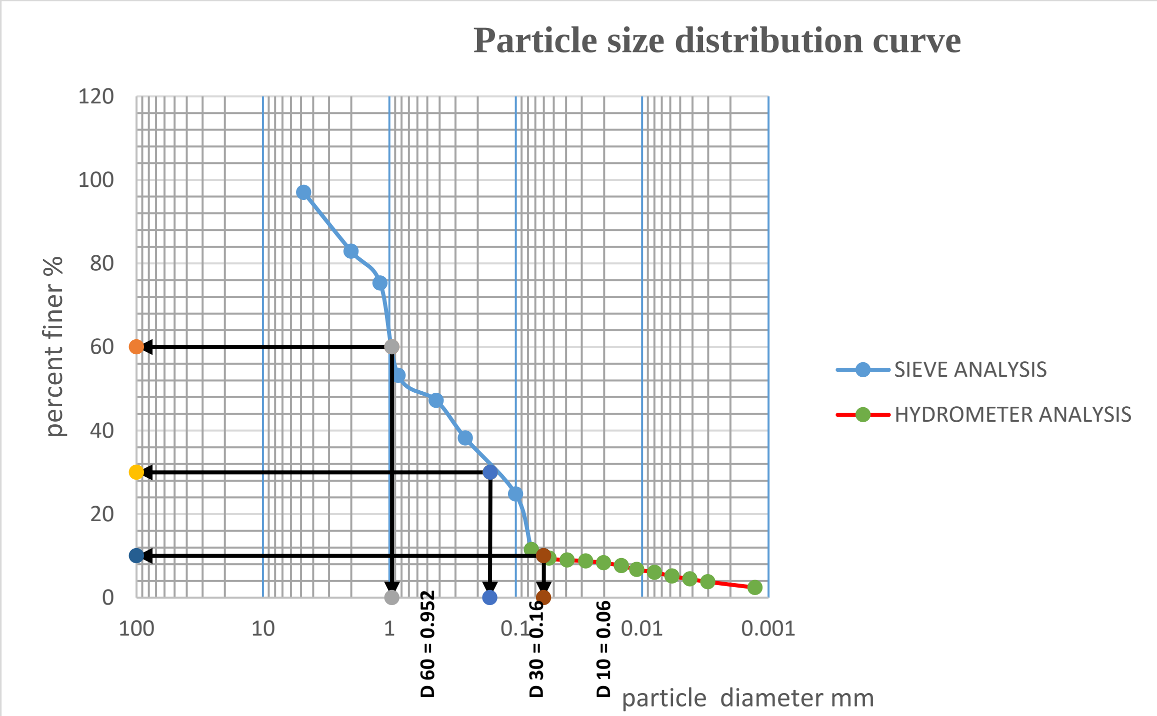

Figure 5.1 Particle size distribution curve

5.2.2 Atterberg limit

A liquidity curve or a flow curve is plotted on a semi-logarithmic graph representing water content on the arithmetical scale and the number of drops on the logarithmic scale. The flow curve is a straight line drawn as nearly as possible through the four or more plotted points, it represents the liquid limit at 25 numbers blows which equals 51.983 and the plastic limit is equal to 31.93, resulting a plasticity index of 20.053.

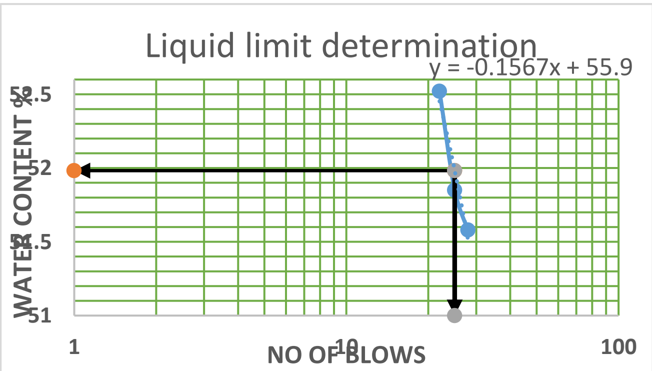

Figure 5.2 Liquid limit determination curve

5.2.3 Soil classification

The soil is classified as high plasticity clay soil with a 31.93 plastic limit and 51.983 liquid limit value from Figure 5.2. From the AASHTO classification soil was classified as clayey gravel soil. The graph in Figure 5.1 shows a soil with all particles of different size which represent a well-graded soil. The effective size of the soil or D10 is equal to 0.06mm, and the diameter corresponding to 60% finer in the particle-size distribution or D60 has a value equal to 0.952mm and D30 or a diameter corresponding to 30% is 0.16mm. The uniformity coefficient of soil is calculated as 15.87, and the coefficient gradation is equal to 0.45. Generally, the soil is classified as highly plastic well-graded clayey gravel soil.

5.2.4 Compaction test

The compaction test was performed to determine the optimum moisture content, which was 11%, and the maximum dry density with the value of 1.5g/cm^3 for test pit -1 but for test pit -2 the maximum dry density and the optimum moisture content are 1.51gm/cm^{3}and 27.32%respectively.

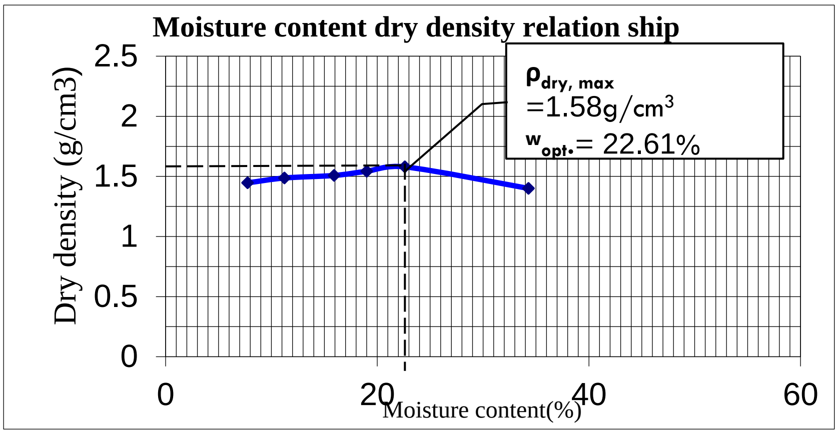

Figure 5.3 Moisture content to dry density relationship curve test pit1

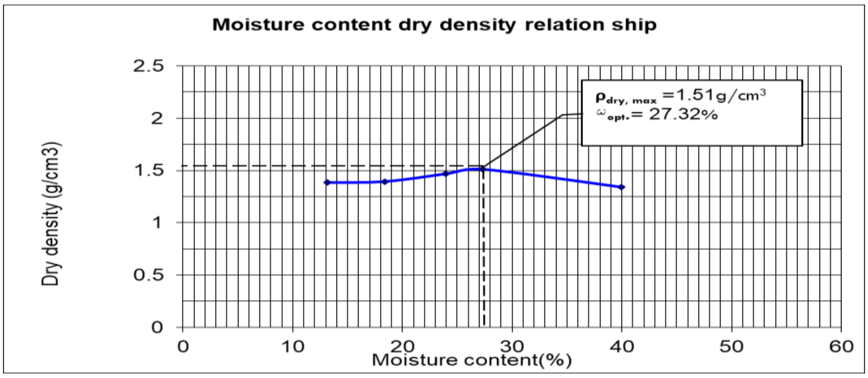

Figure 5.4 Moisture content dry density relationship for test pit2

5.2.5 Direct shear test

The result from the direct shear test gives the cohesion and friction angle of a soil sample. The cohesion of test pit one is 7.12KN/m^2 and the cohesion of test pit two is 9.2KN/m^2 and 25.2° and 20.18° are the friction angle of test pit one and two respectively.

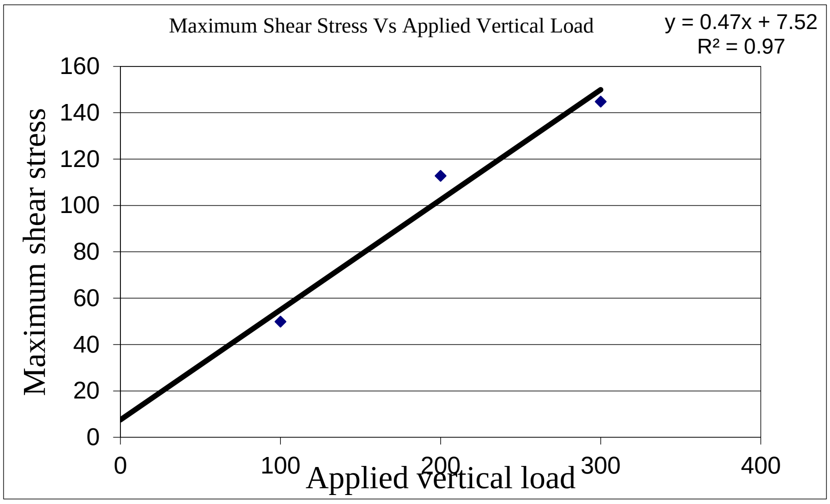

Figure 5.5 Direct shear test result for test pit 1

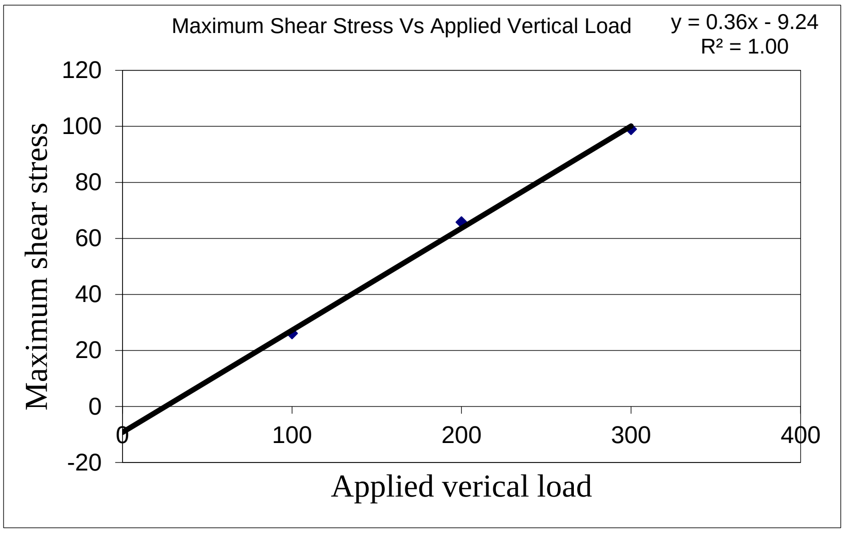

Figure 5.6 Direct shear test result for test pit 2

Table 5.1 Test result for soil samples

<table>
<tr><td colspan="2"></td><td colspan="2">Test results</td></tr>
<tr><td colspan="2">Test conducted</td><td>Soil-1</td><td>Soil-2</td></tr>
<tr><td colspan="2">Test pit depth</td><td>4m</td><td>1.5m</td></tr>
<tr><td colspan="2">Natural water content (%)</td><td>3.6%</td><td>8.76%</td></tr>
<tr><td colspan="2">Specific gravity</td><td>2.68</td><td>2.65</td></tr>
<tr><td rowspan="3">Atterberg limit</td><td>Liquid limit</td><td>51.983</td><td rowspan="3">-</td></tr>
<tr><td>Plastic limit</td><td>31.93</td></tr>
<tr><td>Plastic index</td><td>20.053</td></tr>
<tr><td rowspan="2">Moisture-density relationship</td><td>Maximum dry density gm/cm^3</td><td>1.58gm/cm^3</td><td>1.51gm/cm^3</td></tr>
<tr><td>Optimum moisture content (%)</td><td>21.2%</td><td>27.32%</td></tr>
<tr><td colspan="2">AASHTO classification</td><td>A-2-7</td><td>-</td></tr>
<tr><td colspan="2">USCS classification</td><td>Clayey gravel soil</td><td>Clay</td></tr>
<tr><td rowspan="2">Direct shear test</td><td>Cohesion (KN/m^2)</td><td>7.12</td><td>9.2</td></tr>
<tr><td>Friction angle (˚)</td><td>25.2</td><td>20</td></tr>
</table>

5.3 Engineering properties of rocks

The test was performed for five rock samples with a critical section showing structurally or non-structurally controlled behavior. To determine the strength of the rock a point load was performed and dry and saturated density and slake durability tests were also performed to determine the properties of a rock sample.

5.3.1 Rock strength result

The basalt is slightly to highly weathered rock at outcrop while the rhyolite showed high strength value compared to tuff, ignimbrite, and pyroclastic deposits.

5.3.2 Dry and saturated density of rocks

The observed samples were basalt, rhyolite, ignimbrite, tuff and pumice with ash deposit and the density values for basalt, rhyolite, and ignimbrite are higher than the density of tuff and pumice with ash.

5.3.4 Rock durability result

The durability test was performed for four rock samples The other rock sample (pumice with ash) does not qualify for the slake durability test. The final result of the test showed that all the samples have very high durability values ranging from 99.1% to 99.88%.

Table 5.2 Rock laboratory tests

	Test result				
Type of tests	Rs1	Rs2	Rs3	Rs4	Rs5
Rock type	Tuff	Ignimbrite	Ash pumice deposit	Rhyolite	Basalt
Strength (UCS Mpa)	61.05	90.35	21.96	83.43	140.9
Dry unit weight (KN/m^3)	20.27	20.66	8.799	21.23	28.964
Saturated unit weight (KN/m^3)	25.496	26.415	15.313	24.559	30.45
Slake durability (%)	99.3	99.45	-	99.1	99.88

5.4 Engineering geological map

The study is conducted along the Tercha-Chida Road and the road is outcropped by different lithologies. Pyroclastic deposit is mainly observed in the road sections.

The study area is covered by different lithologies and classified as an engineering geological unit. Unit 1 consists slightly weathered to highly weathered, moderately strong to very strong, brownish and blackish, basalt with glassy texture. Unit 2 consists slightly weathered and highly weathered with lower to moderate strength, white to brown rhyolite rock. Unit 3 consists highly weathered to lower strength, yellowish gray unwelded tuff. Unit 4 consists slightly weathered with moderate strength, gray welded tuff. Unit 5 consists intercalated tuff, pumice, and ash deposit with lower strength purple, white and yellowish pyroclastic deposit. Unit 6 consists the irregular shape of gravel and boulder with pyroclastic deposit. Unit 7 consists colluvial soil, boulders with clayey silt deposit. Unit 8 consists highly plastic, well-graded, red clayey gravel soil. Unit 9 consists high plasticity, black clay soil

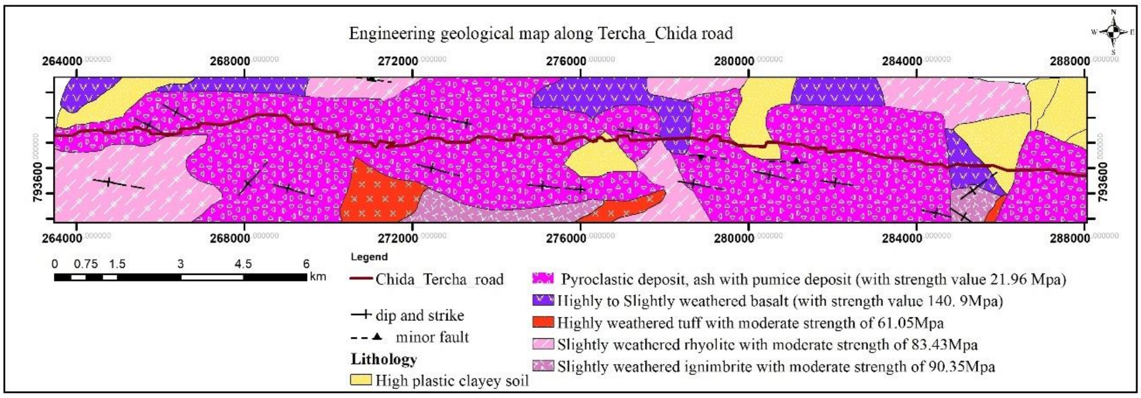

Figure 5.7 Engineering geological map of Tercha-Chida Road section

5.5 Limit equilibrium analysis

Most of the road section has a benching system and some of these slopes show a critical condition. The result is shown using dynamic and static in wet and dry conditions. For this analysis 6 rock slopes and 2 soil slopes have been selected and all slopes showed small factors of safety values. The input parameters that were used for the analysis include the unit weight, cohesion and friction angle of a material. Table 5.3 shows the input parameters for limit equilibrium analysis and finite element analysis.

Table 5.3 Input parameters for limit equilibrium method and finite element method

Sample id	Lithology	Poisson's ratio (μ)	Young's modulus (Em)	Unit weight(γ) ($\frac{KN}{m3}$)	Cohesion (Mpa)	Friction angle (degree)
S1	Clay	0.3	0.6Mpa	29.9	7.12	25.2
S2	Clay	0.3	0.6Mpa	17.7	9.2	20
RS1	Tuff	0.3	2471.94	20.27	1.456	17.33
RS2	Ignimbrite	0.2	9505.79	20.67	3.671	26.25
RS3	Ash pumice deposit	0.4	4687.75	8.799	0.451	16.34
RS4	Rhyolite	0.3	5138.03	20.601	3.254	26.02
RS5	Basalt	0.14	2371.37	28.964	4.119	21.66

5.4.1 Slope model for homogeneous material

A slope with homogenous material was observed for two rock slopes and 1 soil slope and they were analyzed with different slope angles (65˚, 68˚, 71˚ and 79˚), which collected from the field. The analysis was done for four conditions these are dry and wet static and dry and wet dynamic conditions. The factor of safety was interpreted for four limit equilibrium approaches (Bishop, Janbu simplified, Spencer, Morgenstern) and the Janbu simplified method shows the lowest factor of safety. The factor of safety ranges from 0.930 to 1.102 for slope angle 71˚ for basalt rock and 1.029 to 1.739 for 79˚ for rhyolite rock.

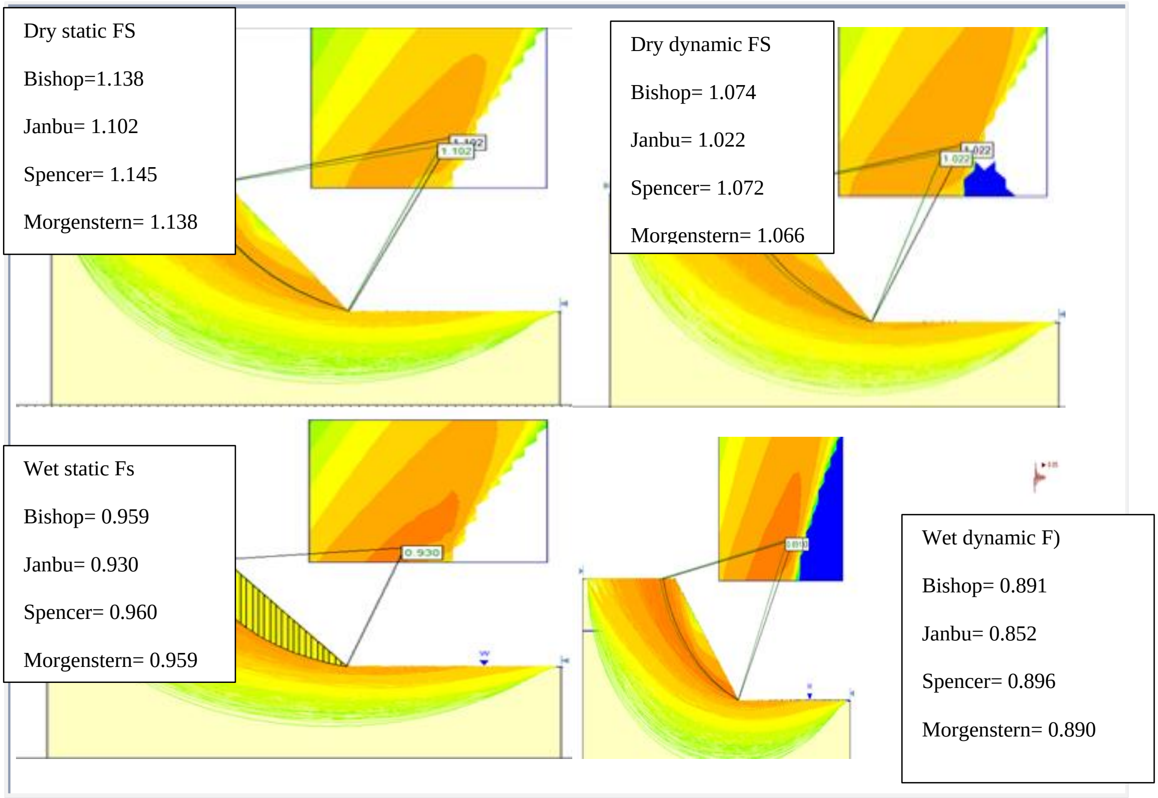

Figure 5.8 Limit equilibrium analysis for rock slope (basalt) for different conditions

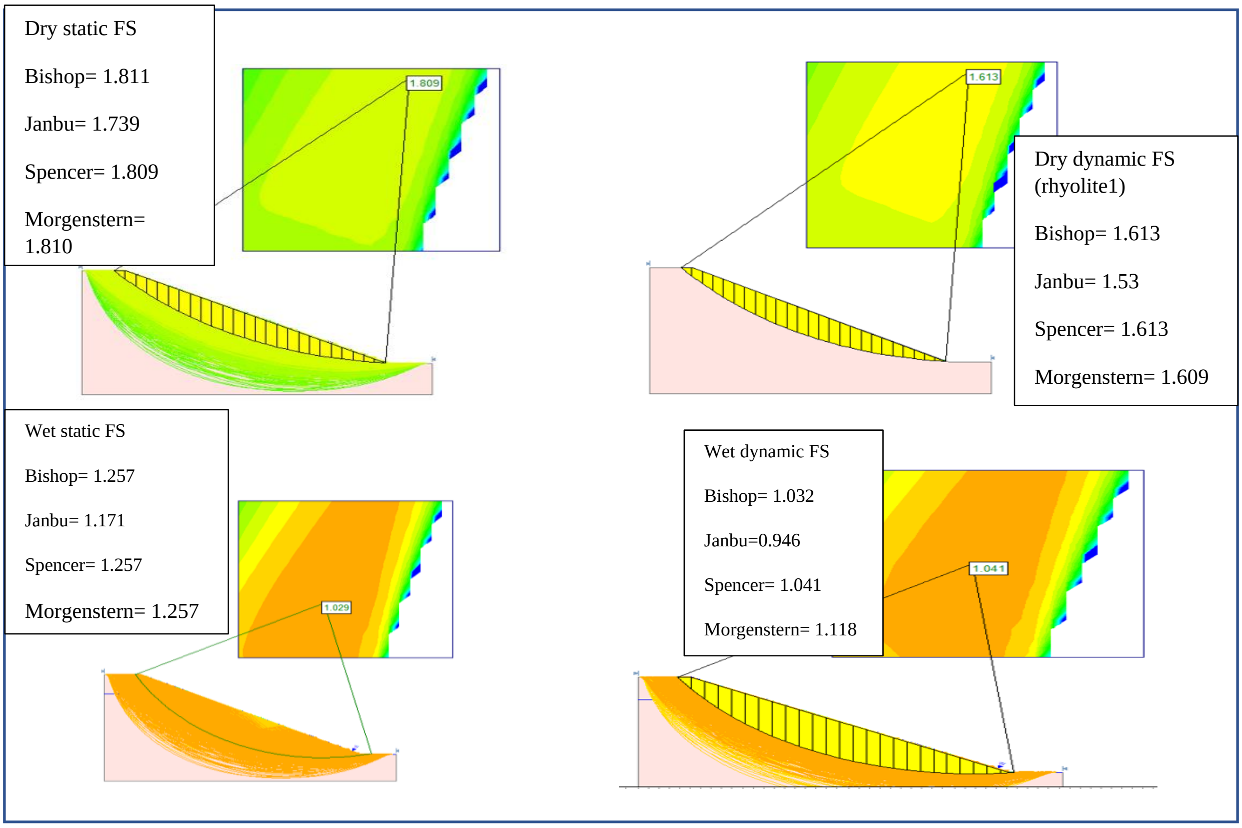

Figure 5.9 Limit equilibrium analysis for rock slope (rhyolite) for a different conditions

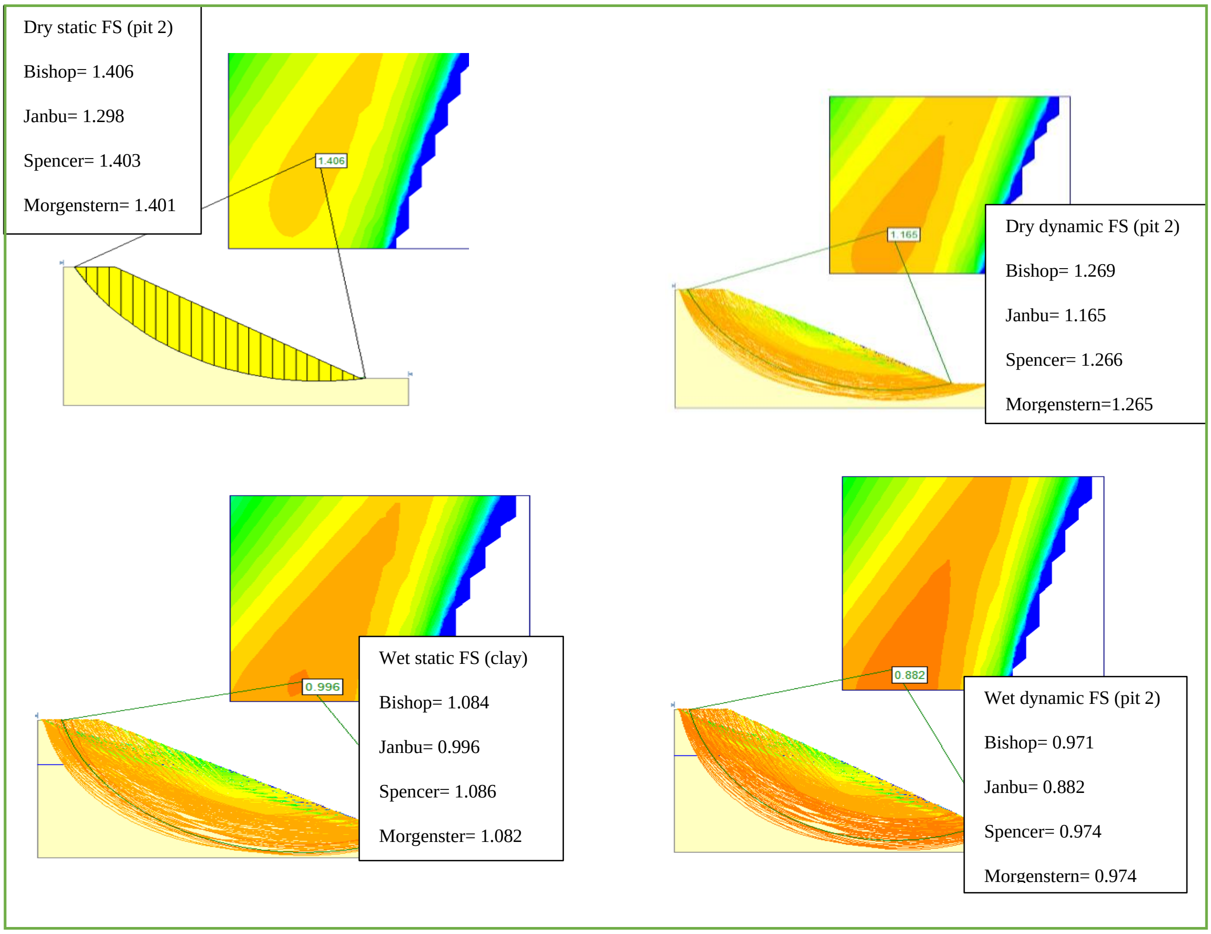

Figure 5.10 Limit equilibrium analysis for soil slope (pit2) for a different conditions

5.4.2 Slope model for heterogeneous slope

A slope with lateral and angular lithologic variation was shown covering some parts of the road section. A lateral variation of 2 rock slopes and 1 soil slope were selected for this analysis. The first slope is ash with pumice rock with a slope angle of 32˚, the factor safety ranges from 0.647 to 1.624. The other slope was a basalt slope with a soil base have a factor of safety ranging from 0.665 to 0.907 with a slope angle of 67˚. The factor of safety ranges from 0.888 to 1.214 for a slope angle of 68˚of clay soil. The slope with the angular unconformity was characterized by slightly weathered ignimbrite and tuff deposit. The model was analyzed by a slope angle of 50.7˚ with varying properties of each lithology. The factor of safety for this slope ranges from 0.439 to 0.477 from the interpretation of the Janbu method.

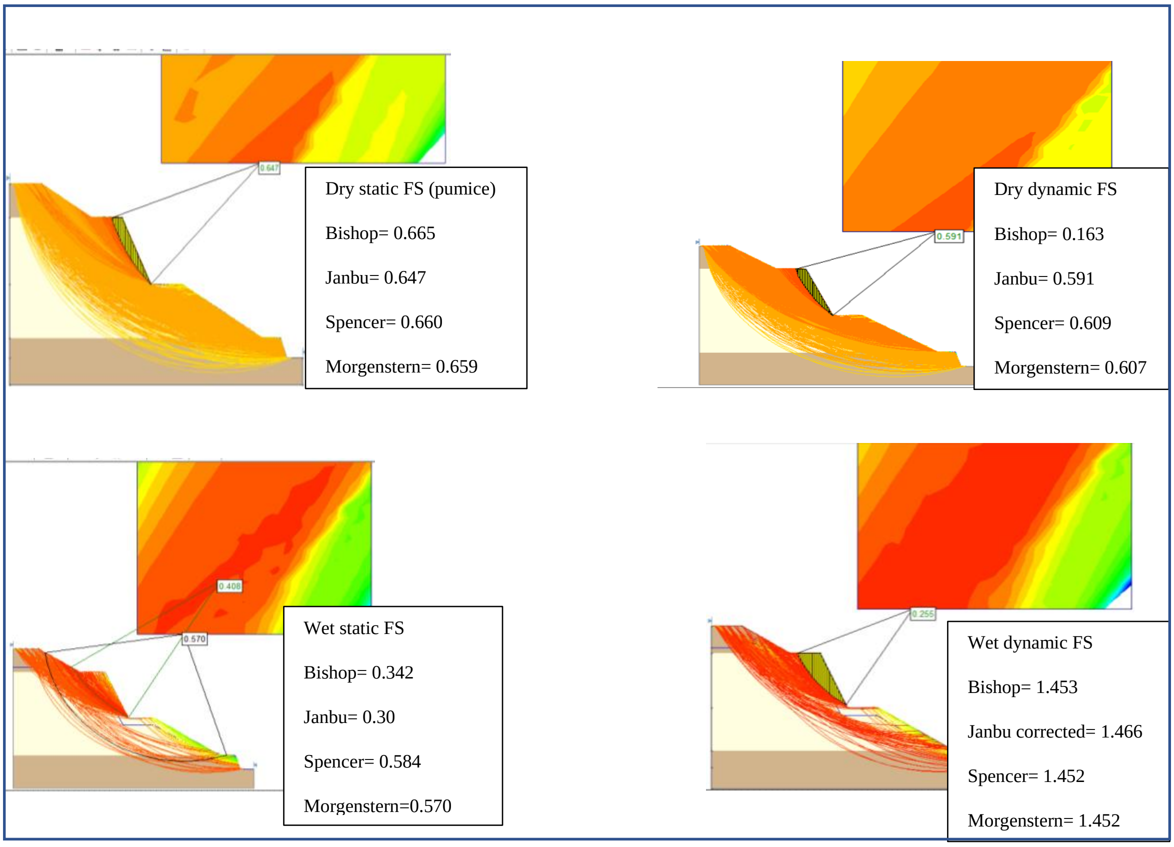

Figure 5.11 Limit equilibrium analysis for rock slope (pyroclastic deposit) for different conditions

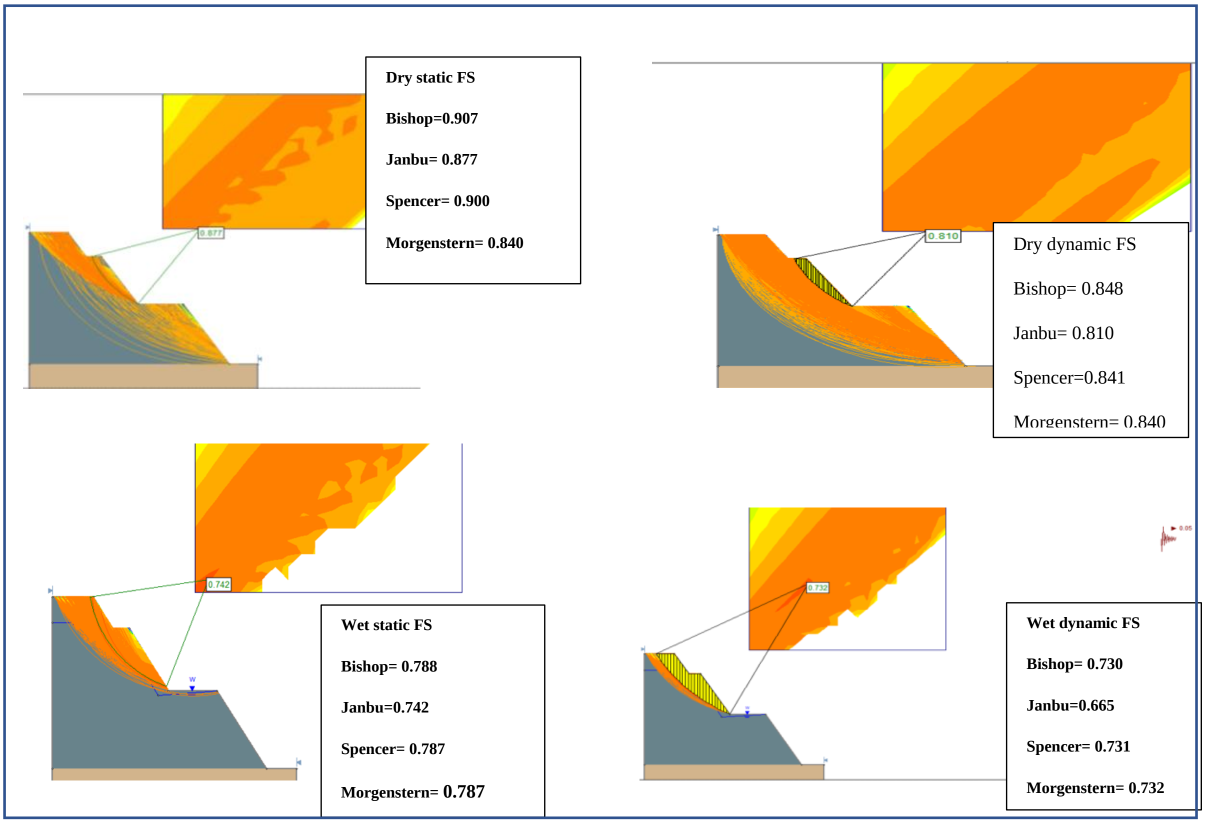

Figure 5. 12 Limit equilibrium analysis for rock slope (basalt2) for different conditions

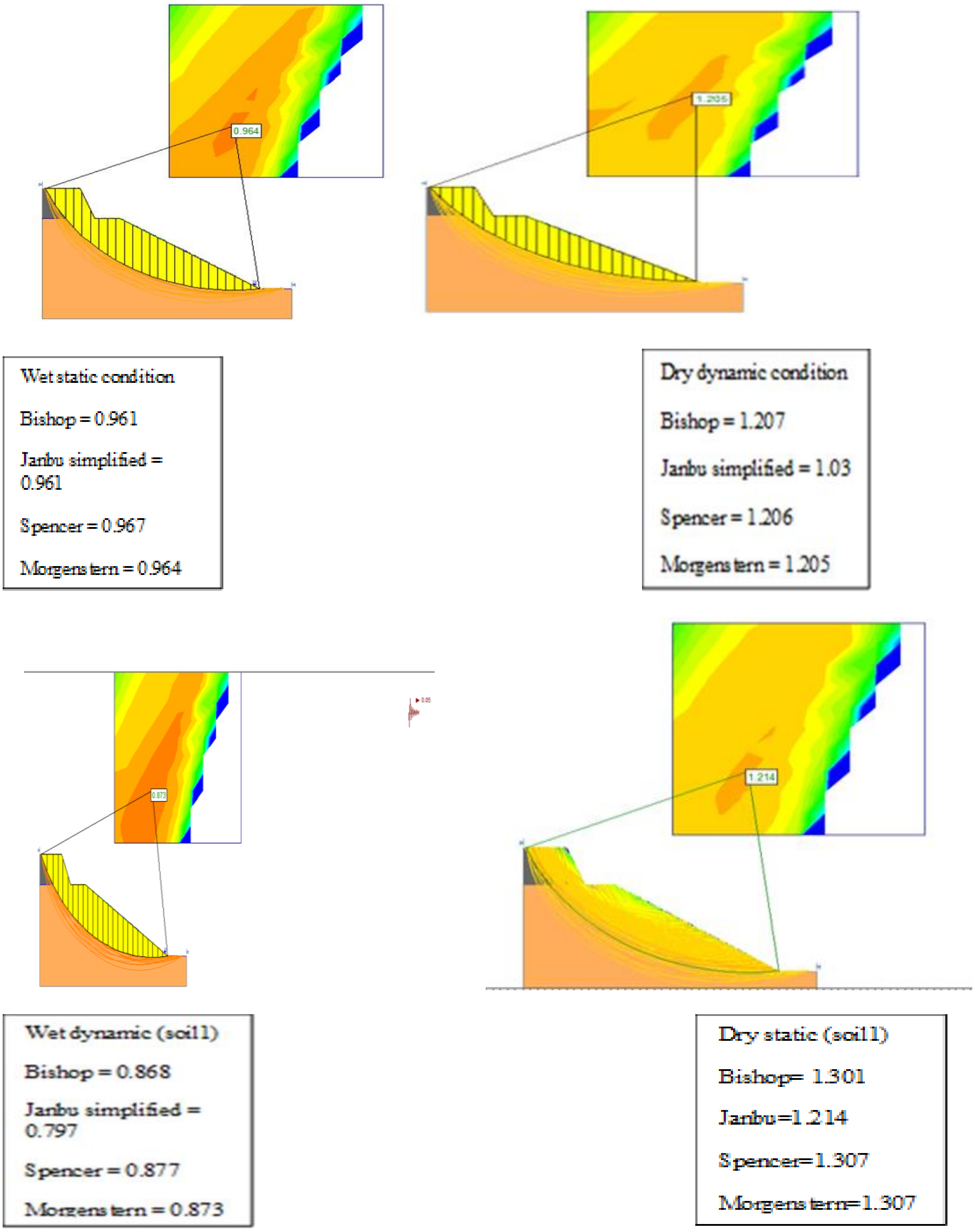

Figure 5.113 Limit equilibrium analysis for soil slope for a different condition

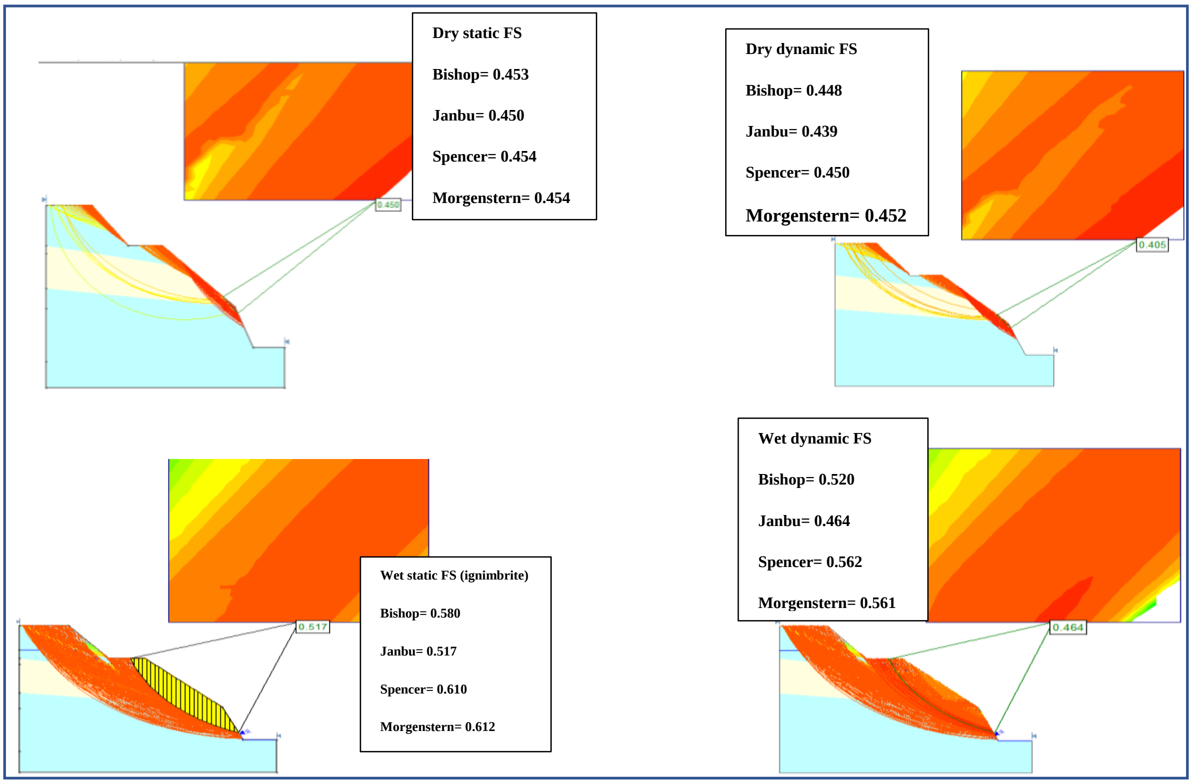

Figure 5.14 Limit equilibrium analysis for ignimbrite with tuff deposit slope

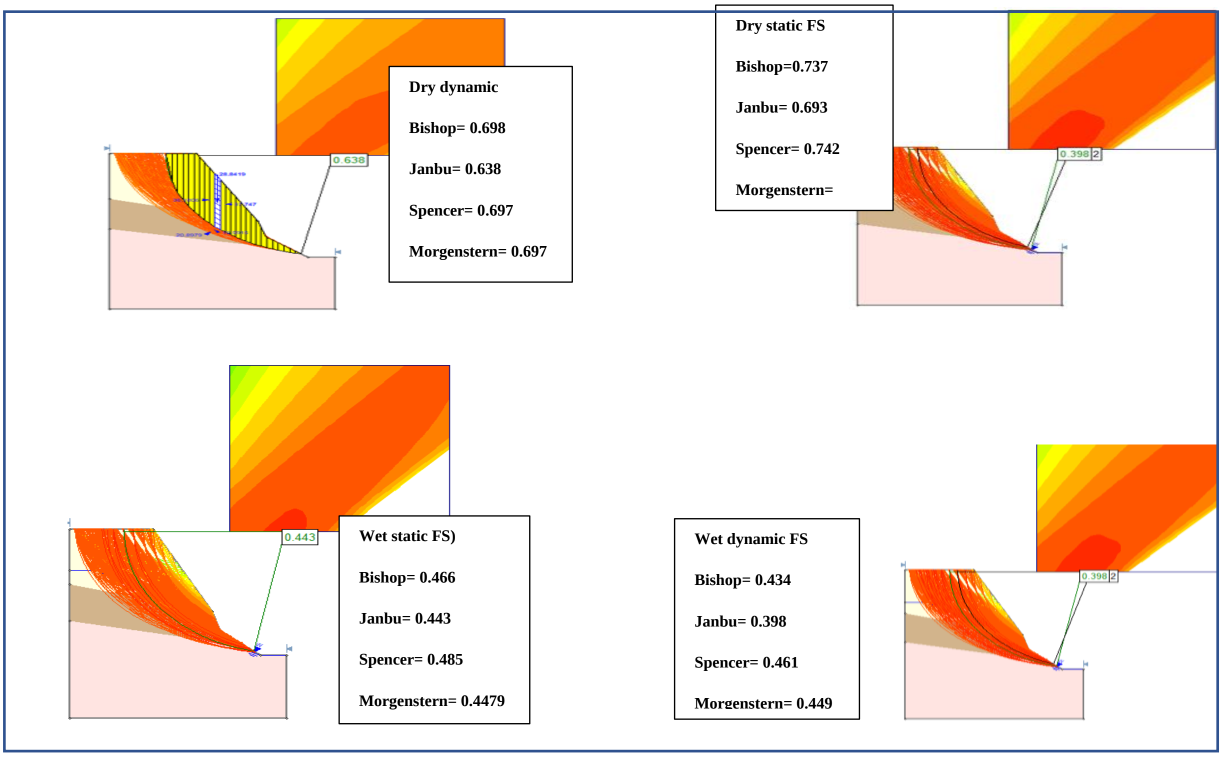

Figure5.15 Limit equilibrium analysis for rhyolite-soil-pumice deposit

5.4 Finite element method

The analysis was done for two soil slopes and six rock slopes with seismic load and with static stage. The factor of safety of slope in the analysis does not have much difference from the factor of safety, which was interpreted using the limit equilibrium method. In this analysis, three cases have been taken one for a homogeneous slope with soil base and a non-homogeneous slope, a slope with a weak layer with parallel orientation with the slope face. The input parameters used in the finite element method were the same as the limit equilibrium method with exception of Poisson ratio and young's modulus.

Table 5.4 Input parameters for finite element method

Sample id	Lithology	Poisson's ratio (μ)	Young's modulus (Em)
S1	Clay	0.3	0.6Mpa
S2	Clay	0.3	0.6Mpa
RS1	Tuff	0.3	2471.94
RS2	Ignimbrite	0.2	9505.79
RS3	Ash pumice deposit	0.4	4687.75
RS4	Rhyolite	0.3	5138.03
RS5	Basalt	0.14	2371.37

5.4.1 Homogeneous slope with a soil base

The analysis was done for four homogeneous slopes, with different properties. The deformed mesh was with 6 node elements.

5.5.1.1 Homogeneous clay slope

There are two clay soil slopes in the study area that seems to cause a problem with a different physical and mechanical property. The soil that was taken from the test pit 1 is the clayey gravel soil and from the test pit, 2 is black clay soil. The SRF of soil-1 ranges from 0.86 to 1.19 for saturated and dry conditions. The SRF of soil slope – 2 ranges from 0.89 to 1.35. The analysis takes place for four conditions. The slope gradient for soil slope was 1H:1V with a slope angle of 30˚ and the slope gradient of soil slope – 2 was 2H:1V with a slope angle of 25˚. Both slopes show a circular type of slope failure.

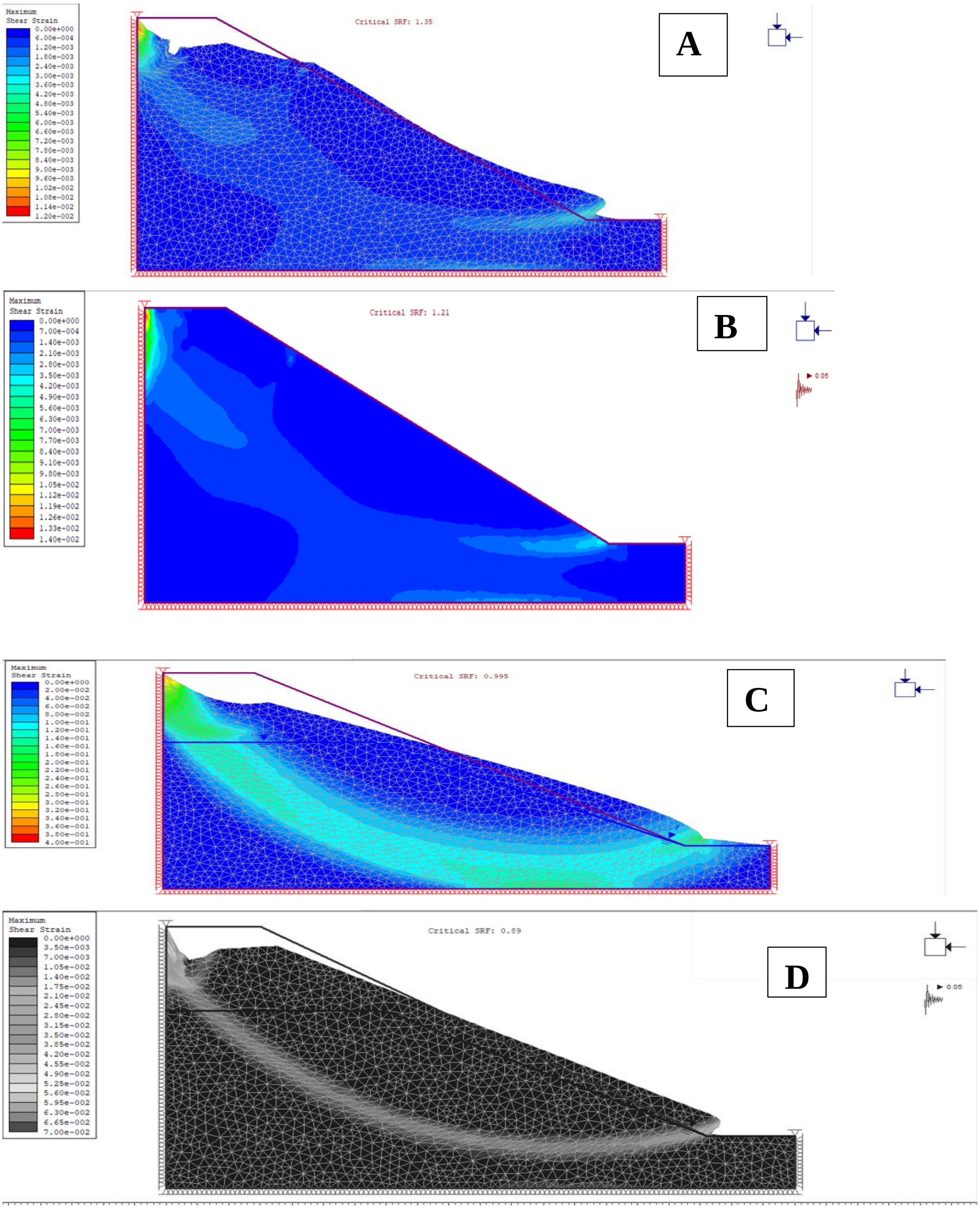

Figure 5.15 Finite element analysis for clay slope – 2 A) analysis for the dry static condition with SRF = 1.35 B) Analysis for a dry dynamic condition with SRF = 1.21 C) Analysis for a wet static condition with SRF = 0.995 and D) Analysis for a wet dynamic condition with SRF = 0.89 and 6 node elements

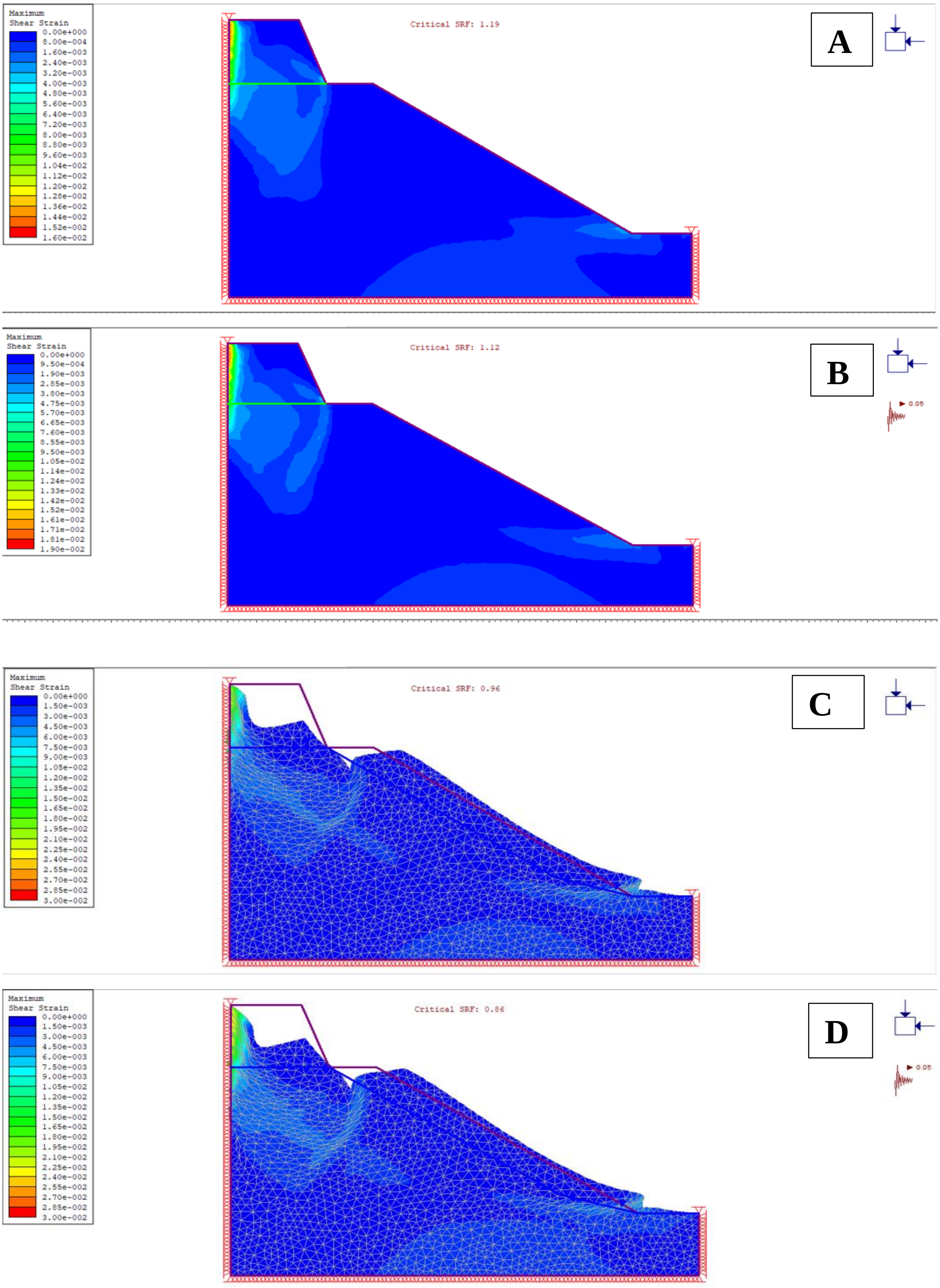

Figure 5.16 Finite element analysis for clay soil slope -1 A) analysis for dry dynamic condition with SRF = 1.19, B) model for dry dynamic condition with SRF = 1.12 C) model

for wet static condition with SRF = 0.96 and D) model for wet dynamic condition with SRF = 0.86 with 6 node elements

5.5.1.2 Homogeneous basalt slope

The analysis is done for slope gradient 2H:1V with a slope angle of 71˚. The SRF result shows a 0.75 lower value for wet dynamic conditions and a 1.11 higher value for dry static conditions compared to other groundwater and seismic conditions.

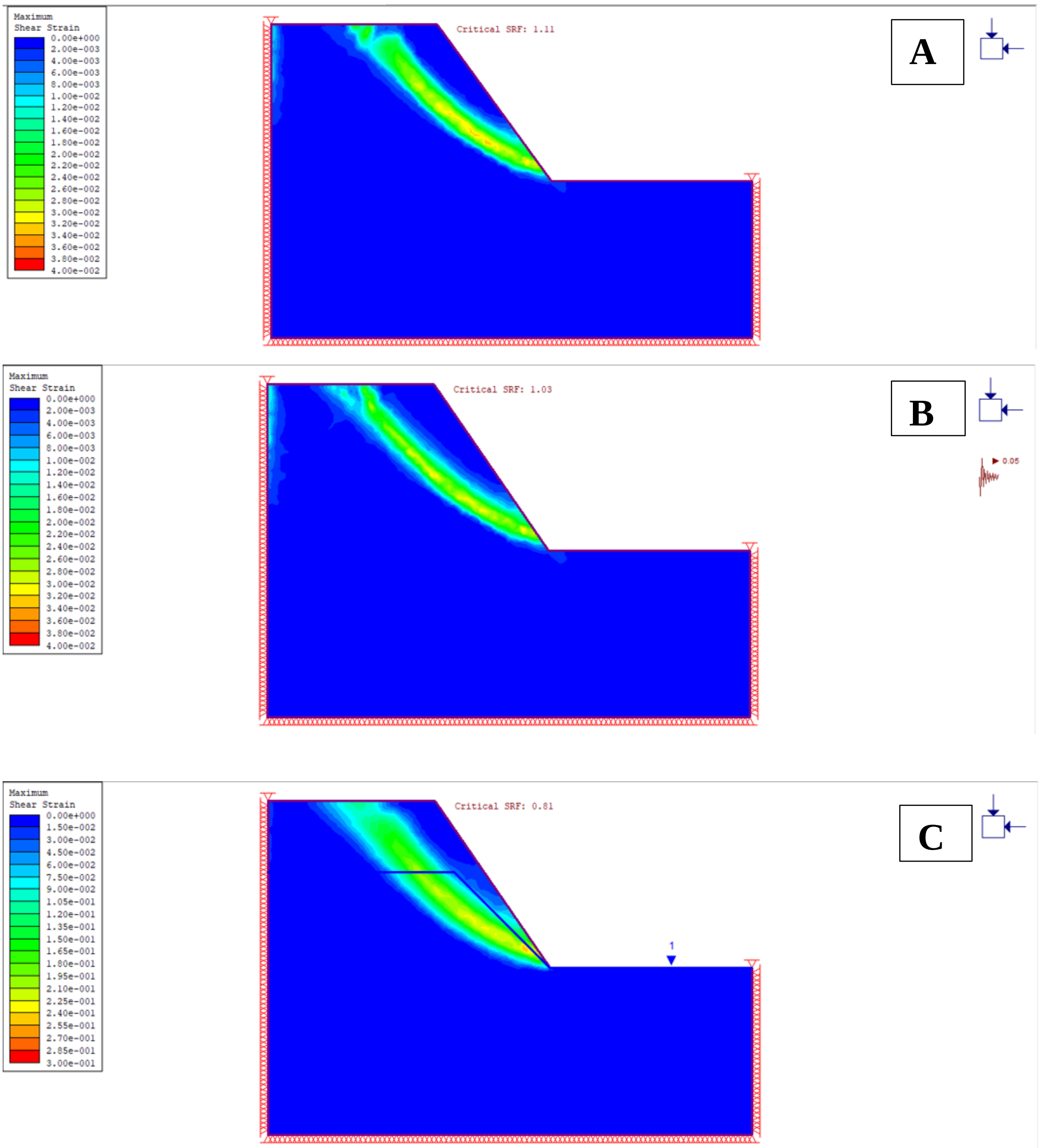

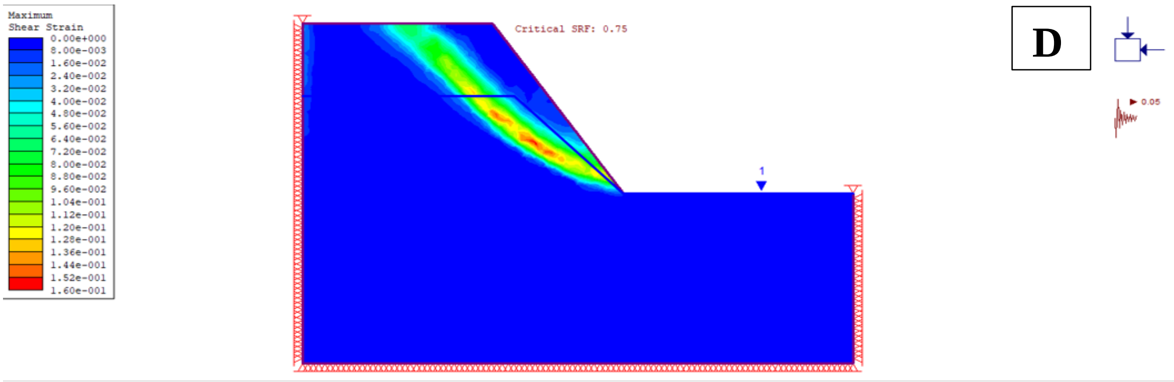

Figure 5. 16 Finite element analysis for basalt slope, A) dry static condition with SRF = 1.11, B) dry dynamic condition with SRF = 1.03 C) wet static condition with SRF = 0.81 and D) wet dynamic condition with SRF = 0.75.

5.5.1.3 Homogeneous rhyolite

The analysis is done with a 2H:1V slope gradient and 79˚ slope angle. The SRF value of this slope ranges from 0.96 to 1.79 which represents the slope stay stable unless it is exposed to seismic force or water pressure. The analysis was done for the conditions and it shows that the slope is stable in dry conditions. Here it shows that the effect of groundwater on the slope is high.

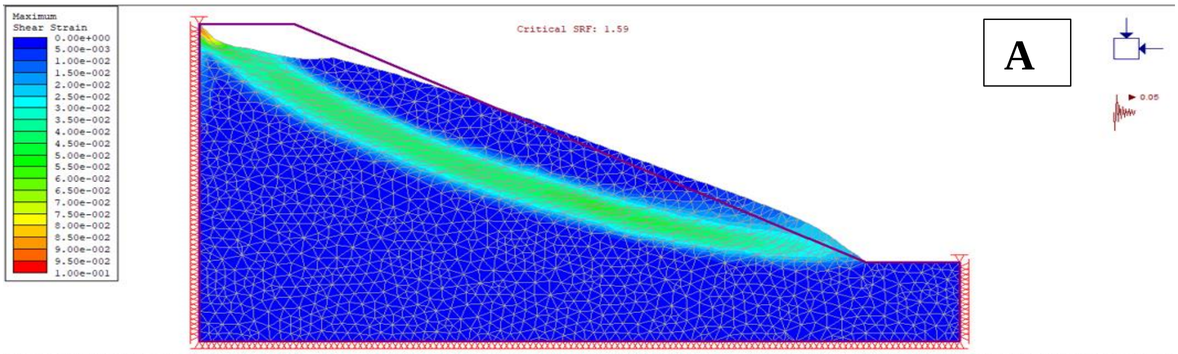

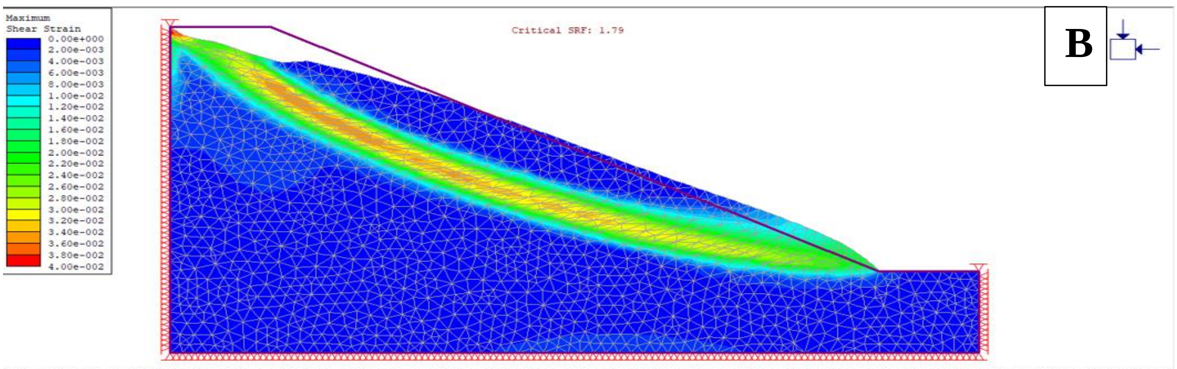

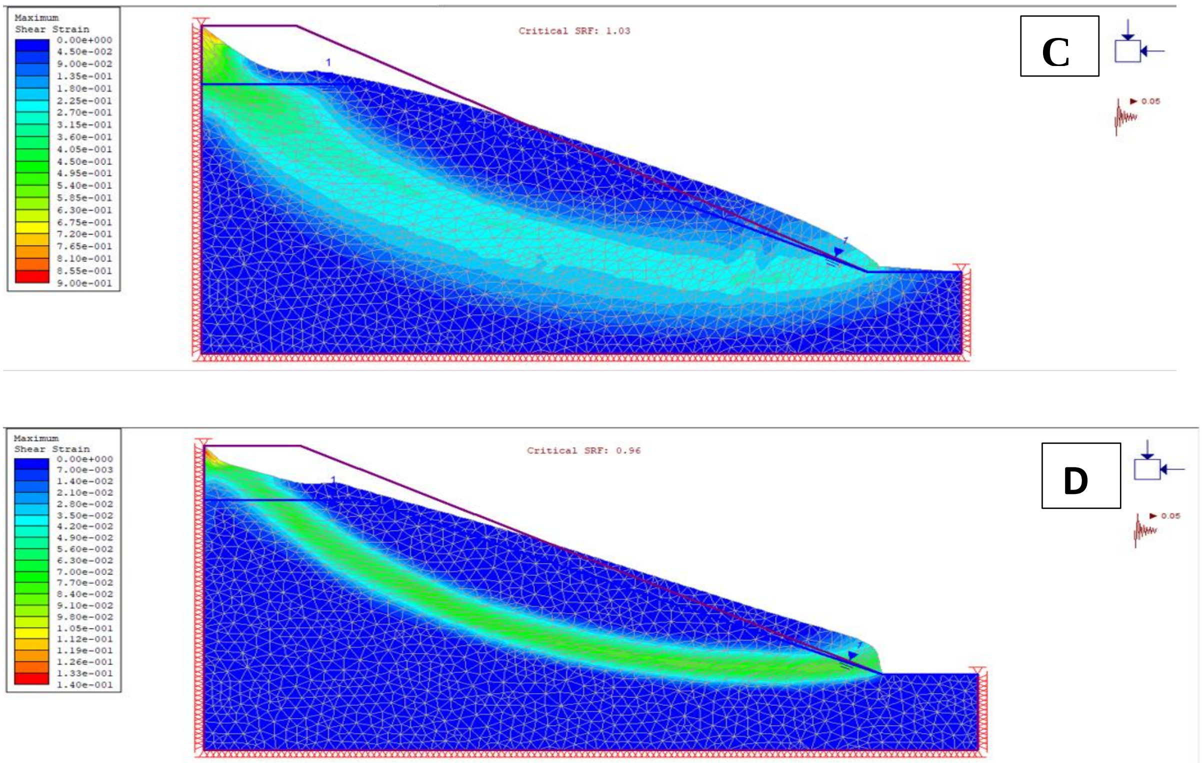

Figure 5.17 Finite element analysis in Rhyolite slope A) dry static condition with SRF = 1.79 B) dry dynamic condition with SRF = 1.59 C) wet static condition with SRF = 1.03 and D) wet dynamic condition with SRF = 0.9 and 6 node element

5.4.2 Non-homogeneous slope

The slope with non-homogeneous behavior were two slopes, these are basalt slope with soil and pyroclastic deposit with soil. The variation between the lithologies was lateral, the soil found at the top and base on both slopes. The analysis was done for dry-dynamic and static and wet-dynamic and static conditions to determine the effect of each pressure on the slope.

5.5.2.1 non-homogeneous basalt slope with soil

The slope represents basalt rock with soil at the top. The gradient of the slope is 1H:1V and 67˚ slope angle. The SRF value ranges from 0.48 to 0.83, where the wet dynamic condition shows a lower value of 0.48 and dry static with a higher value of 0.83 compared to other conditions.

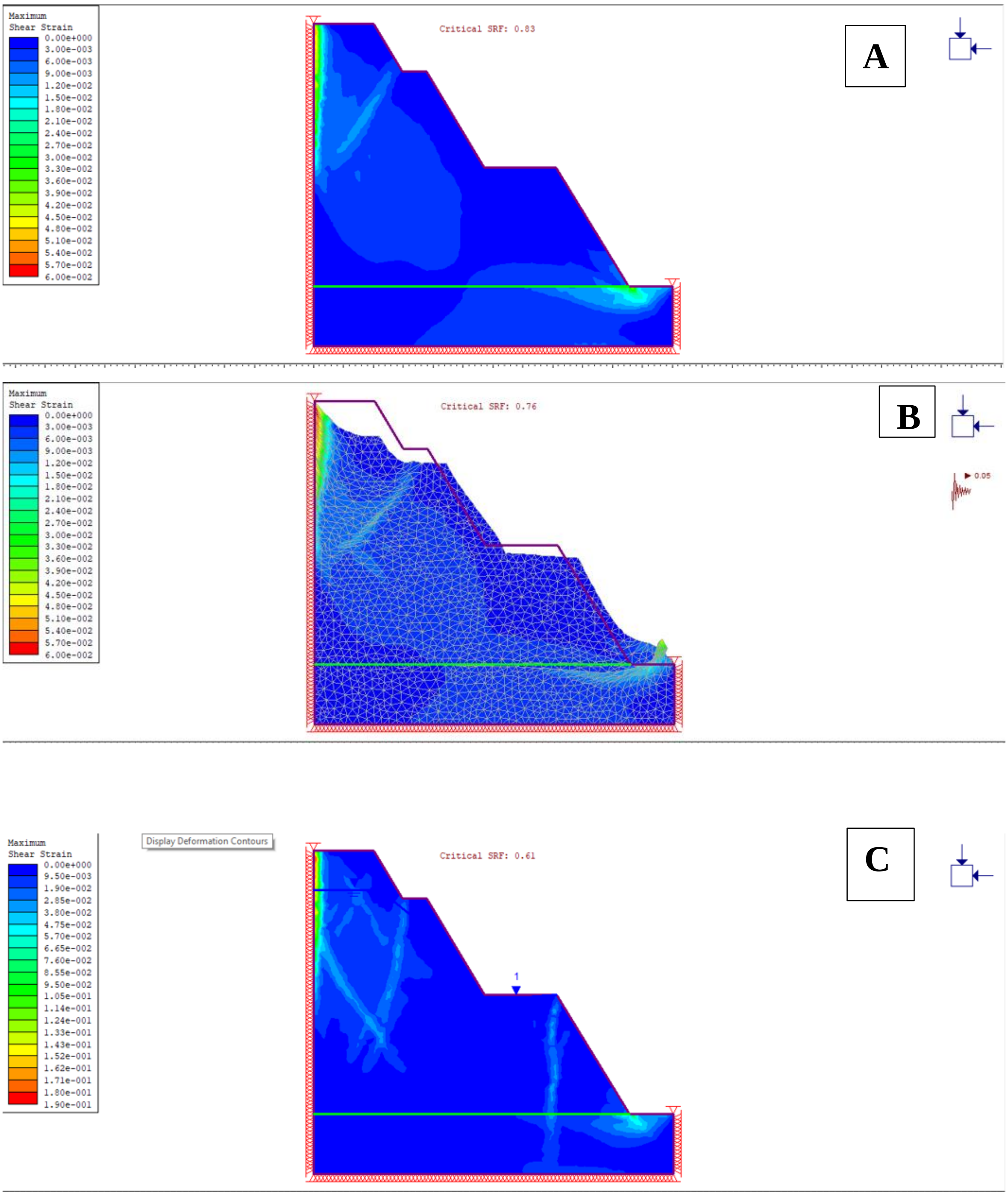
Maximum
Shear Strain
0.00e+000
3.00e-003
6.00e-003
9.00e-003
1.20e-002
1.50e-002
1.80e-002
2.10e-002
2.40e-002
2.70e-002
3.00e-002
3.30e-002
3.60e-002
3.90e-002
4.20e-002
4.50e-002
4.80e-002
5.10e-002
5.40e-002
5.70e-002
6.00e-002
Critical SRF: 0.83
A
Maximum
Shear Strain
0.00e+000
3.00e-003
6.00e-003
9.00e-003
1.20e-002
1.50e-002
1.80e-002
2.10e-002
2.40e-002
2.70e-002
3.00e-002
3.30e-002
3.60e-002
3.90e-002
4.20e-002
4.50e-002
4.80e-002
5.10e-002
5.40e-002
5.70e-002
6.00e-002
Critical SRF: 0.76
B
0.05
Maximum
Shear Strain
0.00e+000
9.50e-003
1.90e-002
2.85e-002
3.80e-002
4.75e-002
5.70e-002
6.65e-002
7.60e-002
8.55e-002
9.50e-002
1.05e-001
1.14e-001
1.24e-001
1.33e-001
1.43e-001
1.52e-001
1.62e-001
1.71e-001
1.80e-001
1.90e-001
Display Deformation Contours
Critical SRF: 0.61
1
C

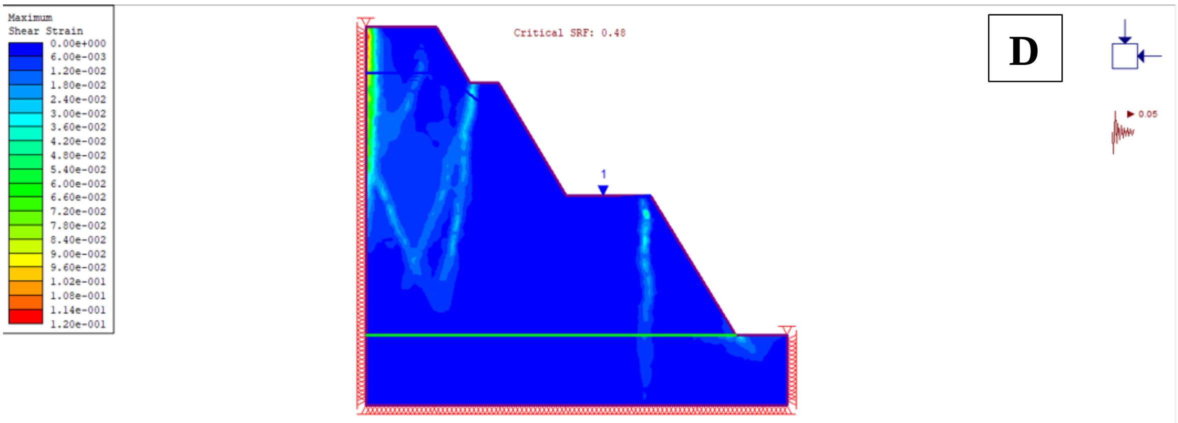

Figure 5.18 Finite element analysis non-homogeneous basalt dominated slope A) dry static condition with SRF = 0.83, B) dry dynamic condition with SRF = 0.76 C) wet static condition with SRF = 0.61 and D) wet dynamic condition with SRF = 0.48

5.5.2.2 non-homogeneous pyroclastic deposit with soil slope

The slope is characterized as an ash-pumice deposit and soil at the top and base. The slope was dominated by the deposit and has a gradient of 1.5H:1V with 32˚slope angel. From the analysis, the SRF value ranges from 0.11 to 0.64. The lowest value goes to the wet dynamic condition. The highest value of SRF represents the dry static condition.

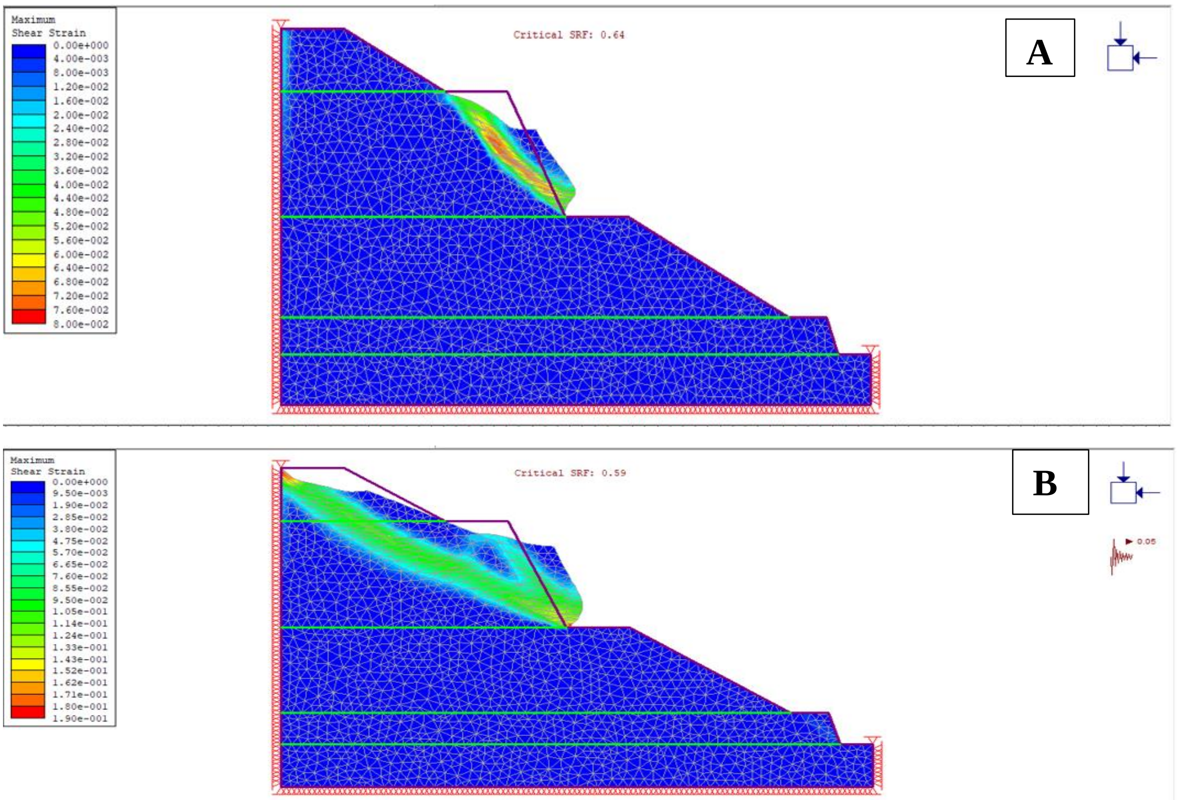

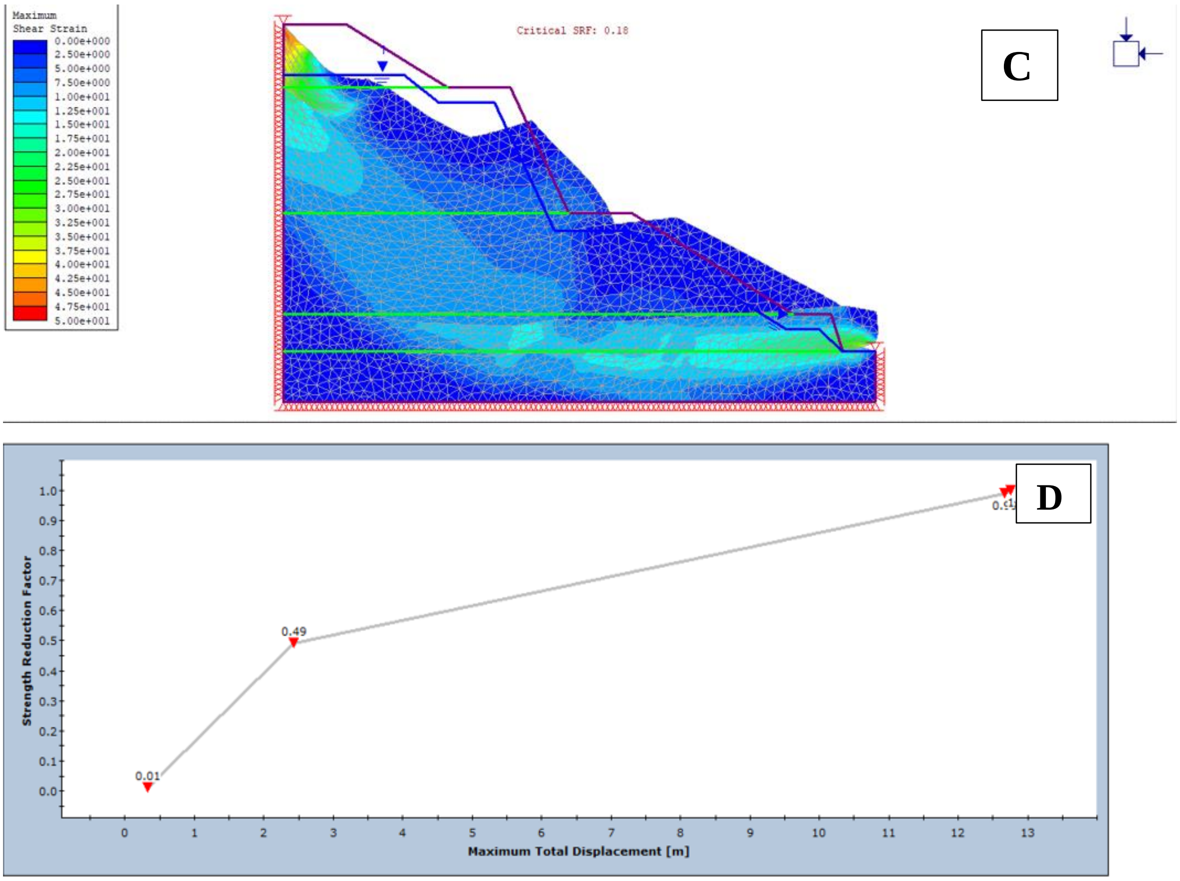

Figure 5.19 Finite element analysis pyroclastic deposit with soil slope model A) dry static condition with SRF = 0.64, B) dry dynamic condition with SRF = 0.59 C) wet static condition with SRF = 0.18 D) graph for wet dynamic condition showing the relationship between maximum total displacement with a strength reduction factor

5.4.3 Non-homogeneous slope with a weak layer

5.5.3.1 non-homogeneous rhyolite with weak layer slope

The slope comprises rhyolite rock with soil and pumice deposit, where the soil is shown as a sub horizontal layer to the rhyolite slope. The slope gradient of this section is 1H:1V, with a 57˚ slope angle. The FOS from the FEM ranges from 0.25 to 0.68, the smallest value goes to the wet dynamic condition and the highest value of SRF represents the dry static condition.

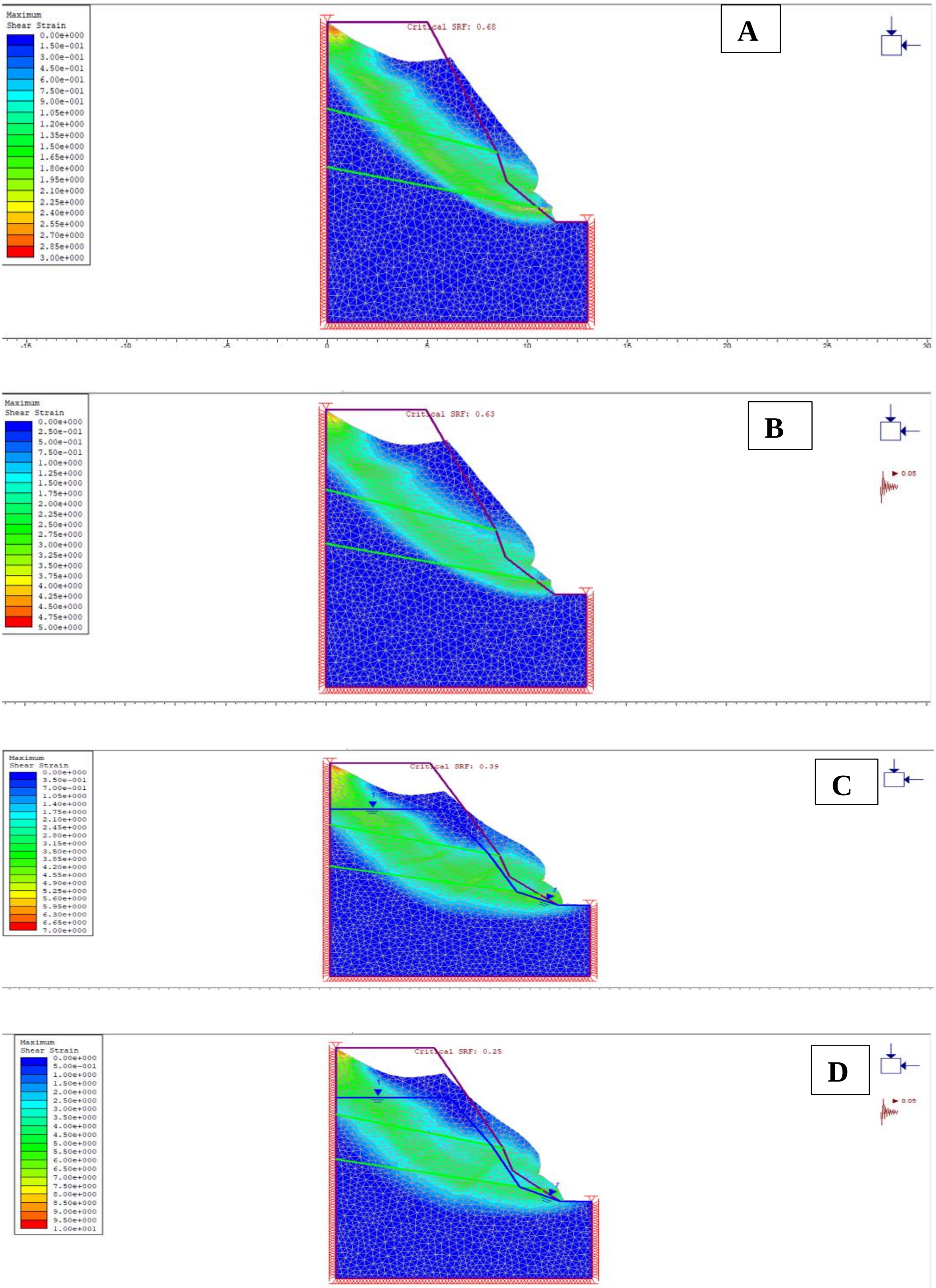

Figure 5. 20 Finite element analysis Non-homogeneous rhyolite slope with weak layer A) dry static condition with SRF = 0.68, B) dry dynamic condition with SRF= 0.63, C) wet static condition with SRF= 0.39 and D) wet dynamic condition with SRF= 0.25

5.5.3.2 Non-homogeneous Ignimbrite with weak layer slope

The slope is characterized by ignimbrite with a tuff deposit, tuff being the weak layer. The slope gradient is 1H:1V with a 50.7˚ slope angle. The SRF value ranges from 0.57 to 0.38, the smallest value represents the wet dynamic condition and the highest value represents the dry static condition.

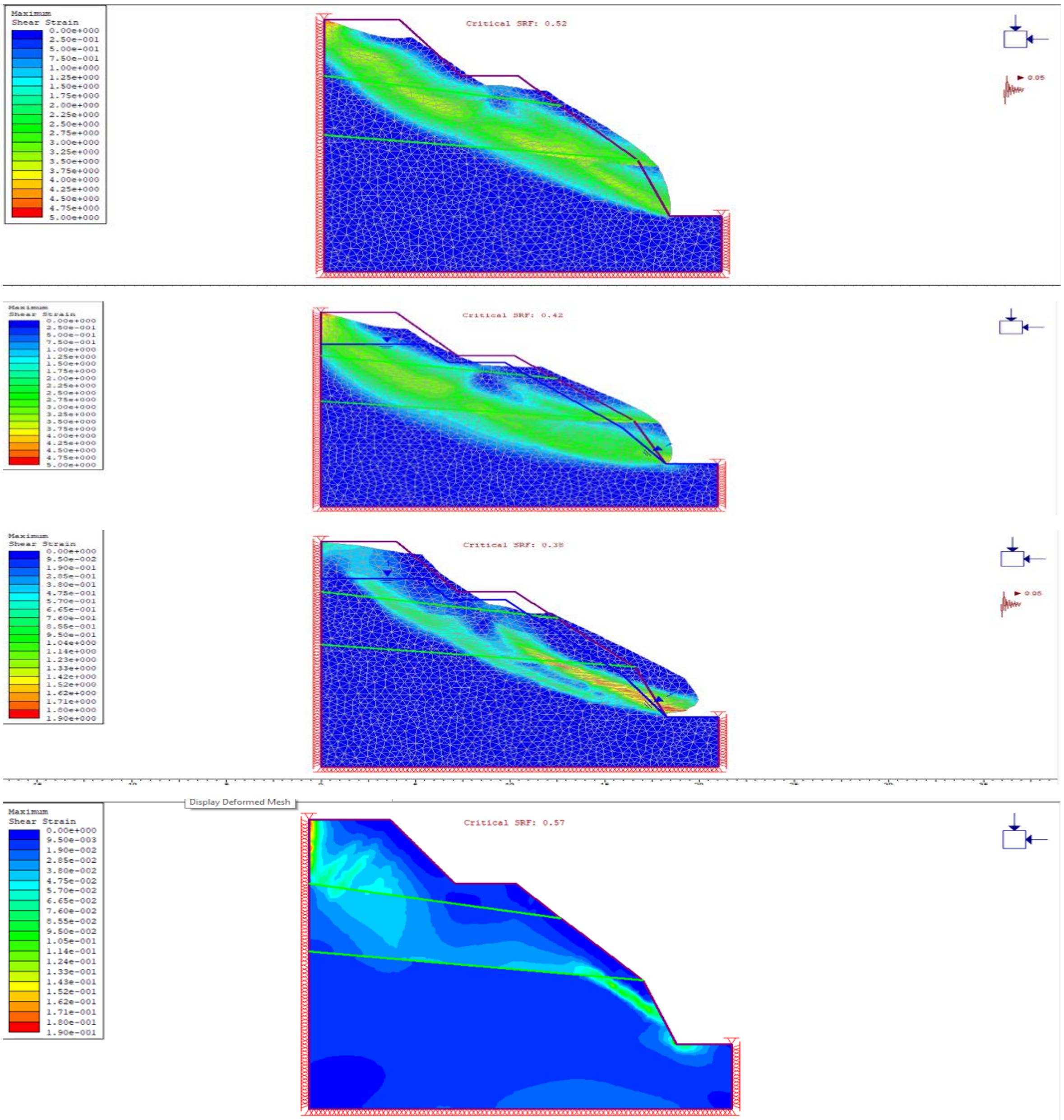

Figure 5. 21 Finite element analysis Non-homogeneous ignimbrite with weak layer slope, A) dry static condition with SRF=0.57, B) dry dynamic condition with SRF= 0.52, C) wet static condition with SRF= 0.42 and D) wet dynamic condition with SRF= 0.38 and with 6 node element slope model

5.6 Kinematic analysis

The analysis identified plane failure, toppling failure in both rock slopes, and one wedge failure. The slope section for the present study is classified into two, these are mainly covered by basalt slope (basalt -slope) and a slope covered by rhyolite flow (rhyolite slope). Table 5.5 shows the input parameters for kinematic analysis.

Table 5.5 Input parameters for kinematic analysis

		J1	J2	J3	J4	J5	J6	Estimated failure type	Slope
Rhyolite (RS4)	Dip amount	40˚	78˚	25˚	46˚	12˚	25˚	Toppling failure	57.2
	Dip direction	191˚	192˚	156˚	154˚	185˚	230˚		195.9
Basalt (RS5)	Dip amount	14˚	78˚	70˚	88˚	83˚	44˚	Planar failure	67˚
	Dip direction	166˚	162˚	177˚	161˚	53˚	166˚		181˚

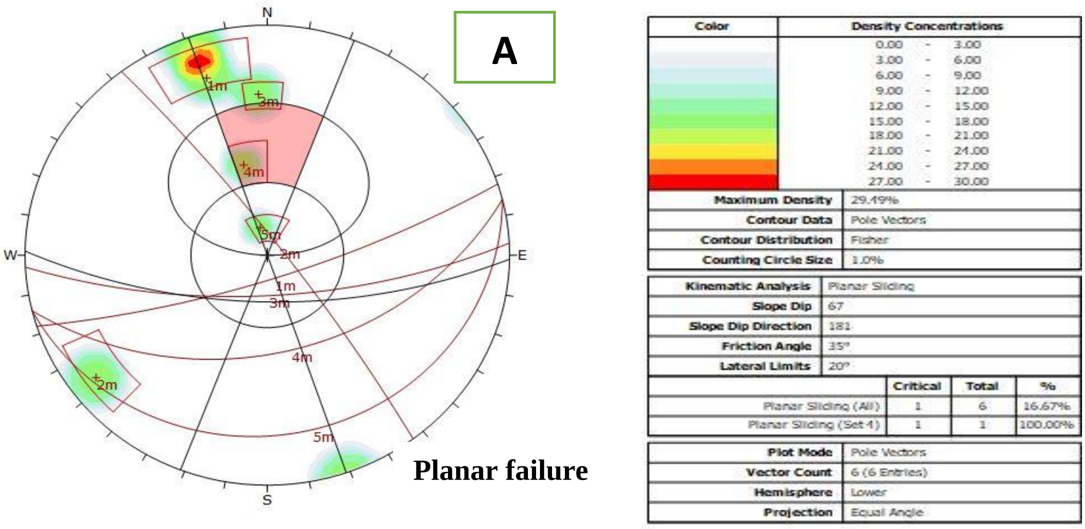

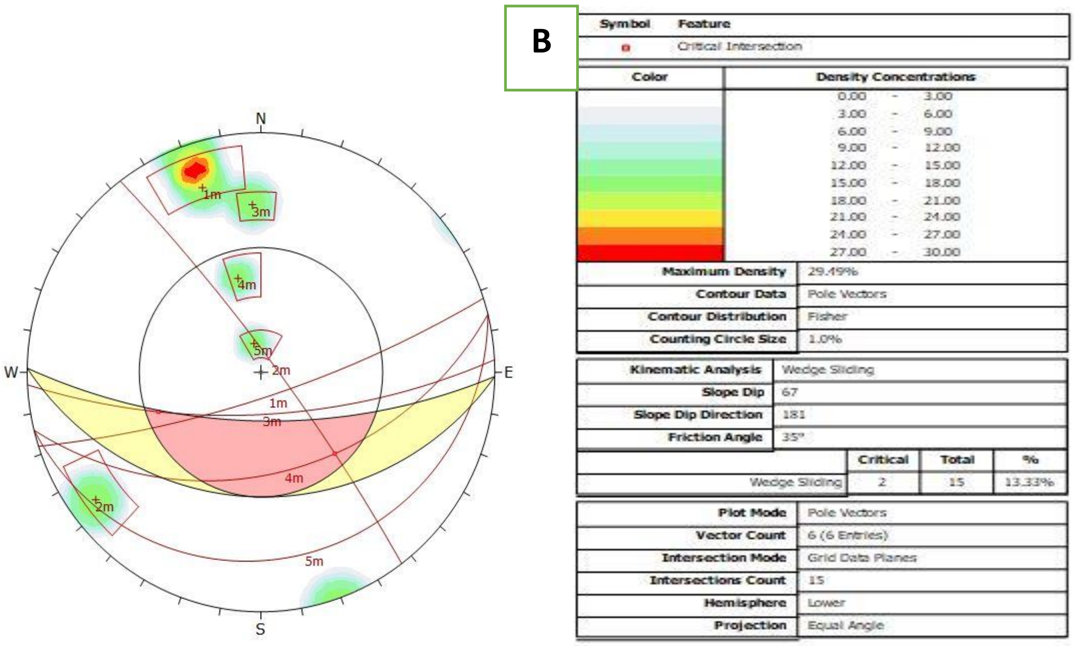

Wedge failure

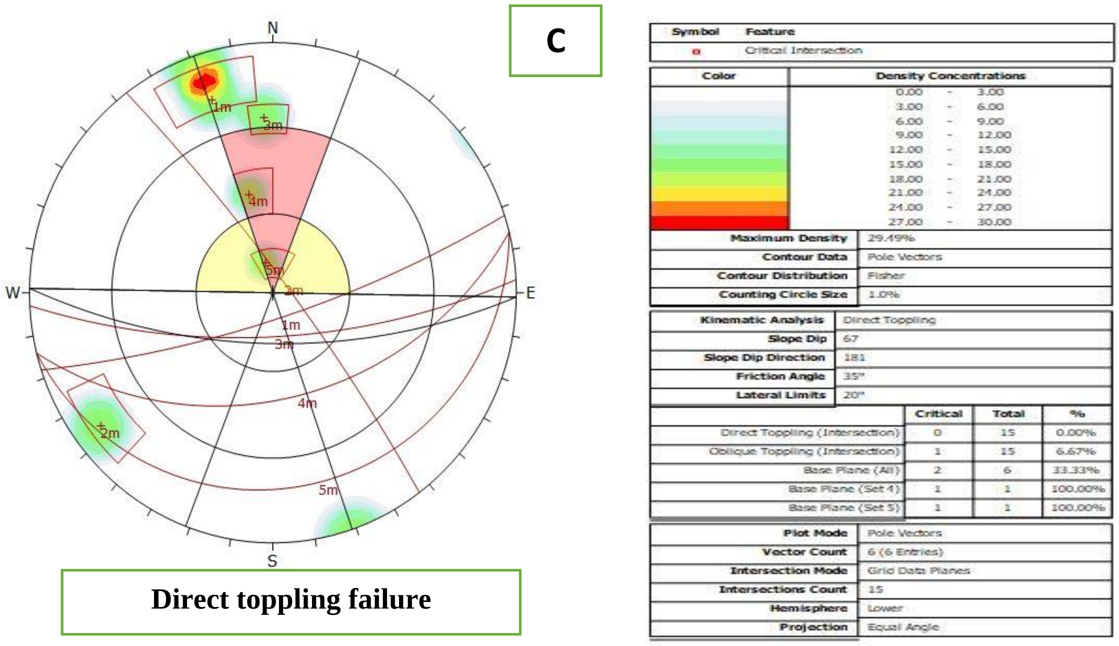

Direct toppling failure

Figure 5.22 kinematic analysis for basalt slope (RS5) A) stereographic projection of a planar failure, B) a stereographic projection showing a wedge failure, C) a stereographic projection for toppling failure and potential of failure for each failure mode

A

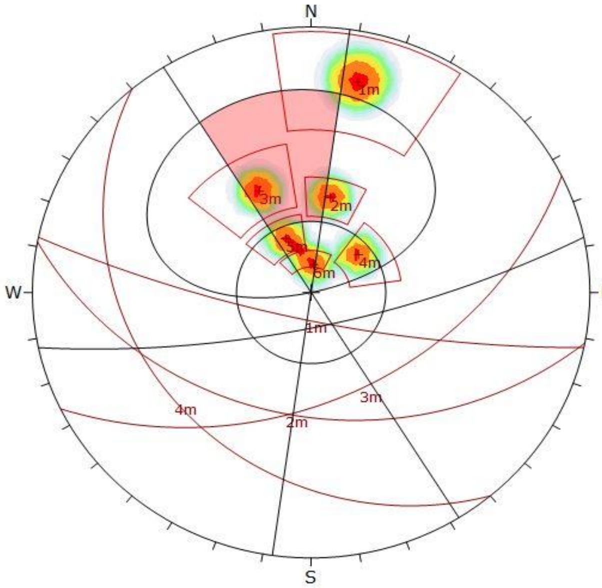

Color	Density Concentrations
	0.00 - 1.80
	1.80 - 3.60
	3.60 - 5.40
	5.40 - 7.20
	7.20 - 9.00
	9.00 - 10.80
	10.80 - 12.60
	12.60 - 14.40
	14.40 - 16.20
	16.20 - 18.00
Maximum Density	17.22%
Contour Data	Pole Vectors
Contour Distribution	Fisher
Counting Circle Size	1.0%

Kinematic Analysis	Planar Sliding		
Slope Dip	75		
Slope Dip Direction	168		
Friction Angle	30°		
Lateral Limits	20°		
	Critical	Total	%
Planar Sliding (All)	1	6	16.67%
Planar Sliding (Set 3)	1	1	100.00%

Plot Mode	Pole Vectors
Vector Count	6 (6 Entries)
Hemisphere	Lower
Projection	Equal Angle

Planar failure

B

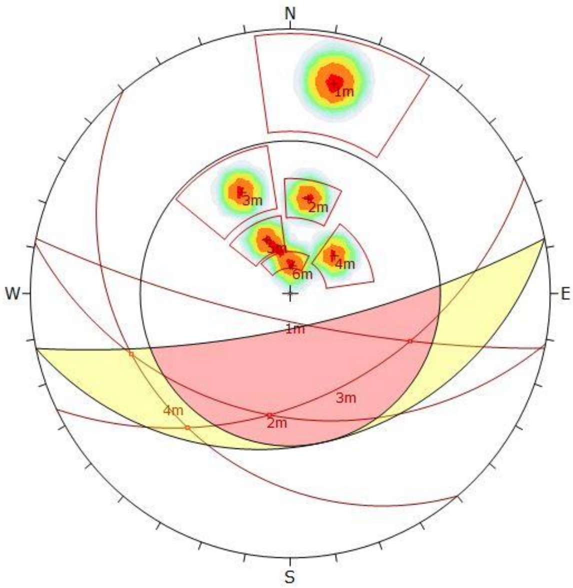

Symbol	Feature
▫	Critical Intersection

Color	Density Concentrations
	0.00 - 1.80
	1.80 - 3.60
	3.60 - 5.40
	5.40 - 7.20
	7.20 - 9.00
	9.00 - 10.80
	10.80 - 12.60
	12.60 - 14.40
	14.40 - 16.20
	16.20 - 18.00
Maximum Density	17.22%
Contour Data	Pole Vectors
Contour Distribution	Fisher
Counting Circle Size	1.0%

Kinematic Analysis	Wedge Sliding		
Slope Dip	75		
Slope Dip Direction	168		
Friction Angle	30°		
	Critical	Total	%
Wedge Sliding	4	15	26.67%

Plot Mode	Pole Vectors
Vector Count	6 (6 Entries)
Intersection Mode	Grid Data Planes
Intersections Count	15
Hemisphere	Lower
Projection	Equal Angle

Wedge failure

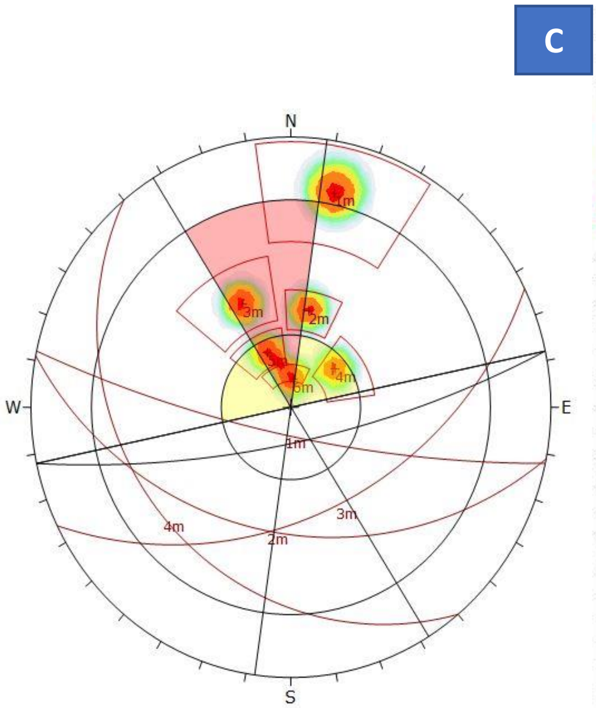

Symbol	Feature
▫	Critical Intersection

Color	Density Concentrations
	0.00 - 1.80
	1.80 - 3.60
	3.60 - 5.40
	5.40 - 7.20
	7.20 - 9.00
	9.00 - 10.80
	10.80 - 12.60
	12.60 - 14.40
	14.40 - 16.20
	16.20 - 18.00
Maximum Density	17.22%
Contour Data	Pole Vectors
Contour Distribution	Fisher
Counting Circle Size	1.0%

Kinematic Analysis	Direct Toppling
Slope Dip	75
Slope Dip Direction	168
Friction Angle	30°
Lateral Limits	20°

	Critical	Total	%
Direct Toppling (Intersection)	0	15	0.00%
Oblique Toppling (Intersection)	0	15	0.00%
Base Plane (All)	4	6	66.67%
Base Plane (Set 3)	1	1	100.00%
Base Plane (Set 4)	1	1	100.00%
Base Plane (Set 5)	1	1	100.00%
Base Plane (Set 6)	1	1	100.00%

Plot Mode	Pole Vectors
Vector Count	6 (6 Entries)
Intersection Mode	Grid Data Planes
Intersections Count	15
Hemisphere	Lower
Projection	Equal Angle

Toppling failure

Figure 5.23 Kinematic analysis for rhyolite slope (RS4), A) a stereographic projection for planar failure, B) a stereographic projection showing a wedge failure, C) a stereographic projection showing a toppling failure and potential failure percentage for each failure mode

5.6.1 Results for basaltic slope

From the interpretation of kinematic analysis, all types of failure were identified with a higher possibility of failure except a wedge failure with a lower possibility of failure compared to planar and toppling failure. The analysis was done using rocplane, swedge, and roctopple for planar failure, wedge failure, and toppling failure respectively. From the whole slope face, only one joint set 6 show a high possibility of failure, and its factor of safety range from 0.61 to 0.78. The wedge failure was observed between joint 2 and joint 4 with the possibility of failure at 16.67%. The toppling failure has a high possibility of failure only in direct toppling failure type, it was 0% possibility of failure in flexural toppling. The factor of safety for wedge failure ranges from 0.697 to 0.744 for different conditions. From the result, the seismic effect was low since it does not show a difference from the static condition.

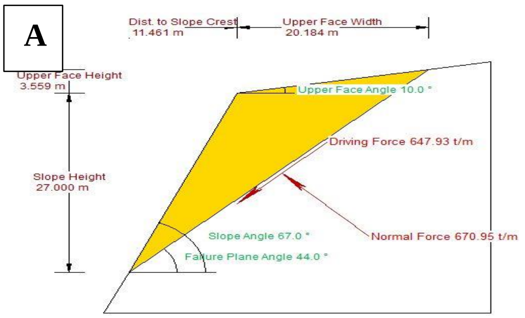

Factor of Safety	0.70
Driving Force	647.93t/m
Resisting Force	453.69t/m
Wedge Weight	932.73t/m
Wedge Volume	252.09m^3/m
Shear Strength	453.69t/m^2
Normal Force	670.95t/m
Plane Waviness	0.0°

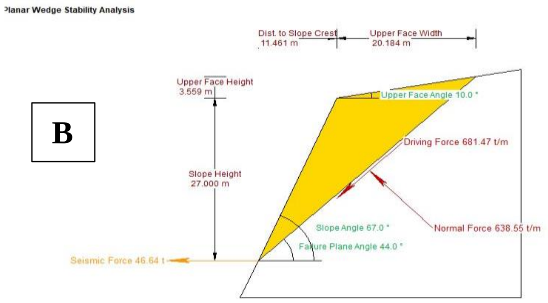

Factor of Safety	0.63
Driving Force	681.47t/m
Resisting Force	431.95t/m
Wedge Weight	932.73t/m
Wedge Volume	252.09m^3/m
Shear Strength	431.95t/m^2
Normal Force	638.55t/m
Seismic Force	46.64t
Plane Waviness	0.0°

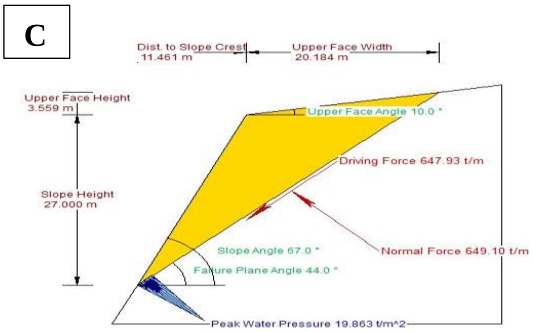

Factor of Safety	0.68
Driving Force	647.93t/m
Resisting Force	439.03t/m
Wedge Weight	932.73t/m
Wedge Volume	252.09m^3/m
Shear Strength	439.03t/m^2
Normal Force	649.10t/m
Plane Waviness	0.0°
Water Force on Failure Plane	21.85t/m

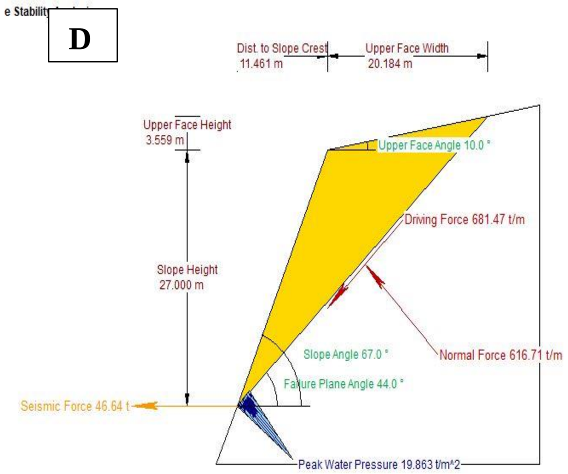

Factor of Safety	0.61
Driving Force	681.47t/m
Resisting Force	417.28t/m
Wedge Weight	932.73t/m
Wedge Volume	252.09m^3/m
Shear Strength	417.28t/m^2
Normal Force	616.71t/m
Seismic Force	46.64t
Plane Waviness	0.0°
Water Force on Failure Plane	21.85t/m

Figure 5.24 A planar failure with and without seismic and saturated condition, A) dry static condition B) dry dynamic condition, C) wet static condition and D) wet dynamic condition

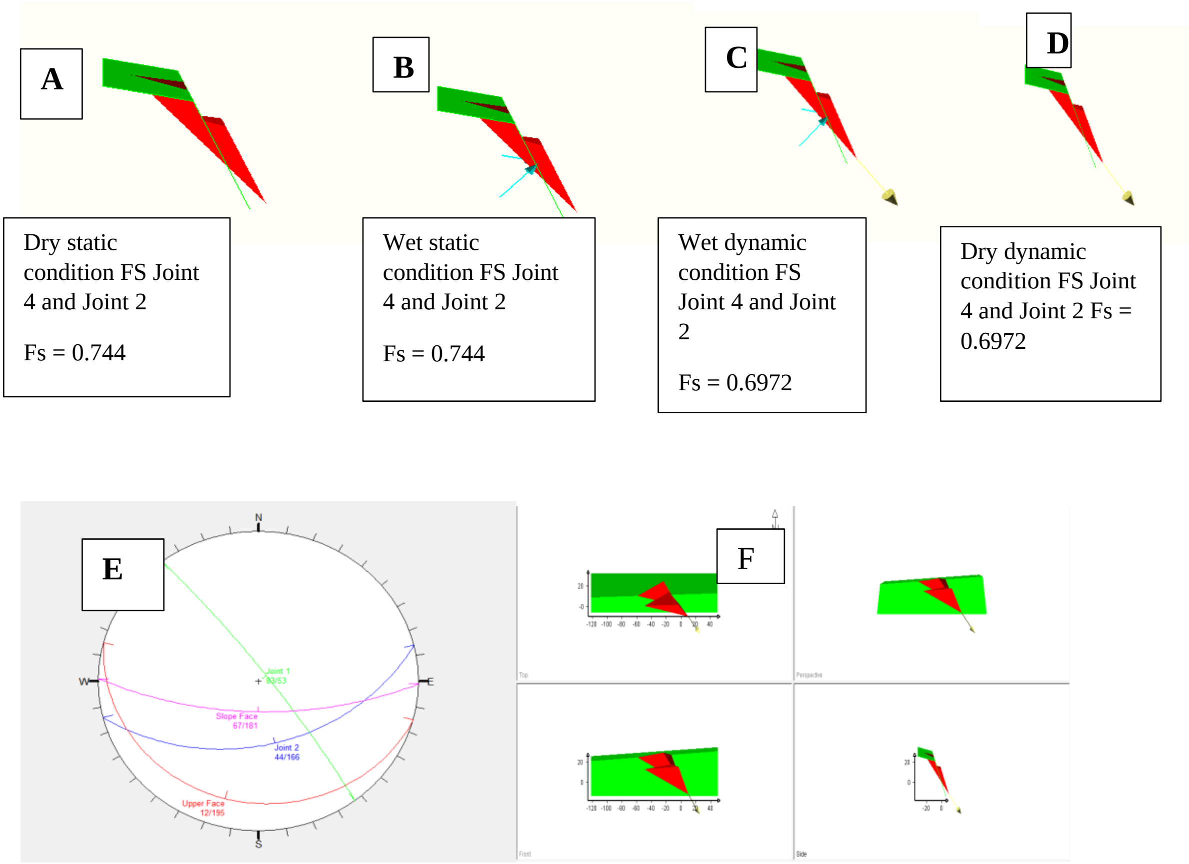

Figure 5.25 Wedge failure for case 1 (basaltic slope) for different conditions A) showing for dry static condition, B) wet static condition C) wet dynamic D) wet static condition E) stereographic projection for case 1 slope F) the whole view of the slope failure

5.6.2 Result for rhyolite slope

From the kinematic analysis result, the slope has two failure types, these are a planar and a direct toppling failure no wedge failure. Both failure types show a high percentage of failure. The planar failure was shown only in joint set 4, with the factor of safety ranging from 0.76 to 0.86.

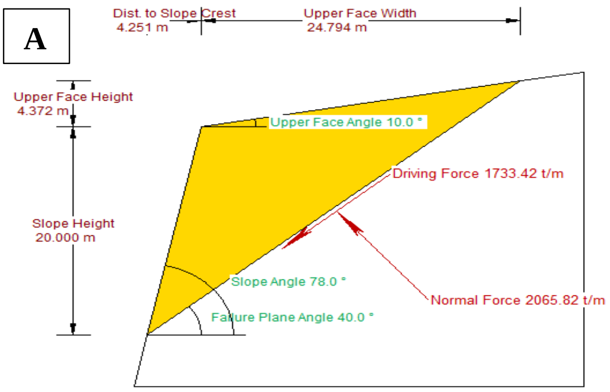

Factor of Safety	0.86
Driving Force	1733.42t/m
Resisting Force	1491.18t/m
Wedge Weight	2696.73t/m
Wedge Volume	238.65m^3/m
Shear Strength	1491.18t/m^2
Normal Force	2065.82t/m
Plane Waviness	0.0°

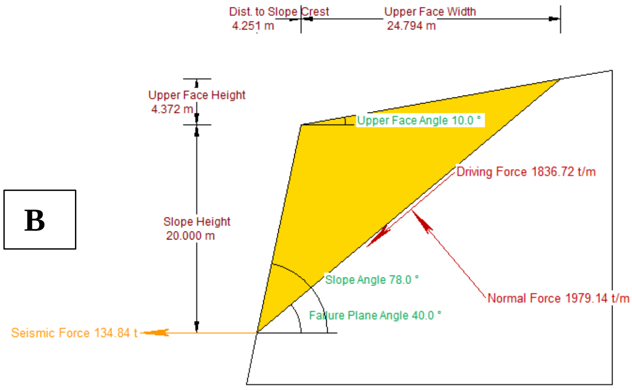

Factor of Safety	0.78
Driving Force	1836.72t/m
Resisting Force	1428.70t/m
Wedge Weight	2696.73t/m
Wedge Volume	238.65m^3/m
Shear Strength	1428.70t/m^2
Normal Force	1979.14t/m
Seismic Force	134.84t
Plane Waviness	0.0°

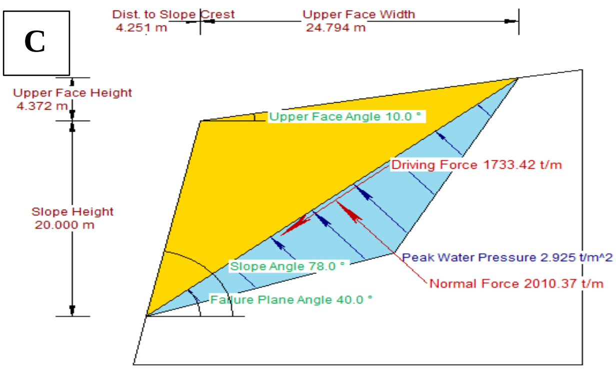

Factor of Safety	0.84
Driving Force	1733.42t/m
Resisting Force	1451.21t/m
Wedge Weight	2696.73t/m
Wedge Volume	238.65m^3/m
Shear Strength	1451.21t/m^2
Normal Force	2010.37t/m
Plane Waviness	0.0°
Water Force on Failure Plane	55.44t/m

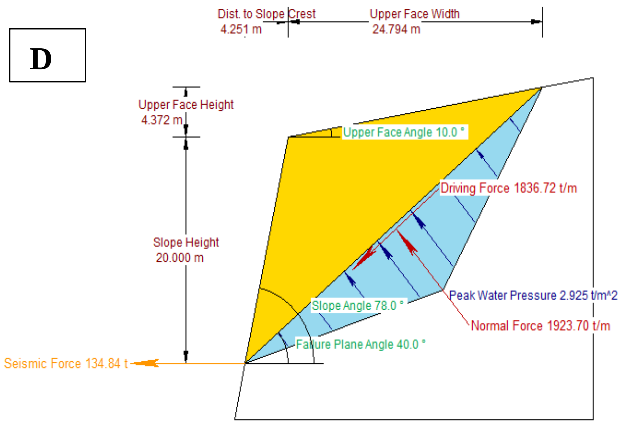

Factor of Safety	0.76
Driving Force	1836.72t/m
Resisting Force	1388.73t/m
Wedge Weight	2696.73t/m
Wedge Volume	238.65m^3/m
Shear Strength	1388.73t/m^2
Normal Force	1923.70t/m
Seismic Force	134.84t
Plane Waviness	0.0°
Water Force on Failure Plane	55.44t/m

Figure 5.26 Figure showing a planar failure with its factor of safety for different conditions, A) dry static B) Dry dynamic C) Wet static and D) wet dynamic conditions

Planar failure

The planar failure was shown in both sites, showing different percentages of the possibility of failure. The first slope that is characterized by mainly basalt rock has a 67˚ dip and 181˚ dip direction slope face. The output from dip software shows joint 6 with 44˚ dip and 166˚ dip direction as a critical surface with a percentage of failure of 100%. The data was interpreted in rocplane to determine the factor of safety with four conditions, these are dry-static, dry-dynamic, wet-static, and wet-dynamic conditions.

The other slope is a rhyolite rock slope with a 75˚ dip and 168˚ dip direction slope face. The critical surface from the dip software was joint set 3 with 46˚ dip and 154˚ dip direction showing 100% failure.

Wedge failure

Wedge failure was not shown in the field but the analysis showed a possibility of failure less than that of planar and toppling failure. The wedge failure in basalt slope were two critical surfaces with a 13.33% possibility of failure. The other, which is characterized as the rhyolite rock had four joint sets showing a wedge failure with a 26.67% possibility of failure.

Toppling failure

A kinematic test for toppling failure shows high possibility of failure in both sites up to 100%. For slope covered by basalt two joint sets and 4 joint sets for rhyolite slope showed potential of failure. Dip and dip direction of basalt's joints were 44˚/166˚(J6) and 83˚/53˚(J5), J3, J4, J5, and J6 of rhyolite slope were the critical surfaces that were shown as toppling failure.

5.7 Comparison of limit equilibrium method and finite element method

The analysis for different slope sections in the study area was done by limit equilibrium and finite element method. The factor of safety for the sections is close to the strength reduction factor of the same section. To compare the LEM and FEM the Janbu and SRF of the slope respectively were selected for different sections.

Table 5.6 Comparison of LEM with FEM for non-homogeneous pumice deposit

Methods	Dry static condition	Dry dynamic condition	Wet static condition	Wet dynamic condition
FOS (LEM)	0.647	0.591	0.255	0.301
SRF (FEM)	0.64	0.59	0.18	0.11

Table 5.7 Comparison of LEM with FEM of a homogenous rhyolite slope

Methods	Dry static condition	Dry dynamic condition	Wet static condition	Wet dynamic condition
FOS (LEM)	1.739	1.53	1.171	1.029
SRF (FEM)	1.79	1.59	1.03	0.96

Table 5.8 Comparison of LEM and FEM for homogeneous basalt slope

Methods	Dry static condition	Dry dynamic condition	Wet static condition	Wet dynamic condition
FOS (LEM)	1.102	1.022	0.930	0.852
SRF (FEM)	1.11	1.03	0.81	0.75

Table 5.9 Comparison of LEM and FEM for soil-1

Methods	Dry static condition	Dry dynamic condition	Wet static condition	Wet dynamic condition
FOS (LEM)	1.214	1.129	0.888	0.797
SRF (FEM)	1.19	1.12	0.961	0.86

Table 5.10 Comparison of LEM and FEM for non-homogeneous basalt slope

Methods	Dry static condition	Dry dynamic condition	Wet static condition	Wet dynamic condition
FOS (LEM)	0.877	0.810	0.774	0.665
SRF (FEM)	1.19	1.12	0.961	0.86

Table 5.11 Comparison of LEM and FEM for homogenous soil-2 slope

Methods	Dry static condition	Dry dynamic condition	Wet static condition	Wet dynamic condition
FOS (LEM)	1.29	1.165	0.996	0.882
SRF (FEM)	1.35	1.21	0.995	0.89

Table 5.12 Comparison of LEM and FEM for non-homogeneous ignimbrite-tuff deposit slope

Methods	Dry static condition	Dry dynamic condition	Wet static condition	Wet dynamic condition
FOS (LEM)	0.450	0.405	0.464	0.517
SRF (FEM)	0.57	0.52	0.42	0.38

Table 5.13 Comparison of LEM and FEM for non-homogeneous rhyolite-soil slope

Methods	Dry static condition	Dry dynamic condition	Wet static condition	Wet dynamic condition
FOS (LEM)	0.693	0.638	0.443	0.398
SRF (FEM)	0.68	0.63	0.39	0.25

The above tables and results of FOS obtained from LEM using the Janbu method and FEM using the shear strength reduction method showed a close values with 0.099 to 0.666 average difference. The FOS obtained from FEM is smaller than the FOS obtained from LEM with a minor difference.

CONCLUSION AND RECOMMENDATION

CONCLUSION

From the present study the following main conclusion has been made:

- The local geology of the study area is categorized into four lithologic units: basalt, sedimentary rocks, felsic rocks, and pyroclastic deposits. The study area is outcropped by Oligocene to Miocene volcanic rocks. The area is the makeup of different geological discontinuities, like faults, joints and exfoliation. These geological structures are developed in different units with diverse orientations. The orientations of the discontinuities are vertical to sub horizontal. The main structural feature observed in the study area was oriented in the NW-SE direction.
- The slope surface around the road section is mainly characterized by unwelded pyroclastic deposits, unconsolidated sediments, and weathered rocks that have a high possibility of failure.
- Along the road sections; eight critical slope sections were selected. Out of which six of them are rock slopes and the other two slopes are soil mass. The subsurface conditions of the critical slope section studied through six boreholes and seismic refraction which is helped to classify into three lithological layers namely; (1) top soils and pyroclastic deposit with 10m thickness (2) weathered and fractured rock (20m thickness) and (3) bed rock.
- As part of geotechnical characterization of the rock slope both disturbed and remolded sample were collected from 2 pit excavations. The dominant soil type in the site is clayey gravel soils which brown in color with a specific gravity of 2.68, natural water content of 3.6%, plastic limit 31.93, liquid limit value of 51.983. The optimum moisture content was 11%, and maximum dry density with the value of 1.5g/cm3. The direct shear test result showed the cohesion and friction angle 12.2KN/m^2 and 30.5° respectively. Similarly, for all rock units observed in the critical slope sections including tuff, ignimbrite, rhyolite, basalt and unwelded tuff are identified and their respective point load strength, dry and saturated density and slake durability were determined.
- The critical slope sections were analyzed using limit equilibrium, finite element and kinematic analysis method. Two structurally controlled rock slope failure have been

identified and each of them showed a planar and a toppling failure. The factor of safety and SRF were obtained from limit equilibrium and finite element methods.

- The analysis was done for four conditions, these are dry-dynamic, dry-static, wet-static, and wet-dynamic. The effect of the loading condition on the slope showed a high difference in the value of FOS. A wet dynamic condition has the smallest value compared to other conditions and the dry static condition has the highest value in the entire slope stability analysis. Moreover, the effect of the seismic condition is high. Generally, the slope is more sensitive to mechanical properties, physical properties, and loading conditions than slope height.

RECOMMENDATION

Based on site investigation, laboratory test result and numerical analysis result of the critical slope section the following are recommended:

- Further detail geotechnical investigation particularly on shear strength behavior of soils under saturated conditions is needed to analyze their effect on slope stability. For better understanding of the failure surface and factor of safety of the slope further research can be carried out by physical modeling and finite difference method of analysis. Detailed investigation in stabilization analysis is recommended including shotcrete, soil nailing and drainage system installations. A further study about the groundwater condition is essential since the assumption of a water table depth of 4.70m may not be realistic in the factor of safety determination. Slope stabilization techniques for proposed slope sections: - Preparing a drainage system, planting shrubs and grasses to reduce soil erosion and proving a bench and berm system at the slope head and toe is recommended.

RESEARCH FUND ACKNOWLEDGMENT

This research project is funded by Adama Science and Technology University under grant number ASTU/SM-R/394/22, Adama, Ethiopia.

REFERENCES

Abramson, A. R. (2002). *Interface and strain effects on the thermal conductivity of heterostructures.* J. Heat Transfer.

Amritpal Kaur, S. R. (2016). *SLOPE STABILITY ANALYSIS TECHNIQUES:.*

Ashkan Gholipoor, A. H. (2015). The Effects of Various Factors on Slope Stability.

authority, E. r. (2013). *Geotechnical design manual.* Addis Ababa: FEDERAL DEMOCRATIC REPUBLIC OF ETHIOPIA.

Azeze, A. W. (2020). *Assessments of Geotechnical Condition of Landslide Sites and Slope Stability Analysis Using Limit Equilibrium Method around Gundwin Town Area, Northwestern Ethiopia.*

Bacicn, B. (2014). *Slope stability analysis.*

Beicip. (1990). *Landsat structural study of southwest Ethiopia, Gambela-Omo area.* unpl. Report, Petroleum Operations Department.

Berhe, S. B. (1987). *Geology, Geochronology and Geodynamics implications of Cenozoic magmatic provinces in Wand SE, Ethiopia.* Geological society London.

Bieniawski, Z. T. (1989). *Engineering rock mass classifications: a complete manual for engineers and geologists in mining, civil, and petroleum engineering.* John Wiley & Sons.

Bosselini, A. (1989). *The Continental Margin of Somalia: their structural evolution and.* Memorie Di Sciencze Geologsche.

Burman. A, S. P. (2015). *Comparative study of slope stability anlysis using traditional limit equilibrium method and finite element method.*

Cannon, R. T. (1981). *The proto Indian Ocean and a probable Paleozoic/ Mesozoic triradial rift system in East Africa.* Earth and Planetary Science Letters.

Carol Matthews and Zeena Farook, A. a. (2014). *Slope stability analysis – limit equilibrium or the finite element method?* ground engineering.

Davidson, A. (1984). *Reconnaissance geology and geochemistry of Illubabor, Keffa, Garno Gofa and Sidamo, Ethiopia.* Addis Ababa.: EIGS Bulletin 2.

de Coulomb, C. A. (1972). *Coulomb's Memoir on Statics: An Essay in the History of Civil Engineering.* Cambridge University Press.

De Mulder et. al, E. H. (2012). Sustainable Development and Management of the Shallow Subsurface. *The Geological Society, London. ISBN: 978-1-86239-343-1*, 192.

Digvijay P. Salunkhe, G. C. (2017). *An Overview on Methods for Slope Stability.* International Journal of Engineering Research & Technology (IJERT).

Digvijay P. Salunkhe, G. C. (2017). *An Overview on Methods for Slope Stability.* International Journal of Engineering Research & Technology (IJERT), Vol. 6 Issue 03.

Dulbal. (2020). *seismic zone of ethiopia according to EBCS-8:95.* https://data-humdata.org/.

Duncan, J. a. (2005). *Soil Strength and Slope Stabilty.* John Wiley & Sons.

Guide, A. (2002). *The Stabiity of the Slope.*

Hack, R. (2016). *Slope Stability by Classification SSPC RMR GSI.*

Hoek E, B. E. (1980). *Empirical strength criterion for rock masses.* .

Hoek E, C.-T. C. (2002). *Hoek-Brown Failure criterion-2002 edition.* Toronto: Proceedings of the North American Rock Mechanics Symposium.

Hoek, E. &. (1981). *Rock slope engineering.* CRC Press.

K.M. Bushira, Y. G. (2018). *Cut soil slope stability analysis along national highway at wozeka–gidole road, Ethiopia, model.*

Khaled Farah et.al, M. L. (2015). *The study of probabilistic FEMs for a slope reliability analysis using the stress fields.* The Open Civil Engineering Journal.

Li, A. J. (2008). *Stability charts for rock slopes based on the Hoek–Brown failure criterion.* International Journal of Rock Mechanics and Mining Sciences.

Mahmud Sazzad, M. M. (2017). *STABILITY ANALYSIS OF SLOPES FOR HOMOGENEOUS AND LAYERED* .

Marinos, P. a. (2000). *GSI: a geologically friendly tool for rock mass strength estimation.* In ISRM international symposium. OnePetro.

Mengesha Tefera, T. C. (1996). *Explanation to the Geological map of Ethiopia.* Ethiopian Institute of Geological Survey.

Merifield RS, L. A. (2006). *Limit analysis solutions for the bearing capacity of rock masses using the generalised Hoek-Brown criterial.* Int J Rock Mech Min Sci .

Merla, G. A. (1979). *The Geology of Ethiopia and Somalia; with accompanied map of 1:2000000.*

Mohr, P. (1963). *The Geology of Ethiopia.* . Univ. Coll. Of Addis Ababa press.

N, B. (2002). *Some new Q-value correlations to assist in site characterisation and tunnel design.* Int J Rock Mech Min Sci.

Nelson, S. A. (2013). *Slope Stability, Triggering Events, Mass Movement Hazards.*

Pourhosravani, A. (2011). *A Review of Current Methods for Slope.* Journal of Geotechnical Engineering .

Rocscience. (2004). A New Era in Slope Stability Analysis: Shear Strength Reduction. *Rocscience* .

S.P. Pradhan, T. S. (2020). *Stability assessment of landslide-prone road cut rock slopes in Himalayan terrain: a finite element method based approach.*

Sangrey, M. N. (1978). *Methods of stability analysis.* Transportation Research Board Special Report.

Sangrey, M. R. (1978). *Methods of stability analysis, Chapter 7. Landslides—Analysis and Control.* Washington DC: National Academy of Sciences.

Shi, G. H. (1989). *Generalization of two-dimensional discontinuous deformation analysis for forward modelling.* International Journal for Numerical and Analytical Methods in Geomechanics,.

Stead, D. &. (2015). *A critical review of rock slope failure mechanisms: the importance of structural geology*. Journal of Structural Geology, 74, 1-23.

Tadlwos Chernet, W. H. (1996). *EXPLANATION OF THE GEOLOGICAL MAP OF ETHIOPIA Scale 1:2,000,000 2.. edition.* Addis Ababa: ETHIOPIAN INSTITUTE OF GEOLOGICAL SURVEYS.

v2.0.0, P. D. (2022). *climatology data of southwestern ethiopia.* available at: https://power.larc.nasa.gov/.

Valenta, J. M. (2021). *Ground fissures within the Main Ethiopian Rift: Tectonic, lithological and piping controls.* Earth Surface Processes and Landforms, 46(15), 3158-3174.

viwer, N. d. (2022). *Climatology data for southwestern Ethiopia.* Available at http://power.larc.nasa.gov/.

Woldearegay, K. (2013). *Review of the occurrences and influencing factors of landslides in the highlands of Ethiopia: With implications for infrastructural development.* Momona Ethiopian Journal of Science, 5(1), 3-31.

Worikineh Haro et al., A. B. (2010). *Geological map of the Jima Area.* Geological Survey of Ethiopia.

Workneh Haro, A. B. (2012). *GEOLOGY, GEOCHEMISTRY, AND GRAVITY SURVEY OF JIMA AREA.* Addis Ababa.

Wube, K. B. (2003). *REPORT ON THE GEOLOGY AND HYDROCARBON POTENTIAL OF GOJEB-CHIDA-LALA AREAS SOUTH WEST ETHIOPIA.*

Wyllie, D. C. (2004). *Rock slope engineering.* CRC Press.

Yang., H. (2021). *An overview of slope stability.*

ZT, B. (1976). *Rock mass classification in rock engineering.* . Balkema: Cape Town: Proceedings of the rock mechanics symposium.

APPENDICES

Appendix 1: Soil property determination

Appendix 1.1 Natural moisture content determination of test pit-1

Natural water content is determined from laboratory tests. Natural soil is put in the oven and the dry sample is measured and water content is the mass of water to the ratio of the mass of soil. it is expressed in percentages.

Specimen no	1	2	3
Moisture can id	E-16	C-16	C-25
Mc = mass of empty can	39.4	24.2	22.8
Mcms = mass of can + moist soil	73.9	74.6	75.6
Mcds = mass of can + dry soil	72.8	72.8	73.7
Ms = mass of soil solid	33.4	48.6	50.9
Mw = mass of pore water	1.1	1.8	1.9
W%	3.3	3.7	3.73

Calculation

Mw = moist soil – dry soil

$$Ww = \frac{weight\ of\ water}{weight\ of\ soil\ solid} \times 100$$

Appendix 1.2 Specific gravity determination test pit-1

The specific gravity of soil was determined from the weight of soil to the weight of water using the density bottle procedure.

Calculation

Specific gravity = $\frac{weight\ of\ a\ soil\ solid}{weight\ of\ water}$

Mass of a dry soil = 10g	Trial 1	Trial 2	Trial 3
Bottle id	38	57	75
Mass of a bottle (g)	35.4	35.6	35.8
Mass of bottle + dry soil (g)	45.4	45.6	45.8
Mass of a bottle + dry soil + water (g)	139.7	141.4	143
Mass of a bottle + water (g)	133.4	135.2	136.7
Specific gravity	2.703	2.632	2.703

Appendix 1.3 Raw data sieve test for test pit-1

Sieve no	Opening (mm)	Weight of empty sieve (A)	Weight of sieve and weight of soil retained (B)	Weight of soil retained (B-A)	Percent of retained	Cumulative retained	Percent of passing
4	4.75	560.6	575.6	15	3	3	97
10	2.00	525.5	595.9	70.4	14.1	17.1	83
	1.18	503.1	573.1	70	7.6	24.7	75.3
20	0.85	468.9	506.8	38	22.12	46.82	53.2
40	0.425	447.6	558.2	110.6	6	52.82	47.2
60	0.25	414.8	444.7	30	8.42	61.24	38.2
100	0.15	397.9	440	42.1	14	75.24	24.8
200	0.075	391.2	457.8	66.6	13.32	88.56	11.5
Pan	-	379.7	436	56.3	11.25	99.8 =100	0
Total				500			

Appendix 1.4 Raw data of hydrometer test for test pit -2

Elapsed time in (min)	Hydrometer reading (R_h)	R'_h=(R_h+C_m)	Corrected hydrometer reading, R_{h1}= R'_h+(Ct-Cd)	L, effective depth	K	L/T	Particle size D=K√L/T (mm) 0.075	Percent finer N%	% Finer on the total wt. N 11.46
30''	46	47	41.65	8.592	0.0131	17.18	0.054	82.467	9.45
1'	44	45	36.65	8.92	0.0131	8.92	0.039	78.507	8.99
2'	43	44	38.65	9.084	0.0131	4.542	0.0279	76.527	8.77
4'	41	42	36.65	9.412	0.0131	2.353	0.0201	72.567	8.32
8'	38	39	33.65	9.904	0.0131	1.238	0.015	66.627	7.63
15'	34	35	29.65	10.56	0.0131	0.704	0.011	58.707	6.73
30'	31	32	26.65	11.052	0.0131	0.36	0.008	52.767	6.04
1 hr	27	28	22.65	11.708	0.0131	0.19	0.006	44.847	5.14
2hr	24	25	19.65	12.2	0.0131	0.10	0.004	38.907	4.46
4hr	21	22	16.65	12.692	0.0131	0.053	0.003	32.967	3.77
24hr	15	16	10.65	13.676	0.0131	0.009	0.0012	21.087	2.41

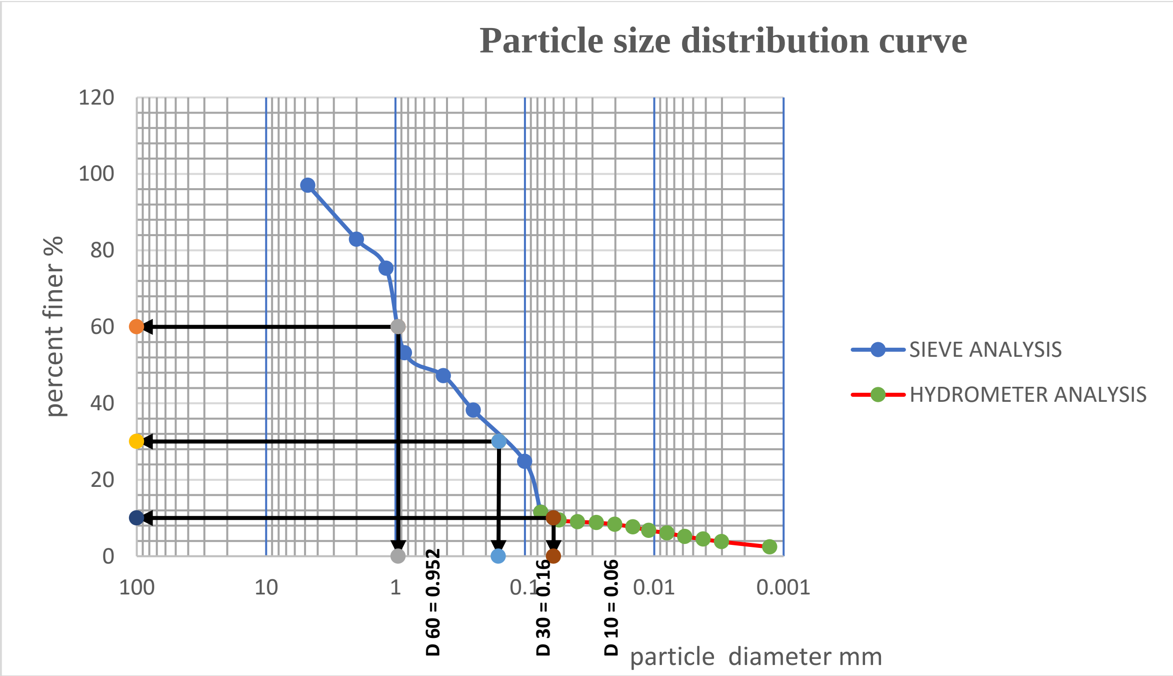

Appendix 1.5 Raw data for Atterberg test for test pit -1

Appendix 1.5.1 liquid limit test for test pit -1

Sample no	1	2	3	4
Mc = mass empty can	23.8	24.1	24.3	23.8
Mcms = mass of can + moist soil	41.3	48.7	45.5	38.2
Mcds = mass of can + dry soil	35.2	40.3	38.2	33.3
Ms = mass of soil solid	11.4	16.2	13.9	9.5
Mw = mass of pore water	6.1	8.4	7.3	4.9
W%	53.51	51.852	52.52	51.58
No of drops	17	25	22	28

Appendix 1.5.2 Plastic limit test for test pit -1

Sample no	1	2	3	4
Mc = mass of empty can	24.3	23.6	23.4	38.1
Mcms = mass of can + moist soil	26.7	32.3	27.7	41.7
Mcds = mass of can + dry soil	26	30.4	26.6	41
Ms = mass of soil solid	1.7	6.8	3.2	2.9
Mw = mass of pore water	0.7	1.9	1.1	0.7
W%	41.2	28	34.37	24.14

Appendix 1.5 Compaction test data and result

Appendix 1.5.1 Compaction test Raw data for test pit-1

sl no	Water added (ml)	Wt. of mold with soil	Water content determination				Wt. of soil (gm)	Bulk density (γ) in gm/cc	Dry density (γd) gm/cc
			Empty wt. of container (gm) W1	Wt. of container +soil (gm) W2	Wt. of container + dry soil (gm)W3	W%			
1	50	6960	22	166.70	156.3	0.077	1471	1.56	1.45
2	100	7050	24	142.9	130.9	0.112	1561	1.65	1.49
3	100	7139	21	138.2	122.1	0.159	1650	1.75	1.51
4	100	7222	22	156.6	135.1	0.190	1733	1.84	1.54
5	100	7317	23	151.00	127.4	0.226	1828	1.94	1.58
6	100	7270	21	156.00	121.5	0.343	1781	1.89	1.4

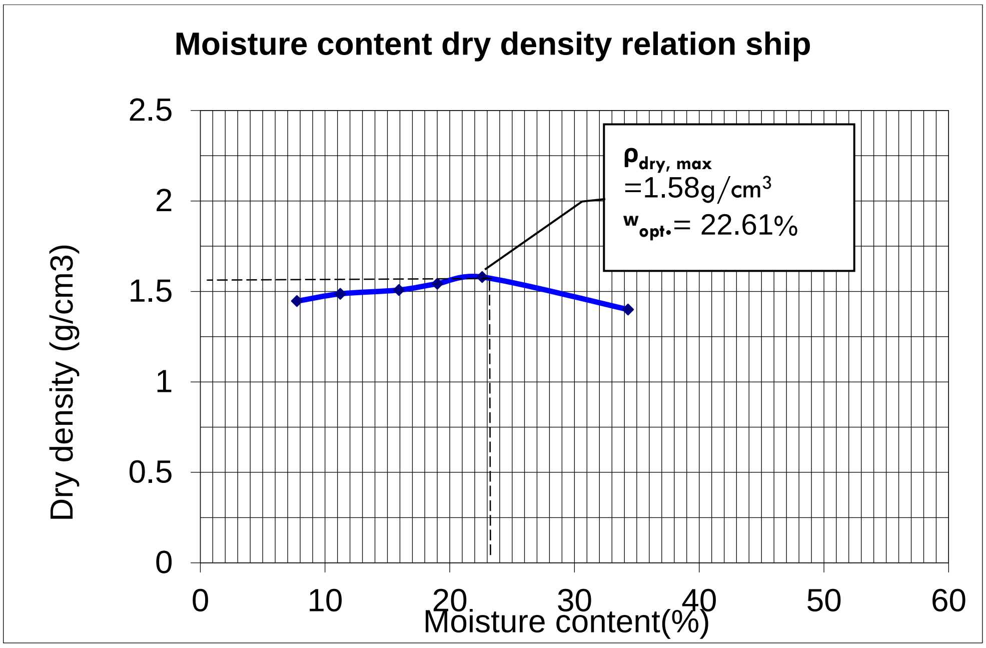

Appendix 1.5.2 Compaction test Raw data for test pit-2

Trial no.	1	2	3	4	5
Wt. of mold	5489	5489	5489	5489	5489
Wt. of wet soil + wt. of mold	6968	7046	7209	7309	7259
Wt. of wet soil	1479	1557	1720	1820	1770
Volume of mold, cm^3	944	944	944	944	944
Bulk density,BD	1.57	1.65	1.82	1.93	1.88
Trial no.	1	2	3	4	5
Wt. of can	22.2	22	24.1	21.2	23
Wt. of wet soil + wt. of can	115.1	120	127	127	141
Wt. of dry soil + wt. of can	104.3	104.8	107.1	104.3	107.3
Moisture content, MC	0.132	0.184	0.240	0.273	0.400
Dry density, DD	1.38	1.39	1.47	1.51	1.34

Test Method: AASHTO T-99 [Using Standard Effort]						
Moisture Content Vs Dry Density Computation Table						
Determination No.	1	2	3	4	5	
Bulk density	1.57	1.65	1.82	1.93	1.88	
Water Content, %	13.15	18.36	23.98	27.32	39.98	
Dry density	1.38	1.39	1.47	1.51	1.34	

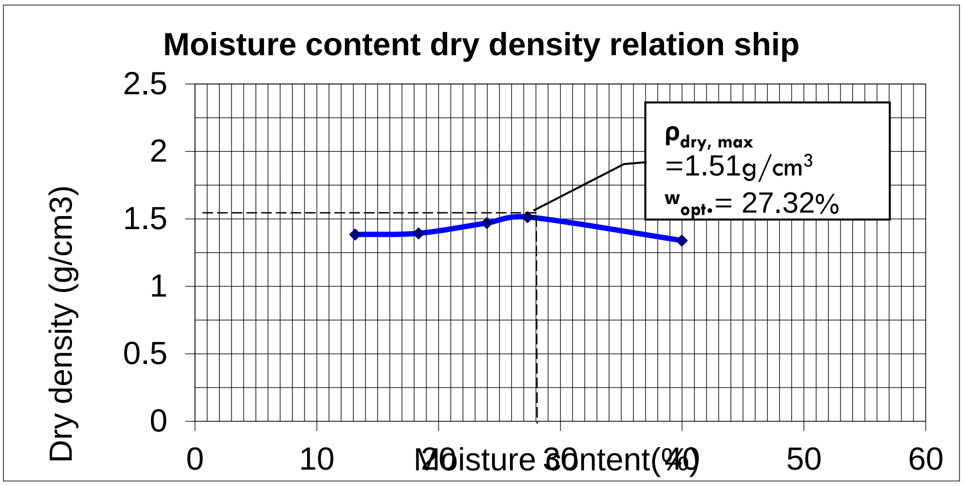

Appendix 1.6 Raw data and results for direct shear test

Appendix 1.6.1 Direct shear test for test pit -1

Horizontal displacement (mm)	Shear load (N) 100kpa	Shear load (N) 200kpa	Shear load (N) 300kpa
0.0	00	00	00
0.5	11	15	17
1	13	19	22.5
1.5	15	23	25
2	16.5	26.5	27
2.5	17.5	29	30
3	18	31	32.5
3.5	18.5	33	33
4	20	35	34.5
4.5	20	36	35
5	20	37	36
5.5	20.5	38.5	37
6	20.5	40	39.5
6.5	20.5	41	42
7	20.5	42	44
7.5	21	43	46.5
8	21	44	48
8.5	21.5	45.5	50.5
9	22	46.5	53
9.5	21	47.5	56.5
10	20.5	48.5	58
10.5		49.5	61
11			61

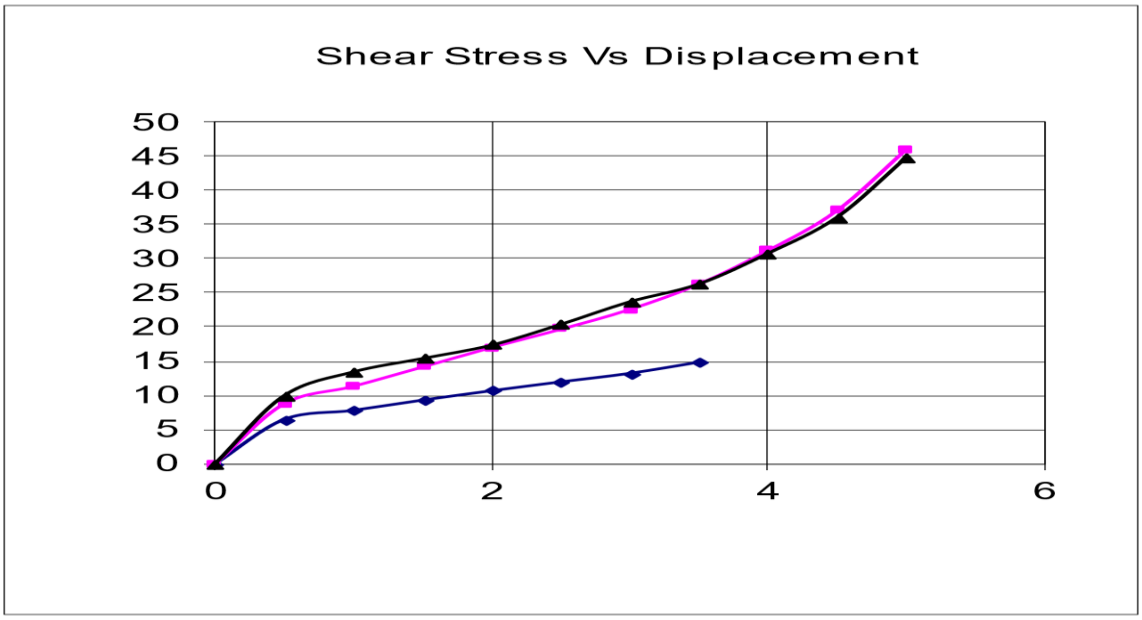
Shear Stress Vs Displacement
50
45
40
35
30
25
20
15
10
5
0
0
2
4
6

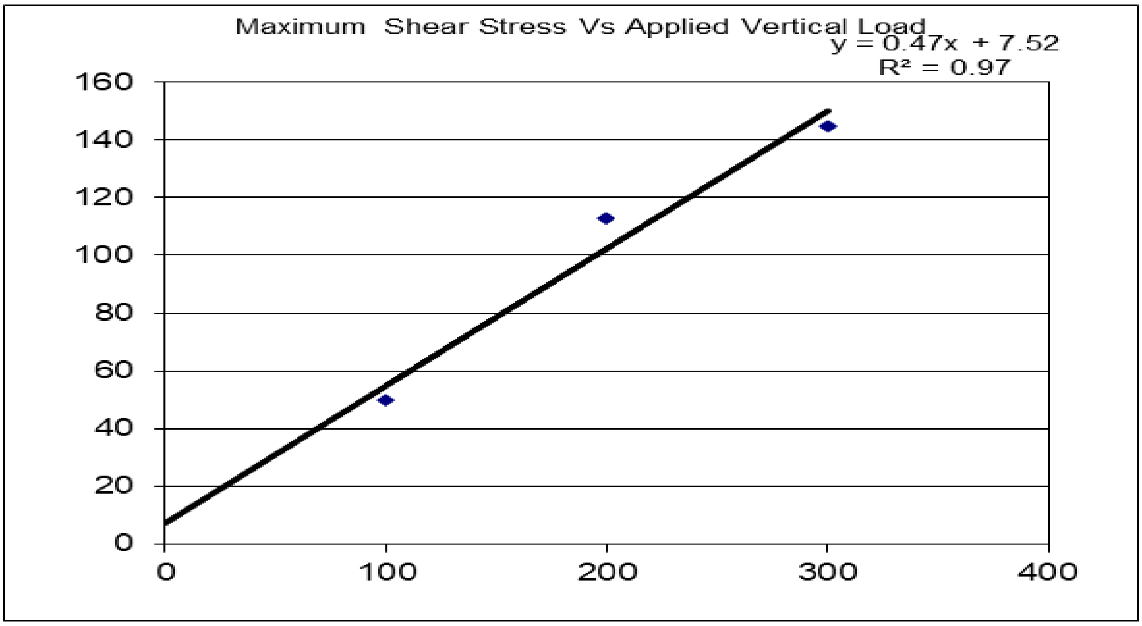
Maximum Shear Stress Vs Applied Vertical Load
y = 0.47x + 7.52
R² = 0.97
160
140
120
100
80
60
40
20
0
0
100
200
300
400

Appendix 1.6.2 Direct shear test pit -2

Sample No. TP-2				Sample Depth, m: 2.50		Water Content26.52	
The thickness of sample: 20mm				Rate of strain : 0.1 mm/min		Unit Weight 16.11	
Ring Area, cm^2: 30.19				Sample Condition: disturbed			
Height of sample, mm: 20				Ring Calibration Factor 1.8018			
		Applied Vertical Stress		Applied Vertical Stress		Applied Vertical Stress	
		100 kPa		**200 kPa**		**300 kPa**	
Horizontal	Corrected	Dial Gauge	Shear	Dial Gauge	Shear	Dial Gauge	Shear
Displacem't	Area	Reading	Stress	Reading	Stress	Reading	Stress
[mm]	[mm^2]	[mm]	[kPa]	[mm]	[kPa]	[mm]	[kPa]
0.0	3099	0.00	0.00	0.00	0.00	0.00	0.00
0.5	3069	7.00	4.11	21.00	12.33	28.00	16.44
1.0	3009	11.50	6.89	34.00	20.36	35.00	20.96
1.5	2919	18.00	11.11	44.50	27.47	41.00	25.31
2.0	2799	21.00	13.52	48.50	31.22	47.00	30.26
2.5	2649	21.00	14.28	50.00	34.01	49.00	33.33
3.0	2469	22.00	16.05	50.00	36.49	51.00	37.22
3.5	2259	23.00	18.35	49.00	39.08	52.00	41.48
4.0	2019	26.00	23.20	47.50	42.39	53.00	47.30
4.5	1749	23.00	23.69	45.50	46.87	53.00	54.60
5.0	1449	21.00	26.11	43.50	54.09	53.00	65.90
5.5	1689	20.00	21.34	41.00	43.74	53.00	56.54
6.0	1659	19.00	20.64	40.00	43.44	52.00	56.48
6.5	1359		0.00	38.50	51.04	51.00	67.62
7.0	1329		0.00	37.00	50.16	50.00	67.79
7.5	999		0.00	36.50	65.83	48.00	86.57
8.0	1209		0.00	36.00	53.65	47.50	70.79

8.5	1149		0.00		0.00	45.00	70.57
9.0	819		0.00		0.00	45.00	99.00
9.5	759		0.00		0.00		0.00
Maximum shear stress, kPa			**26.11**	*Max. shear stress, kPa*	**65.83**	*Max. shear stress, kPa*	**99.00**

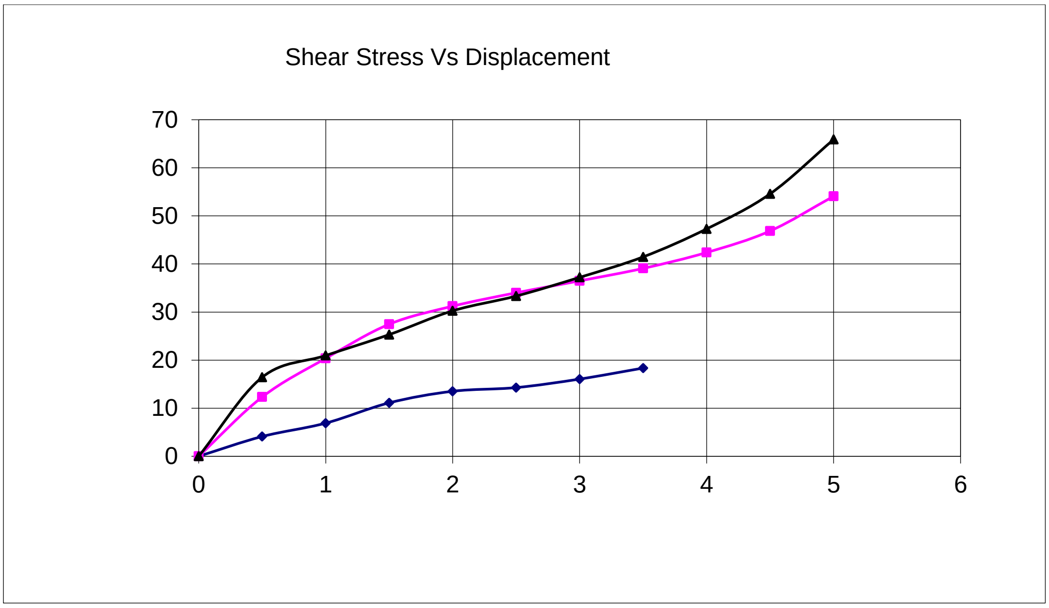

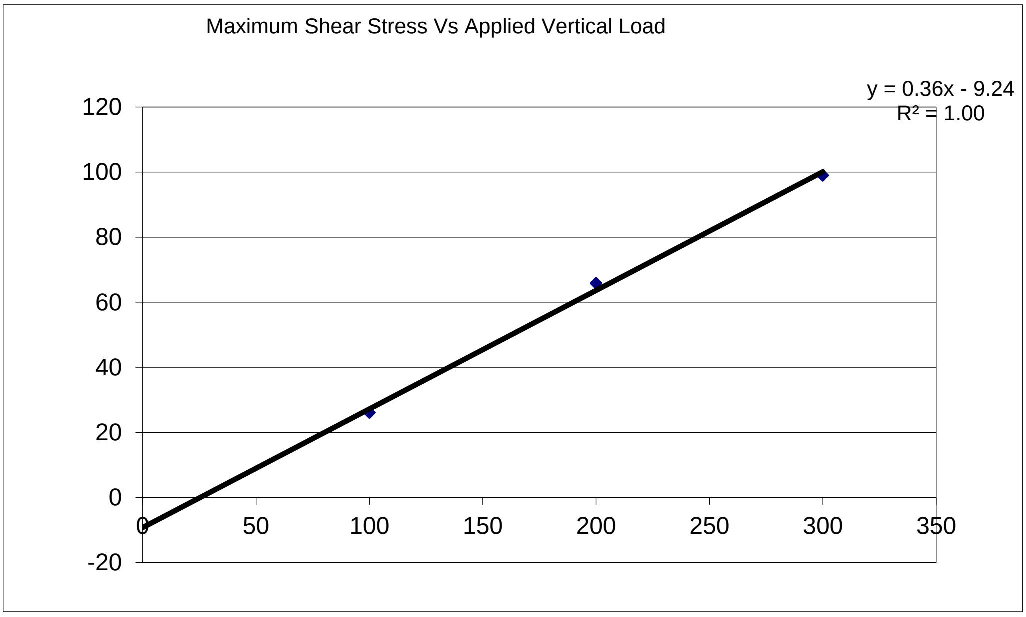

Appendix 2 Rock material characterization

Appendix 2.1 Raw data point load test

Sample ID	Rock types	W1 (mm)	W2 (mm)	Ave W(mm)	D (mm)	P (KN)	De (mm)	De^2 (mm^2)	A $(mm)^2$	P/1000	Is Mpa	F	Is (50) Mpa	UCS (Mpa)
Rs_1-01	Welded tuff	69.5	64.22	66.86	60.15	13	71.575	5123.1	4021.63	0.013	2.54	1.2	2.5	71.3
Rs_1-02	Welded tuff	53.02	60	56.51	28.01	4.5	44.904	2016.37	1582.85	0.0045	2.23	0.9	2.2	50.8
Rs_2-01	Ignimbrite	89.15	64.46	78.8	60.1	15	77.67	6033	4735.9	0.015	2.48	1.2	2.5	72
Rs_2-02	Ignimbrite	65.66	73.19	69.42	40.47	15	59.823	3578.9	2809.43	0.015	4.19	1.1	4.2	108.7
Rs_3-01	Pyroclastic deposit	81.03	68.53	74.78	58.51	3.5	74.662	5574.4	475.4	0.0035	0.62	1.2	0.6	17.9
Rs_3-02	Pyroclastic deposit	76.94	47.15	62.04	43.71	3.5	58.775	3454.5	2711.77	0.0035	1.01	1.07	1.01	26.02
Rs_4-01	Rhyolite	62.07	87.51	74.79	43.35	15	64.266	4130.11	3242.14	0.015	3.63	1.12	3.6	97.5
Rs_4-02	Rhyolite	92.25	86.54	89.4	47.91	15	73.866	5456.24	4283.15	0.015	2.76	1.2	2.76	78.9
Rs_4-03	Rhyolite	74.03	88.95	81.49	56.72	15	76.733	5888.03	4622.11	0.015	2.54	1.21	2.54	73.9
Rs_5-01	Basalt	95.55	71.72	83.63	58.06	24.3	78.647	6185.41	4855.55	0.0243	3.93	1.22	3.9	115
Rs_5-02	Basalt	100.68	72.32	86.5	70.72	42	88.276	7792.7	6117.3	0.042	5.39	1.29	5.4	166.8

Appendix 2.2 Dry density determination

Sample id	Rock types	m (g)	V1 (ml)	V2 (ml)	V2-V1 (ml)	Dry m (g)	$\rho = \frac{M}{V}$ g/cm^3	$\gamma = \rho * g$ KN/m^3
Rs1-01	Welded tuff	195	700	790	90	192.9	2.14	20.972
Rs1-02	Welded tuff	155	700	770	70	153.5	2.193	21.513
Rs1-03	Welded tuff	151.1	700	780	80	149.1	1.864	18.285
Rs2-01	Ignimbrite	130.1	500	550	50	128.7	2.574	25.251
Rs2-02	Ignimbrite	189.3	500	600	100	187.3	1.873	18.374
Rs2-03	Ignimbrite	170.8	500	590	90	168.6	1.873	18.374
Rs3-01	Pyroclastic deposit	191.2	600	790	190	187.6	0.987	9.6824
Rs3-02	Pyroclastic deposit	60	400	470	70	56.5	0.807	7.9167
Rs4-01	Rhyolite	189.3	500	595	95	188.8	1.987	19.492
Rs4-02	Rhyolite	218.7	600	700	100	217.3	2.173	21.317
Rs4-03	Rhyolite	322.9	700	850	150	320.9	2.14	20.993
Rs4-04	Rhyolite	271.9	500	615	115	270.9	2.355	23.103
Rs5-01	Basalt	351	700	810	110	350.5	3.186	31.225
Rs5-02	Basalt	326.8	600	720	120	326.6	2.722	26.703

Appendix 2.3 Saturated density determination

Sample Id	Rock type	Wet m (g)	V1 ml)	V2 (ml)	V2-V1 (ml)	$\rho = \frac{M}{V}$ g/cm^3	$\gamma = \rho * g$ N/m^3
Rs1-01	Welded tuff	204.8	500	575	75	2.731	26.791
Rs1-02	Welded tuff	164.8	500	570	70	2.354	23.093
Rs1-03	Welded tuff	162.7	500	560	60	2.712	26.604
Rs2-01	Ignimbrite	135.4	600	650.5	50.5	2.681	26.3
Rs2-02	Ignimbrite	198.4	500	570	70	2.834	27.801
Rs2-03	Ignimbrite	179.4	600	670	70	2.563	25.143
Rs3-01	Pyroclastic deposit	249.7	700	860	160	1.561	15.313
Rs4-01	Rhyolite	198.6	600	680	80	2.482	24.348
Rs4-02	Rhyolite	227.1	600	700	100	2.271	22.278
Rs4-03	Rhyolite	337.5	600	740	140	2.411	23.652
Rs4-04	Rhyolite	285	700	800	100	2.85	27.958
Rs5-01	Basalt	352.1	700	820	120	2.934	28.782
Rs5-02	Basalt	327.4	600	700	100	3.274	32.118

Appendix 2.4 Slake durability test

Sample id	Rock type	Initial weight	Weight after 1st cycle	Weight after 2nd cycle	% Retained after 1st cycle	% Retained after 2nd cycle
Sample – 1	Welded tuff	512.3	494.5	491	3.6%	99.3%
Sample – 2	Ignimbrite	503.1	494.4	491.7	1.76%	99.45
Sample – 4	Basaltic tuff	469.7	461.4	457.2	1.8%	99.1%
Sample – 5	Basalt	523.1	520.2	519.6	0.56%	99.88%

Appendix 3. Rock mass property determination

Appendix 3.1 Field estimates of uniaxial compressive strength of intact rock according to (Marinos, 2000)

Grade*	Term	Uniaxial Comp. Strength (MPa)	Point Load Index (MPa)	Field estimate of strength	Examples
R6	Extremely Strong	> 250	>10	Specimen can only be chipped with a geological hammer	Fresh basalt, chert, diabase, gneiss, granite, quartzite
R5	Very strong	100 - 250	4 - 10	Specimen requires many blows of a geological hammer to fracture it	Amphibolite, sandstone, basalt, gabbro, gneiss, granodiorite, peridotite , rhyolite, tuff
R4	Strong	50 - 100	2 - 4	Specimen requires more than one blow of a geological hammer to fracture it	Limestone, marble, sandstone, schist
R3	Medium strong	25 - 50	1 - 2	Cannot be scraped or peeled with a pocket knife, specimen can be fractured with a single blow from a geological hammer	Concrete, phyllite, schist, siltstone
R2	Weak	5 - 25	**	Can be peeled with a pocket knife with difficulty, shallow indentation made by firm blow with point of a geological hammer	Chalk, claystone, potash, marl, siltstone, shale, rocksalt,
R1	Very weak	1 - 5	**	Crumbles under firm blows with point of a geological hammer, can be peeled by a pocket knife	Highly weathered or altered rock, shale
R0	Extremely Weak	0.25 - 1	**	Indented by thumbnail	Stiff fault gouge

Appendix 3.2 Values of the constant mi for intact rock, by a rock group. (Marinos, 2000)

Note that values in parenthesis are estimates. The range of values quoted for each material depends upon the granularity and interlocking of the crystal structure – the higher values being associated with tightly interlocked and more frictional characteristics.

Rock type	Class	Group	Texture: Coarse	Texture: Medium	Texture: Fine	Texture: Very fine
SEDIMENTARY	Clastic		Conglomerates * Breccias *	Sandstones 17 ± 4	Siltstones 7 ± 2 Greywackes (18 ± 3)	Claystones 4 ± 2 Shales (6 ± 2) Marls (7 ± 2)
	Non-Clastic	Carbonates	Crystalline Limestone (12 ± 3)	Sparitic Limestones (10 ± 2)	Micritic Limestones (9 ± 2)	Dolomites (9 ± 3)
		Evaporites		Gypsum 8 ± 2	Anhydrite 12 ± 2	
		Organic				Chalk 7 ± 2
METAMORPHIC	Non Foliated		Marble 9 ± 3	Hornfels (19 ± 4) Metasandstone (19 ± 3)	Quartzites 20 ± 3	
	Slightly foliated		Migmatite (29 ± 3)	Amphibolites 26 ± 6	Gneiss 28 ± 5	
	Foliated**			Schists 12 ± 3	Phyllites (7 ± 3)	Slates 7 ± 4
IGNEOUS	Plutonic	Light	Granite 32 ± 3 Granodiorite (29 ± 3)	Diorite 25 ± 5		
		Dark	Gabbro 27 ± 3 Norite 20 ± 5	Dolerite (16 ± 5)		
	Hypabyssal		Porphyries (20 ± 5)		Diabase (15 ± 5)	Peridotite (25 ± 5)
	Volcanic	Lava		Rhyolite (25 ± 5) Andesite 25 ± 5	Dacite (25 ± 3) Basalt (25 ± 5)	
		Pyroclastic	Agglomerate (19 ± 3)	Breccia (19 ± 5)	Tuff (13 ± 5)	

* Conglomerates and breccias may present a wide range of m_i values depending on the nature of the cementing material and the degree of cementation, so they may range from values similar to sandstone, to values used for fine grained sediments (even under 10).

** These values are for intact rock specimens tested normal to bedding or foliation. The value of mi will be significantly different if failure occurs along a weakness plane.

Appendix 3.3 Geological strength index for jointed rock masses (Marinos, 2000)

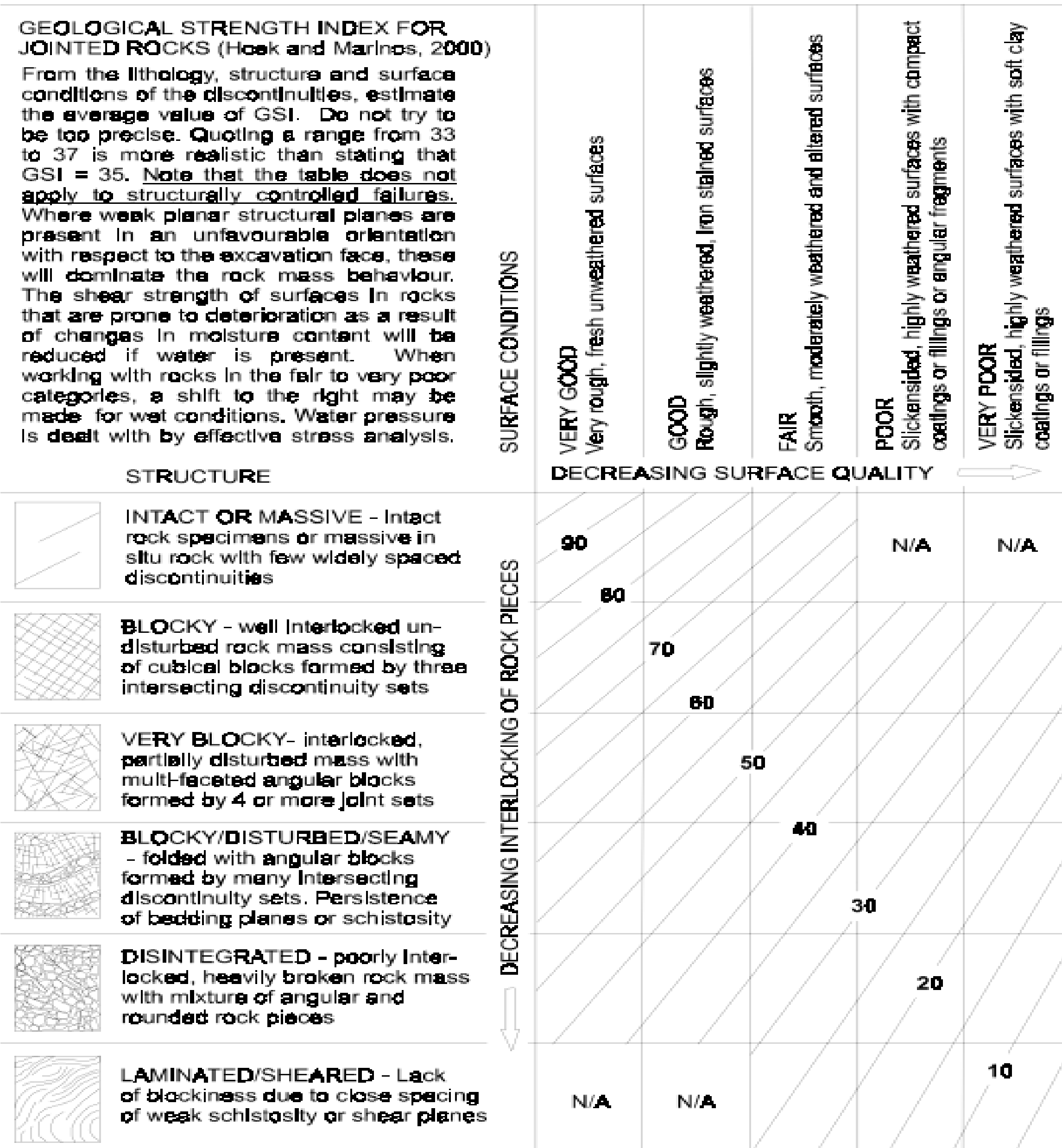

Appendix 3.4 rock mass property determination using Rocdata

RS1

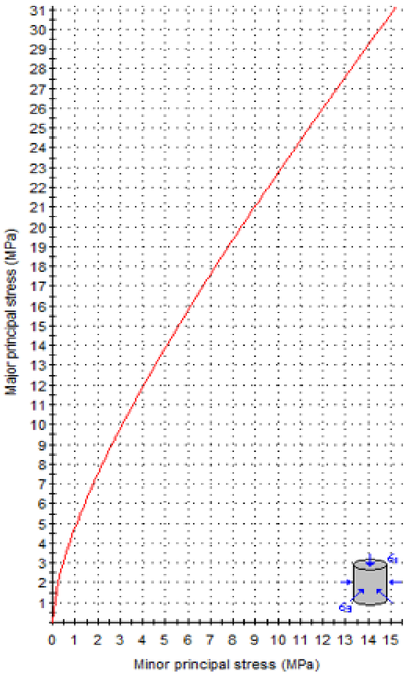

Analysis of Rock/Soil Strength using RocData

Hoek-Brown Classification
intact uniaxial compressive strength = 61.1 MPa
GSI = 30 mi = 14.19 Disturbance factor = 0.7

Hoek-Brown Criterion
mb = 0.303 s = 3.93e-5 a = 0.522

Mohr-Coulomb Fit
cohesion = 1.456 MPa friction angle = 17.33 deg

Rock Mass Parameters
tensile strength = -0.008 MPa
uniaxial compressive strength = 0.305 MPa
global strength = 3.958 MPa
modulus of deformation = 1606.70 MPa

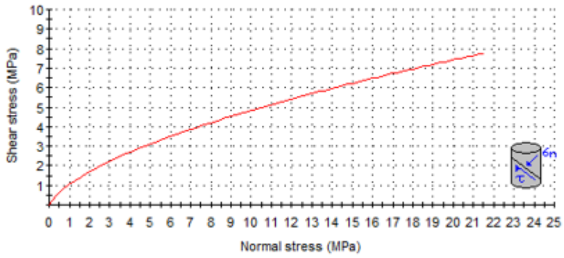

RS2

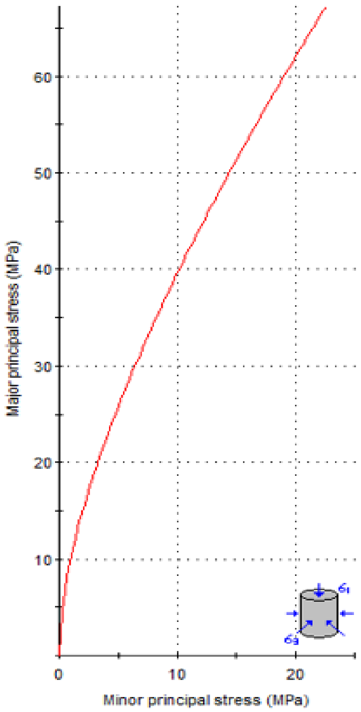

Hoek-Brown Classification
intact uniaxial compressive strength = 90.36 MPa
GSI = 50 mi = 15.45 Disturbance factor = 0.7

Hoek-Brown Criterion
mb = 0.990 s = 0.0007 a = 0.506

Mohr-Coulomb Fit
cohesion = 3.671 MPa friction angle = 26.25 deg

Rock Mass Parameters
tensile strength = -0.065 MPa
uniaxial compressive strength = 2.314 MPa
global strength = 11.807 MPa
modulus of deformation = 6178.76 MPa

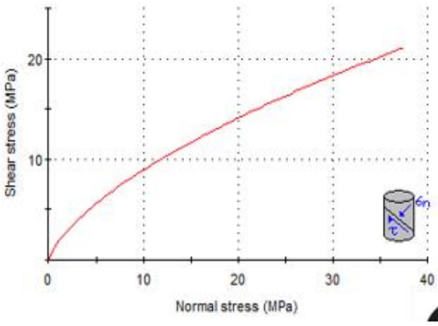

RS3

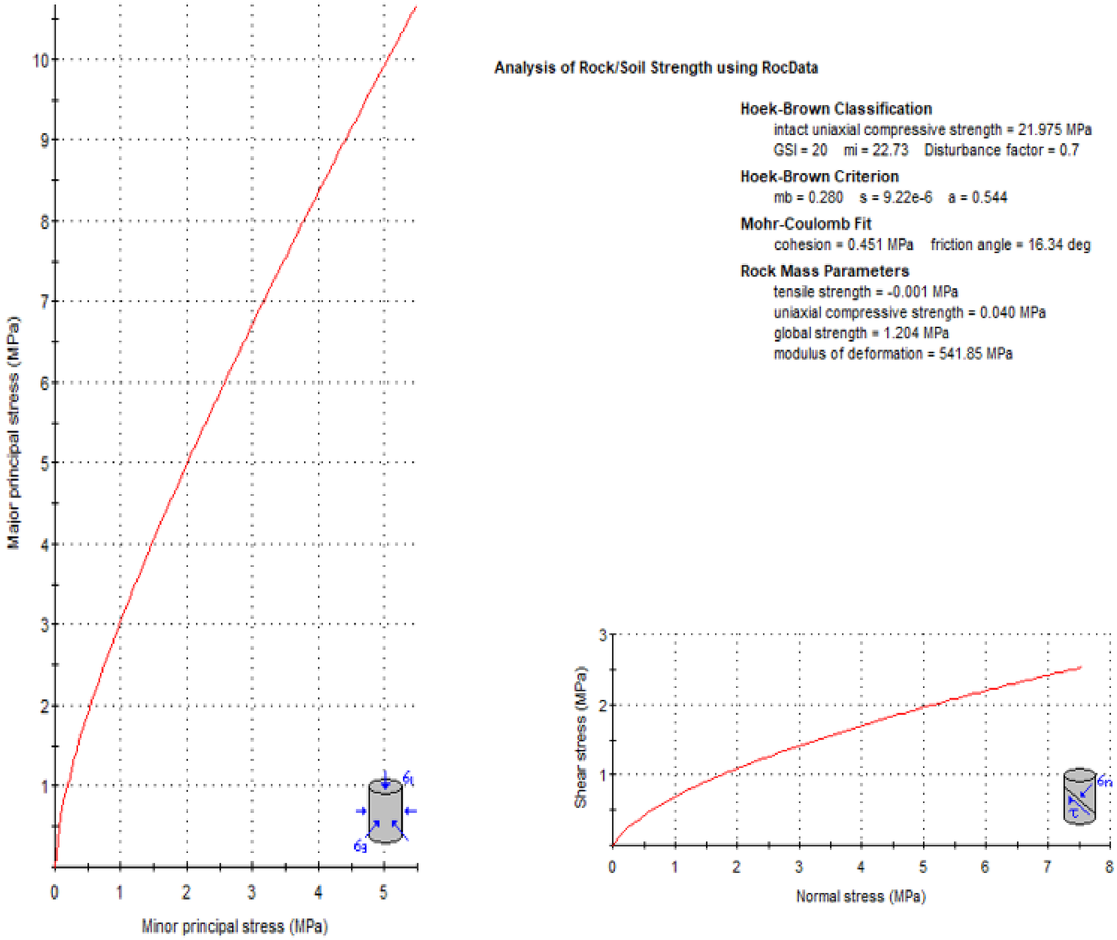
Analysis of Rock/Soil Strength using RocData
Hoek-Brown Classification
intact uniaxial compressive strength = 21.975 MPa
GSI = 20 mi = 22.73 Disturbance factor = 0.7
Hoek-Brown Criterion
mb = 0.280 s = 9.22e-6 a = 0.544
Mohr-Coulomb Fit
cohesion = 0.451 MPa friction angle = 16.34 deg
Rock Mass Parameters
tensile strength = -0.001 MPa
uniaxial compressive strength = 0.040 MPa
global strength = 1.204 MPa
modulus of deformation = 541.85 MPa
Major principal stress (MPa)
Minor principal stress (MPa)
Shear stress (MPa)
Normal stress (MPa)

RS-4

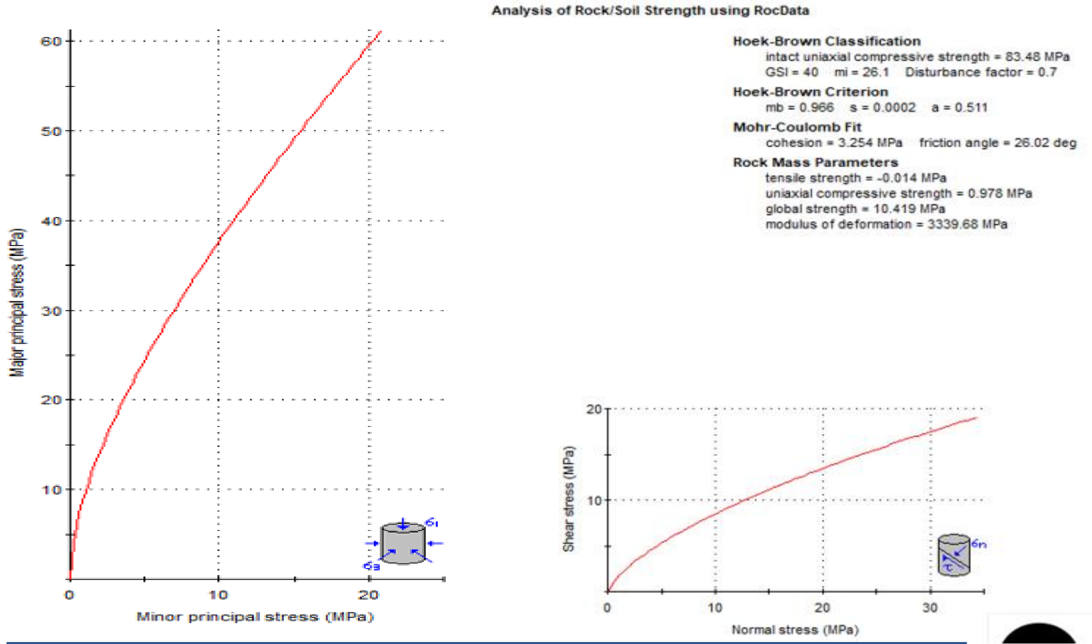

Analysis of Rock/Soil Strength using RocData
Hoek-Brown Classification
intact uniaxial compressive strength = 83.48 MPa
GSI = 40 mi = 26.1 Disturbance factor = 0.7
Hoek-Brown Criterion
mb = 0.966 s = 0.0002 a = 0.511
Mohr-Coulomb Fit
cohesion = 3.254 MPa friction angle = 26.02 deg
Rock Mass Parameters
tensile strength = -0.014 MPa
uniaxial compressive strength = 0.978 MPa
global strength = 10.419 MPa
modulus of deformation = 3339.68 MPa
Major principal stress (MPa)
Minor principal stress (MPa)
Shear stress (MPa)
Normal stress (MPa)

RS-5

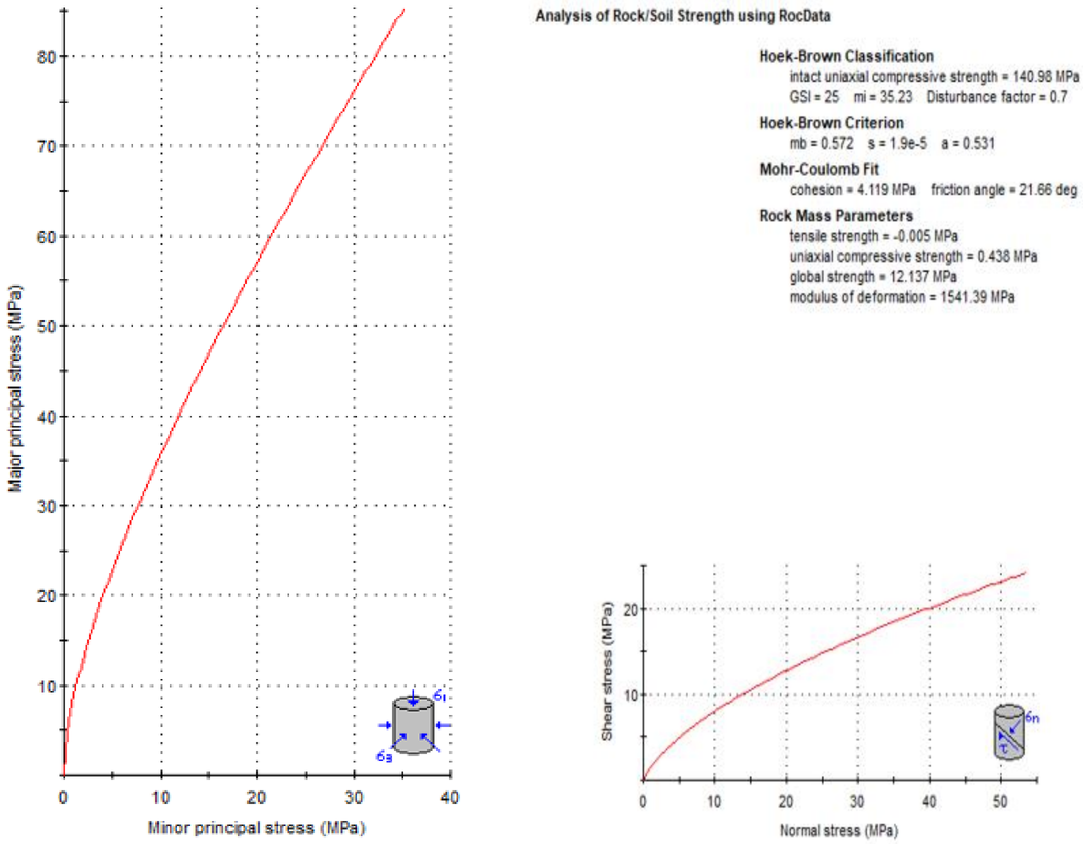

Analysis of Rock/Soil Strength using RocData
Hoek-Brown Classification
intact uniaxial compressive strength = 140.98 MPa
GSI = 25 mi = 35.23 Disturbance factor = 0.7
Hoek-Brown Criterion
mb = 0.572 s = 1.9e-5 a = 0.531
Mohr-Coulomb Fit
cohesion = 4.119 MPa friction angle = 21.66 deg
Rock Mass Parameters
tensile strength = -0.005 MPa
uniaxial compressive strength = 0.438 MPa
global strength = 12.137 MPa
modulus of deformation = 1541.39 MPa
Major principal stress (MPa)
Minor principal stress (MPa)
Shear stress (MPa)
Normal stress (MPa)

Appendix 4 Precipitation data of Tercha-Chida during 11 years (2010-2011)

Month	Jan	Feb	Mar	Apr	May	Jun	Jul	Aug	Sep	Oct	Nov	Dec	Total
2010	1.2	2.35	6.1	8.23	11.28	8.57	5.54	5.02	6.4	5.02	2.21	1.08	63
2011	0.62	0.31	2.73	6.58	8.29	4.18	2.54	2.44	3.22	4.12	7.64	0.56	43.23
2012	0.04	0.34	0.95	10.28	7.5	3.87	4.74	10.85	8.76	5.28	3.2	2.88	58.69
2013	0.99	0.36	5.09	12.25	12.51	7.54	6.4	5.81	5.44	7.86	6.65	0.38	71.28
2014	0.1	1.99	4.47	10.16	15.37	7.44	5.58	6.22	8.94	9.61	4.3	1.57	75.75
2015	0.02	0.81	1.85	4.71	6.65	6.02	5.38	2.89	1.81	7.93	2.92	3.05	44.04
2016	1.32	0.64	3.2	10.16	7.33	3.79	4.03	10.02	7.05	3.77	1.52	0.42	53.25
2017	0.09	2.62	2.74	4.43	9.21	3.87	5.49	4.51	7.77	5.03	1.86	0.03	47.65
2018	0.07	3.69	2.57	8.72	8.56	4.28	1.36	3.15	1.5	3.5	3.93	0.62	41.95
2019	0	1.34	2.43	7.52	4.83	5.64	5.3	6.07	8.28	7.47	4.26	2.66	55.8
2020	2.36	2.75	5.38	12.4	8.21	6.38	6.08	8.17	8.4	3.2	2.55	4.13	70.01
2021	2.21	0.57	0.51	4.74	8.76	2.05	6.53	7.81	5.97	5.73	1.01	1.7	47.59
Average	0.752	1.615	3.456	9.107	9.864	5.784	5.361	6.633	6.685	6.229	3.823	1.735	61.044